

Fighting preterm birth with novel surgical tools and biomaterials engineering

THÈSE N° 8359 (2017)

PRÉSENTÉE LE 5 DÉCEMBRE 2017
À LA FACULTÉ DES SCIENCES DE LA VIE
UNITÉ DU PROF. LUTOLF

PROGRAMME DOCTORAL EN BIOTECHNOLOGIE ET GÉNIE BIOLOGIQUE

ÉCOLE POLYTECHNIQUE FÉDÉRALE DE LAUSANNE

POUR L'OBTENTION DU GRADE DE DOCTEUR ÈS SCIENCES

PAR

Yannick Robert DEVAUD

acceptée sur proposition du jury:

Prof. Ph. Renaud, président du jury
Prof. M. Lütolf, Dr M. Ehrbar, directeurs de thèse
Prof. N. Ochsenbein-Köhlle, rapporteuse
Dr M. Tibbitt, rapporteur
Prof. N. Stergiopoulos, rapporteur



ÉCOLE POLYTECHNIQUE
FÉDÉRALE DE LAUSANNE

Suisse
2017

*To Gabisou, Mamacita and Paps,
You are the true inspiration.*

ABSTRACT

With advances in fetal diagnosis and therapy, fetoscopy has become a good option to treat a series of life threatening diseases like twin-to-twin transfusion syndrome or severe congenital diaphragmatic hernia. The efficacy of fetoscopy for those types of disorders is not debatable; however, it comes with a daunting limitation: iatrogenic preterm premature rupture of the fetal membrane (iPPROM). The injury created by the instruments to access the amniotic cavity is the reason for fetal membrane rupture in almost one third of all interventions. The consequences of very early iPPROM are death or very preterm birth leading to physiological complications for the baby, and psychological burdens for the family. A solution preventing iPPROM is necessary to make fetoscopy a safer procedure.

We first concentrated on developing a minimally invasive medical device to stabilize the fetal membrane defect caused by fetoscopic instruments. Our approach consists in placing bioadhesives at the wounded site from the inside of the amniotic cavity following the intervention. To do so, we designed and produced an umbrella-shape receptor whose mechanical properties enabled its crimping inside the accession catheter and ensured its automatic deployment inside the cavity. The umbrella is then pulled against the membrane and glued by gathering injectable bioadhesives. We demonstrated evidence of the functionality of the method by applying existing biocompatible glues on an ex vivo model replicating physiological conditions.

While the application method is a requirement for a reliable delivery of injectable materials, questions remain about the nature of those materials. Restoration of the native tissue might provide functional advantages over the simple sealing of it. Hence, the development of platforms enabling the in vitro study of cell response to biological cues was the focus of the next investigations. First, we took advantage of the tunability of polyethylene glycol (PEG) synthetic hydrogels to locally bind growth factors (GFs) by affinity. We established a GF gradient in 3D and assessed multiple methods to quantify cell behaviour in response to those gradients.

Next, we utilized a method to pre-fabricate hydrogel gradients in a full 96-well plate and established scripts to automate image acquisition, image processing and data analysis. This platform enabled a fast quantification of the influence of GF concentration on the recruitment of cells in large number of samples in parallel. We then reproduced a wound in a tissue model in vitro, injected PEG hydrogels carrying GF and quantified cell recruitment into the healing hydrogel.

Finally, we used a proteomics approach to investigate the effect of bioactive signals on inducing a differential production of extracellular matrix (ECM) by the cells. This investigation was motivated by the critical role of ECM proteins in tissue functionality and thus by the importance of faithfully reconstituting the native structure of the tissue.

To summarize, our efforts contributed to the advancement of fetal therapy by bringing innovative solutions in two distinct fields. On one side, by the development of a technology to apply materials at the site of defect; and on the other side, by the establishment of platforms allowing the exploration of cell behaviour. Combined, they carry a real potential to engineer methods for precise delivery of healing-inducing biomaterials and consequently to reduce the risks of iPPROM.

Key words: iPPROM, fetal membranes, fetoscopy, hydrogels, 3D cell culture, wound model, gradient, extracellular matrix, growth factors, proteomics

RÉSUMÉ

Avec le progrès en diagnostic et thérapie fœtale, la fétoscopie s'est avérée être une bonne option pour une série de maladies engageant le pronostic vital comme par exemple le syndrome transfuseur-transfusé ou la hernie diaphragmatique congénitale. L'efficacité de la fétoscopie pour ce genre de troubles n'est pas questionnable, cependant, elle est accompagnée d'une importante limitation : la rupture prématurée iatrogène de la membrane fœtale (iPPROM). La blessure créée lors de l'insertion des instruments de fétoscopie dans la cavité amniotique résulte en la rupture de la membrane dans environ un tiers de toutes ces interventions. Les conséquences d'iPPROM précoces sont la mort ou la naissance très prématurée avec pour conséquence des complications physiologiques pour le bébé et un fardeau psychologiques pour la famille. Une solution pour empêcher l'iPPROM est nécessaire afin de rendre cette procédure plus sûre.

Nous nous sommes premièrement concentrés sur le développement d'un dispositif médical à invasion minimale afin de stabiliser la plaie sur la membrane amniotique créée par les instruments de fétoscopie. Notre approche consiste à placer des bio-adhésifs sur le lieu de perforation par l'intérieur de la cavité amniotique suivant l'intervention. Pour ce faire, nous avons designé et produit un élément en forme de parapluie dont les propriétés mécaniques permettent de le plier à l'intérieur du cathéter utilisé durant la fétoscopie et assure son déploiement automatique à l'intérieur de la cavité amniotique. Le parapluie est ensuite placé contre la membrane et collé à celle-ci en recueillant des bio-adhésifs injectables. Nous avons démontré des preuves fonctionnelles de cette méthode en injectant des colles biocompatibles existantes sur un modèle ex vivo reproduisant des conditions physiologiques.

Alors que la méthode d'application est une qualité requise pour déposer des matériaux injectables de manière fiable, la nature de ces matériaux demeure un point d'interrogation. Une restauration du tissu naturel doit sûrement apporter des avantages fonctionnels comparé à l'unique scellage de la plaie. Pour ce faire, dans les investigations suivantes, nous nous sommes attardés sur le développement de plateformes permettant l'étude in vitro de la réponse cellulaire à des signaux biologiques stimulant le processus de guérison. En premier lieu, nous avons profité de la versatilité des gels de polyéthylène glycol (PEG) pour y attacher des facteurs de croissance par affinité. Nous avons établi un gradient 3D de facteurs de croissances et évalué plusieurs méthodes de quantification du comportement cellulaire en réponse à ces gradients.

Nous avons ensuite utilisé une méthode pour pré-fabriquer des gradients d'hydrogel dans une plaque entière de 96 puits et avons établi des scripts afin d'automatiser l'acquisition et le traitement d'images ainsi que l'analyse de données. Cette plateforme a permis la quantification rapide d'un grand nombre d'échantillons en parallèle de l'influence de la concentration des facteurs de croissance sur le recrutement de cellules. Nous avons ensuite reproduit un modèle de plaie in vitro, y avons injecté des

hydrogels de PEG porteurs de facteur stimulant la guérison et avons quantifié le recrutement de cellules dans ces hydrogels injectés.

Pour conclure, nous avons utilisé une approche protéomique afin d'enquêter sur les effets de signaux bioactifs dans l'induction de la production différentielle de matrice extracellulaire (ECM) par les cellules. Cela a été motivé par le rôle critique des protéines de l'ECM sur la fonction d'un tissu et par conséquence, sur l'importance de reconstituer la structure d'un tissu de manière fidèle.

En résumé, nos efforts ont contribué à l'avancement de la thérapie fœtale en apportant des solutions novatrices sur deux plans. D'une part par le développement d'une technologie permettant l'application de matériaux sur l'endroit de perforation et d'autre part, par la création de plateformes permettant l'exploration du comportement cellulaire. Ensemble, ces éléments portent un réel potentiel pour l'ingénierie de méthodes permettant le placement précis de matériaux bioactifs et par conséquence pour la réduction des risques d'iPPROM.

Mots clés: iPPROM, membranes fœtales, fétoscopie, hydrogels, culture cellulaire en 3D, modèle de plaie, gradient, matrice extracellulaire, facteurs de croissance, protéomique

TABLE OF CONTENTS

ABSTRACT	5
RÉSUMÉ	7
CHAPTER 1 _ INTRODUCTION	13
1.1 _ BACKGROUND	13
1.2 _ MOTIVATION	19
1.3 _ SPECIFIC GOALS	19
1.4 _ REFERENCES	21
CHAPTER 2 _ MINIMALLY INVASIVE SURGICAL DEVICE FOR PRECISE APPLICATION OF BIOADHESIVES TO PREVENT IPPROM.	25
2.1 _ ABSTRACT	26
2.2 _ INTRODUCTION	27
2.3 _ MATERIALS AND METHODS	28
2.4 _ RESULTS	32
2.5 _ DISCUSSION	37
2.6 _ REFERENCES	40
CHAPTER 3 _ LOCALLY CONTROLLING MESENCHYMAL STEM CELL MORPHOGENESIS BY 3D PDGF-BB GRADIENTS TOWARDS THE ESTABLISHMENT OF AN IN VITRO PERIVASCULAR NICHE	43
3.1 _ ABSTRACT	44
3.2 _ INTRODUCTION	45
3.3 _ MATERIALS AND METHODS	47
3.4 _ RESULTS	51
3.5 _ DISCUSSION	57
3.6 _ REFERENCES	60
CHAPTER 4 _ IN VITRO CELL RECRUITMENT PLATFORMS TO ASSESS THE HEALING POTENTIAL OF GROWTH FACTOR-DELIVERING HYDROGEL ON A WOUND HEALING MODEL	63
4.1 _ ABSTRACT	64
4.2 _ INTRODUCTION	65
4.3 _ MATERIALS AND METHODS	67

4.4 _ RESULTS	70
4.5 _ DISCUSSION	76
4.6 _ REFERENCES	78
CHAPTER 5 _ LABEL FREE QUANTIFICATION PROTEOMICS FOR THE IDENTIFICATION OF MESENCHYMAL STEM CELL MATRISOME INSIDE 3D POLY-ETHYLENE GLYCOL HYDROGELS	79
5.1 _ ABSTRACT	80
5.2 _ INTRODUCTION	81
5.3 _ MATERIALS AND METHODS	83
5.4 _ RESULTS	87
5.5 _ DISCUSSION	96
5.6 _ REFERENCES	99
CHAPTER 6 _ CONCLUSION	103
6.1 _ GENERAL DISCUSSION	103
6.2 _ FUTURE DIRECTIONS	107
6.3 _ REFERENCES	109
ACKNOWLEDGEMENTS	112
CURRICULUM VITAE	114

CHAPTER 1 _ INTRODUCTION

1.1 _ BACKGROUND

FETAL MEMBRANES

Fetal membranes consist of an organized multilayer system with two overlapping layers, the inner layer, the amnion and the outer one, the chorion. The amnion is a strong tissue of a single layer of epithelial cells, a basement membrane and a thick layer composed of mesenchymal cells, which are multipotent stromal cells having the ability to differentiate into multiple cell. The third layer of the amnion, composed of proteoglycan, enables it to slide over the chorion, on which it lies. The chorion is composed of three different layers. One of those is populated by trophoblasts, which are the first cells to be differentiated during development and are responsible for the implantation of the egg into the uterus and to strong attachment to the maternal decidua (Figure 1.1).^{1,2} Each of those layers are composed of a precise combination of proteins building the extracellular-matrix (ECM) environment. Collagens, proteoglycans and glycoproteins are responsible for ensuring the structural function of the membranes by providing tensile strength, elasticity, anchoring functions, structure maintenance and mechanical stability.¹ The components of those membranes have been reported to vary over time and are closely related to cell apoptosis followed by matrix metalloproteinase (MMP) production.^{3,4} The consequence of such MMP production is the weakening of the membrane and, along with structural changes caused by contractions, the spontaneous rupture of the membrane. Thus, besides its main function to hold the amniotic fluid and protect the foetus from adverse effects, fetal membranes appear to participate to a programmed self-weakening leading to the induction of labour.

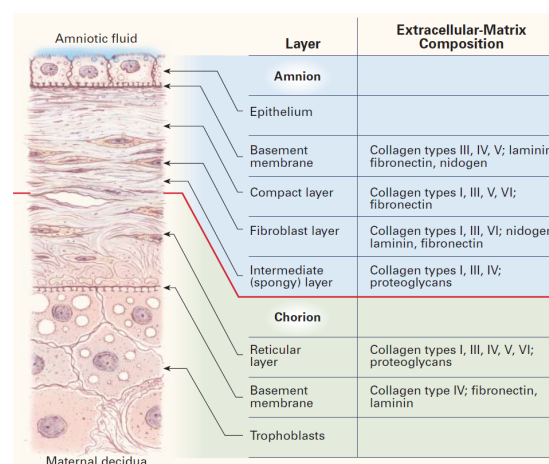


Figure 1.1. Schematic drawing of the structure of the fetal membranes and their compositions in extracellular matrix proteins at term. Figure reproduced with permission from Parry et al.², Copyright Massachusetts Medical Society

FETAL SURGERIES

While spontaneous rupture of the membrane (ROM) is a natural process, premature rupture (PROM) is a complication occurring in 5-10% of all pregnancies and caused by various factors such as inflammation, genetics or external factors.⁵ With advances in fetal diagnosis and therapies, a new origin of membrane rupture has appeared, namely the iatrogenic preterm premature rupture of the fetal membrane (iPPROM). This is caused by fetoscopies, which are endoscopic fetal surgeries aiming to treat life-threatening anomalies on the foetus or the placenta during pregnancy (Figure 1.2). In opposition to open fetal surgery where the foetus is exposed by opening the uterus and the amniotic sac, fetoscopy accesses to the amniotic cavity by minimal invasion through the abdominal wall and the fetal membranes. The most common indications requiring fetoscopy include twin-to-twin transfusion syndrome (TTTS), severe congenital diaphragmatic hernia (CDH), discordant monochorionic twins with a lethal anomaly or reverse arterial perfusion (TRAP).^{6,7} Despite the good efficiency of those treatments, iPPROM occurs in up to 30% of all the surgeries due to the injury of the fetal membrane caused when punching through it when accessing the amniotic cavity. The consequence of such an event can be dramatic for the children suffering from it. Indeed, preterm birth carries a big risk of complication going from morbidity to incurable diseases decreasing life quality and/or expectancy such as cerebral palsy, impaired cognitive skills, vision problems, hearing problems, behavioural, psychological as well as chronic health issues.^{8,9} It is thus safe to say that iPPROM remains the weak spot of those interventions and a solution to prevent iPPROM could considerably improve the success rate of fetal treatment.¹⁰

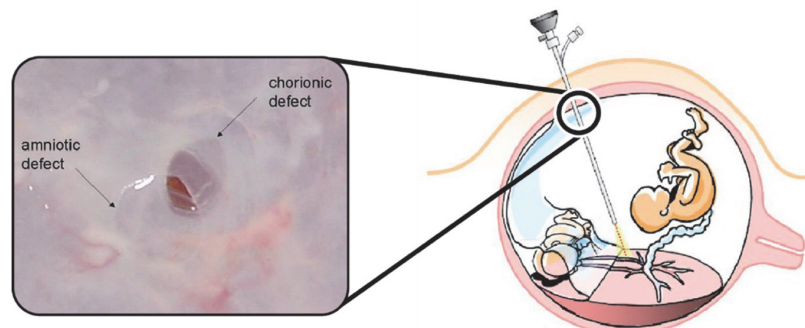


Figure 1.2. Schematic representation of a fetoscopic intervention (in this case a laser fetal surgery treating TTTS) taken from med.brown.edu and a magnified photo of the fetal membrane defect created by the puncture for accessing the amniotic cavity. Photo reprinted from Gratacos et al.¹¹ with permission from Elsevier.

HEALING OF MEMBRANES

Interestingly, human fetal membranes are limited in their healing capacity and holes created by fetoscopy remain open after fetoscopy until the end of pregnancy.¹¹ The reason for that is not yet well understood but is likely due to the lack of support matrix, innervation, vascularization and thus healing signals in vivo. Another reason could be the inhibition of repair mechanism due to MMP activity at the wounded site as observed in a mice model.¹² Considerable effort has been made to try to close the wound in fetal membranes in order to prevent iPPROM. Many attempts have been made to try sealing with glues or plugs and healing with biological triggers.¹³ However, clinicians have not adopted a single of those techniques due to the lack of efficiency and/or

reproducibility of the methods. Many factors, such as the difficulty to access the wound or the localization of the wound, transparency and dimension (thickness of only a few hundred micrometres) of the membranes and wet conditions, make the study of why the healing of human fetal membranes does not occur, very challenging.¹⁴

Some studies investigated healing potential in vitro of fetal membrane by cultivating membrane-derived cells on 2D monolayers or in 3D cell cultures.^{15,16} Healing signals were present in a very limited amount¹⁷⁻¹⁹ but could be stimulated by the exposure to soluble epidermal growth factor (EGF) and insulin-like growth factor-1 (ILGF-1).¹³

The healing potential of fetal membranes has also been studied in animal models. Rat models reported a significant reduction of wound size despite the fact that its integrity was not restored.²⁰ In opposition, a rabbit model showed membrane integrity restoration of up to 40% of the animals.¹² However, none of these promising results have been observed in sheep and monkey studies.²¹ These results attest the very limited spontaneous healing of FMs and confirm the observations made on human fetal membranes.¹¹

Due to the inherent limited healing capacity of membranes, researchers have adopted a strategy consisting in placing cell instructive materials at the defect site to trigger wound healing. This has been done in rabbit mid-gestational models by inserting decellularized amniotic membranes where an increased reepithelization was observed when the scaffolds were inserted alone²², glued with fibrin²³ or loaded with mixed, soluble transforming growth factor beta (TGF β) or fibroblast growth factor 1 (FGF-1).²⁴ The regeneration potential of FMs by their native cells is thus non-questionable. Their combination with scaffolds and precise biological signals are thus hypothesized to be critical determinants for efficient cell recruitment, proliferation and survival, which are essential factors required for a potential clinical application.

SEALING OF MEMBRANES

Another approach consists in applying sealing components instead of healing-triggering materials. Many ex vivo studies have been conducted to try to find potential components for an optimal FM sealant. Materials such as fibrin glue²⁵, platelets rich plasma²⁶, thrombin-containing commercial preparations²⁷ as well as laser welding of the membrane²⁸ were tested. Platelets derivate showed good sealing potential but their use in vivo would require an appropriate application method. Laser welding was possible and efficient but the difficulty of its standardization and the risk of thermal injury discarded it from the list of candidates.

In vivo, animal models have been used to assess fetal membrane sealing. Sealing potential was observed when applying fibrin glue^{25,29,30}, collagen¹⁹ or gelatin sponges²⁰, collagen slurry^{31,32} and MatrigelTM.³³ Similar attempts of applying sealing-inducing patches have been performed on humans. Alternatively, the use of amniopatch (mix of fibrinogen and platelets), which aims to reproduce the blot clot mechanism to seal the wound reported an increase in membrane closure and fetal survival when applied alone^{34,35} or in combination with fibrin.³⁰ However, its relative success came along with reports of fetal death caused by excessive loss of blood.³⁶ A lot of hope has been placed on these naturally derived materials due to their apparent ability to seal fetal membrane ruptures. However, their instability, lack of controlled effect and difficult delivery are reasons why they cannot be used clinically.

MUSSEL GLUE FOR SEALING APPLICATION

A lot of work in the scientific community has focused on the development of injectable candidates for sealing tissues in the body. Their efficiency in a wet environment is one of the main requirements for the successful use of such a glue. Current approaches base their development on gluing mechanisms inspired by nature. The chemical properties conferring the gluing potential of those naturally occurring sealants are deciphered and added into synthetic material backbones able to carry those chemical features. For example, glues have been developed using the principles of geckos or worms to be used as band-aids or help wound closure inside of the body.^{37,38} Similarly, marine and freshwater mussels have also been an inspiration given their ability to adhere to organic and inorganic structures underwater.³⁹⁻⁴¹ Proteins produced in high concentration at the mussel's feet contain a catechol side chain of 2, 3-dihydroxyphenylalanine (DOPA) that confers this very adhesive property. This side chain was synthetically added to star-shaped poly (ethylene glycol) (PEG) macromeres to form a catechol-functionalized PEG (cPEG) giving this injectable synthetic material a strong sealing potential. Crosslinking of cPEG molecules is triggered by the addition of sodium periodate in equal volume.⁴² This second precursor has a potential harmful action on surrounding tissues due to its strong oxidizing potential. However, the very quick and strong reaction with cPEG precursors might ensure rapid use of periodate and fast reduction into less irritating species.⁴³

Recent evidence has shown cPEG's non-toxic, very good sealing potential, leak-proof closure on stretching models *in vitro*^{44,45} and demonstrated good promise on *in vivo* rabbit models.⁴⁶ In addition, advantages over fibrin glue have been proven to reside in its potential to work under wet conditions in an *ex vivo* study.⁴⁷ Its long-lasting adhesion conferred by the slow hydrolysis of the material definitely sets this glue as another very good candidate as a fetal membrane sealing material.

HYDROGELS AS 3D CELL CULTURE PLATFORMS

A strategy used in many laboratories to mimic cell environment is the use of synthetic materials such as cell scaffold for 3D culture. PEG hydrogels have been widely described and have proven their potential to allow recreating similar environments as encountered by cells in nature.^{48,49} The ECM-mimicking structure does not only provide an adequate network for cell survival but also enables stiffness and degradability variation for optimal cell behaviour.⁵⁰ A further advantage, when compared to the use of collagen or Matrigel™, is the lack of biological background, making all the observations inherent to the attributes conferred by gel modification.⁵¹⁻⁵³ From a regenerative medicine point of view, this allows for the careful study of the environment formed by the cells in their hydrogel scaffold. This is particularly important given the structural and bioactive roles that ECM proteins have. Indeed, ECM-cell interaction has a central role in immobilizing biological cues^{54,55} and regulating stem behaviour and fate.^{52,56-61} Thus, deciphering the ECM protein composition can help investigate the effects of biological signals in directing specific protein synthesis.^{16,62-64}

The hydrogels used in our laboratory are based on the cross-linking of PEG substrates triggered by the transglutaminase enzyme factor XIII activated (FXIIIa).^{65,66} This enzyme catalyses the formation of a covalent bond between the acyl group of Glutamine and the amine group of

Lysine contained within peptide substrate domains (Figure 1.3). Adhesion sites such as RGD are added following the same principles. This amino acid sequence, together with a MMP-sensitive domain present in the linker-peptide, is essential to allow cell survival, spreading and migration.⁶⁵⁻⁶⁷ In addition, its chemical structure permits the addition of cell instructive signals to its backbone. This allows a flexible and independent variation of multiple parameters towards the modification of the 3D cellular environment in vitro, which can have a significant influence on the cells.⁶⁸⁻⁷⁰ The possibility to immobilize different motifs to those synthetic gels gives rise to a multitude of options to tune them. For example, biological signals could be modified to possess the peptide recognized by FXIII and be covalently bound to the gel upon gel formation. Alternatively, the addition of streptavidin to the hydrogel backbone would enable the immobilization of biotinylated proteins thanks to the affinity that streptavidin and biotin have.⁷¹ Another option is to covalently bind protein A to the gel and immobilize proteins that have been modified by the addition of the long chain residue of antibodies, which has an affinity to protein A.⁷²⁻⁷⁴ Despite the infinite imaginable options, the challenge remains in how to organize the presentation of those biological cues in 3D. Indeed, while it is straightforward to add biological cues in a homogeneous manner inside a gel during the polymerization of it, it is challenging to immobilize those cues in a spatially controlled manner.

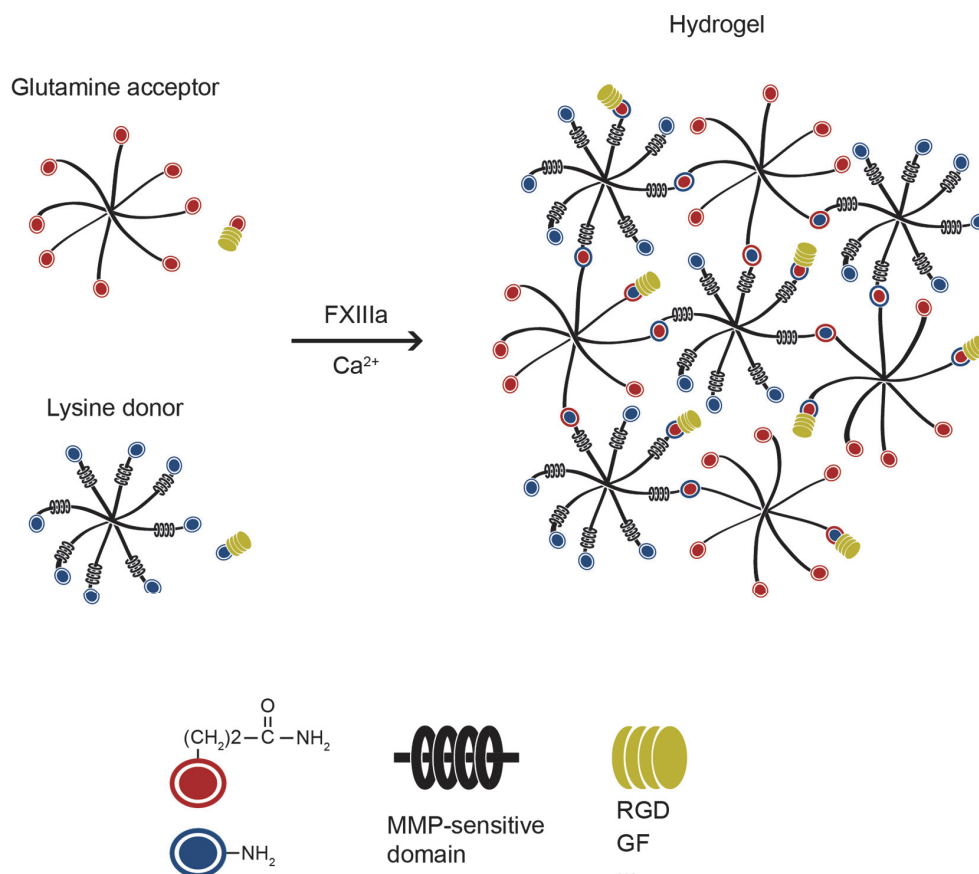


Figure 1.3. PEG polymerization process. 8-arm PEG with Lysine end binds together with the 8-arm PEG with Glutamine end by enzymatic crosslinking lead by FXIIIa in the presence of Calcium ions. 8-arms Lysine PEG has an MMP-sensitive amino acid sequence to permit cleavage. Growth factors (GF), RGD binding sequence or other motifs (...) can be bound to the PEG backbone by the same mechanism.

ELECTROCHEMISTRY TO LOCALLY INHIBIT PEG POLYMERIZATION

While models as described previously are very convenient to mimic tissues in vitro, they are limited in throughput. The dissociation of gel formation and cell seeding may enable to tackle this burden. The objective is to provide with higher throughput models without impairing in the 3D cell culture characteristics. Recent developments in the lab have used the properties of the enzyme-mediated polymerization to this matter.^{75,76} The principle relies on the pH-dependency of enzyme activity. As schematized in Figure 1.4, FXIII works only in a defined pH window. At higher or lower pH, FXIII activity is inhibited and polymerization does not happen. In order to inhibit locally gel formation, a conductive metal placed in the gel is loaded with electric current. By water hydrolysis, protons are produced and the pH drops, inhibiting gel formation around the metal. This principle is used to form hydrogels with softness gradients. These gradients enable cell penetration in 3D even if they are seeded after gel formation. One important advantage of this method is the possibility to pre-fabricate a large number of gels prior to cell seeding and cultivation.

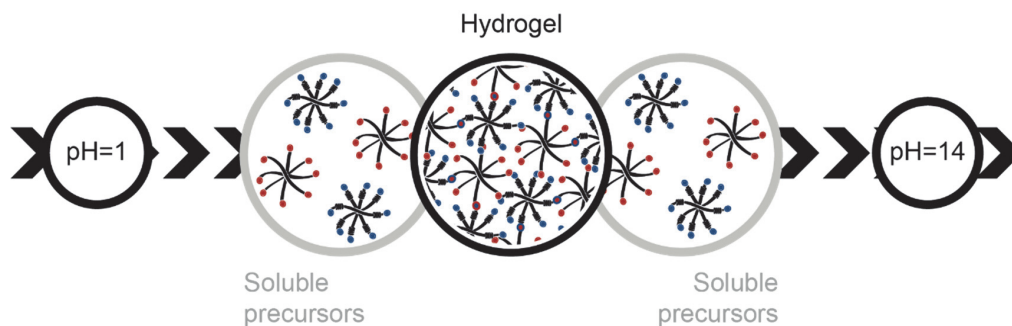


Figure 1.4. Schematic representation of enzymatic polymerization of PEG. The transglutaminase factor XIIIa is active only in a certain range of pH, outside of which it does not initiate polymerization.

1.2 _ MOTIVATION

Preterm birth is the leading cause of child morbidity under the age of 5. It causes approximately 1 million deaths yearly in the world and leaves about 14 million other babies with risks of lifetime disabilities related to the interruption of their development in the maternal womb.⁷⁷ The factors provoking delivery at early stages are partly known and include physiological conditions from the mother and/or the foetus, psychological status, medication, environment, genetics and possibly an overlap of those factors.⁷⁸ One physiological cause of preterm birth is the preterm premature rupture of the fetal membrane (PPROM), which results in the induction of the delivery. PPRM can happen either spontaneously or following fetoscopy (iPPROM). Preventive sealing and stabilization of the defect created when punching the fetal membrane during fetoscopy could significantly decrease the risks of fetoscopy by extending the pregnancy and thus drastically improve fetal health and survival.⁷⁹ It would on one side reduce complications encountered by premature babies and on the other side prevent the huge trauma experienced by parents after the loss of a child. Previous researchers have failed to offer an effective solution to the problem. Thus, this project will seek to combine expertise in various engineering domains in order to step towards the healing of the amniotic membrane and reduce the risks of iPPROM.

1.3 _ SPECIFIC GOALS

Our long-term vision consists in delivering, very precisely, at the site of puncture, a material able to trigger the healing and subsequent closure of the fetal membrane defect. Given the two distinct aspects of our approach, which is composed of a delivery system and a healing material, we subdivided the project into specific goals (Figure 1.5).

1. To develop a minimally invasive surgical device for the application of a membrane sealant on an ex vivo fetal membrane injury model

The first element of the research presented in Chapter 2 aims to develop a prototype of a surgical tool for the application of a bioadhesive at the site of the membrane defect. It is a very translational oriented goal, in which many practical aspects have to be considered. Application technique, glue retention strategy, materials and geometric parameters are all elements that have to be taken into consideration. The objective is to have a tool in hand that respects all the critical criteria for compatibility to actual fetoscopic instruments. The feasibility of the method will be evaluated by assessing the delivery efficacy of multiple glues and the adhesive strength on an ex vivo fetal membrane injury model developed for this study.

2. To rationally establish hydrogel platforms to study cell behaviour in contact with bioactive cues promoting tissue healing

This aim is based on the hypothesis that fetal membranes can undergo healing upon stimulation with appropriate growth factors and the presence of a supportive matrix.

First, we utilized the binding capabilities of engineered hydrogels to expose biological cues in a locally controlled manner in 3D. This work, presented in Chapter 3, quantifies mesenchymal stem cells (MSCs) response upon exposure to a stable platelet-derived growth factor (PDGF) gradient.

In Chapter 4, we harnessed the advantage of the possibility of tailoring locally PEG mechanical properties to establish a method enabling the rapid quantification of cell activity in response to growth factors in a large number of samples simultaneously. Based on the findings, we developed a tissue injury model and assessed the potential of those healing cues to recruit cells into the wound mimic.

3. To study the protein composition of the extra-cellular matrix (ECM) environment generated by the cells cultures in hydrogel

Our work is based on the hypothesis that fetal membrane defects can be healed upon stimulation by the right bioactive cues. To restore the integrity of the injured tissue, it is relevant to detain means to enable the study of growth factor effect on ECM protein production. Chapter 5 demonstrates a proteomics approach to identify the ECM proteins present in the PEG hydrogels hosting MSCs stimulated by healing inducing cues.

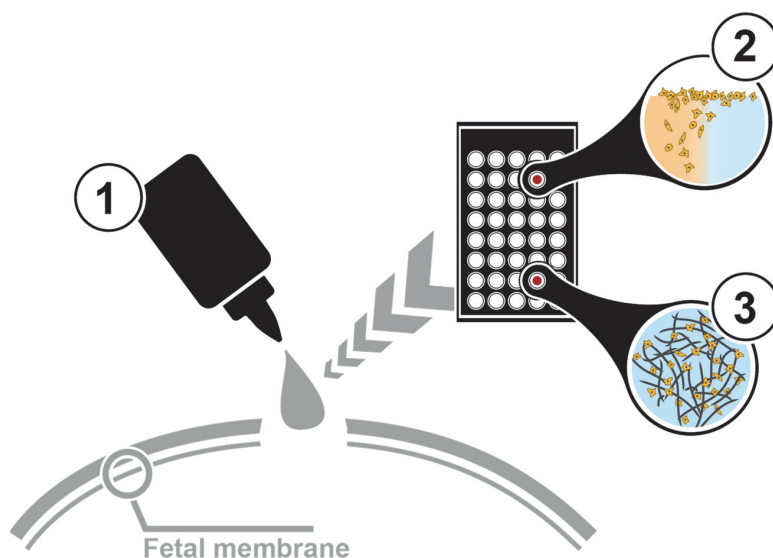


Figure 1.5. Scheme of the aims discussed in this work. Objective 1 focuses on the delivery method of materials and is presented in Chapter 2. Objective 2 focuses on the engineering of smart materials in vitro, which is presented in Chapters 3 and 4. Objective 3 presents in Chapter 5 a method to assess the ECM produced in synthetic hydrogels.

1.4 _ REFERENCES

1. Bryant-Greenwood, G.D. The extracellular matrix of the human fetal membranes: Structure and function. *Placenta* 19, 1-11 (1998).
2. Parry, S. & Strauss, J.F., 3rd. Premature rupture of the fetal membranes. *N Engl J Med* 338, 663-670 (1998).
3. Malak, T.M. & Bell, S.C. Structural Characteristics of Term Human Fetal Membranes - a Novel Zone of Extreme Morphological Alteration within the Rupture Site. *Brit J Obstet Gynaec* 101, 375-386 (1994).
4. Moore, R.M., Mansour, J.M., Redline, R.W., Mercer, B.M. & Moore, J.J. The physiology of fetal membrane rupture: insight gained from the determination of physical properties. *Placenta* 27, 1037-1051 (2006).
5. van der Ham, D.P., et al. Methods for the diagnosis of rupture of the fetal membranes in equivocal cases: a systematic review. *Eur J Obstet Gynecol Reprod Biol* 157, 123-127 (2011).
6. Peiro, J.L., et al. Therapeutic indications of fetoscopy: a 5-year institutional experience. *Journal of laparoendoscopic & advanced surgical techniques. Part A* 19, 229-236 (2009).
7. Shue, E.H., Miniati, D. & Lee, H. Advances in prenatal diagnosis and treatment of congenital diaphragmatic hernia. *Clinics in perinatology* 39, 289-300 (2012).
8. Gibson, A.T. Outcome following preterm birth. *Best Pract Res Clin Obstet Gynaecol* 21, 869-882 (2007).
9. Saigal, S. & Doyle, L.W. An overview of mortality and sequelae of preterm birth from infancy to adulthood. *Lancet* 371, 261-269 (2008).
10. Beck, V., Lewi, P., Gucciardo, L. & Devlieger, R. Preterm prelabor rupture of membranes and fetal survival after minimally invasive fetal surgery: a systematic review of the literature. *Fetal diagnosis and therapy* 31, 1-9 (2012).
11. Gratacos, E., et al. A histological study of fetoscopic membrane defects to document membrane healing. *Placenta* 27, 452-456 (2006).
12. Devlieger, R., et al. Matrix metalloproteinases -2 and -9 and their endogenous tissue inhibitors in fetal membrane repair following fetoscopy in a rabbit model. *Molecular human reproduction* 6, 479-485 (2000).
13. Devlieger, R., Millar, L.K., Bryant-Greenwood, G., Lewi, L. & Deprest, J.A. Fetal membrane healing after spontaneous and iatrogenic membrane rupture: a review of current evidence. *American journal of obstetrics and gynecology* 195, 1512-1520 (2006).
14. Zisch, A.H. & Zimmermann, R. Bioengineering of foetal membrane repair. *Swiss medical weekly* 138, 596-601 (2008).
15. Devlieger, R., et al. An organ-culture for in vitro evaluation of fetal membrane healing capacity. *Eur J Obstet Gynecol Reprod Biol* 92, 145-150 (2000).
16. Kiveliö, A., Ochsenein-Koelble, N., Zimmermann, R. & Ehrbar, M. Engineered cell instructive matrices for fetal membrane healing. *Acta biomaterialia* 15, 1-10 (2015).
17. Bilic, G., Ochsenein-Kolble, N., Hall, H., Huch, R. & Zimmermann, R. In vitro lesion repair by human amnion epithelial and mesenchymal cells. *American journal of obstetrics and gynecology* 190, 87-92 (2004).
18. Devlieger, R., Gratacos, E., Verbist, L., Pijnenborg, R. & Deprest, J. Gestational age-dependent repair kinetics of microsurgical defects in monolayers of human amniocytes. *Gynecol Obstet Invest* 69, 62-66 (2010).
19. Quintero, R.A., Carreno, C.A., Yelian, F. & Evans, M.I. Repair kinetics of amnion cells after microsurgical injury. *Fetal diagnosis and therapy* 11, 348-356 (1996).
20. Sopher, D. The response of rat fetal membranes to injury. *Annals of the Royal College of Surgeons of England* 51, 240-249 (1972).
21. Devlieger, R., et al. Matrix metalloproteinases-2 and -9 and their endogenous tissue inhibitors in tissue remodeling after sealing of the fetal membranes in a sheep model of fetoscopic surgery. *J Soc Gynecol Investig* 9, 137-145 (2002).
22. Ochsenein-Kolble, N., et al. Enhancing sealing of fetal membrane defects using tissue engineered native amniotic scaffolds in the rabbit model. *American journal of obstetrics and gynecology* 196, 263 e261-267 (2007).
23. Mallik, A.S., et al. Fetoscopic closure of punctured fetal membranes with acellular human amnion plugs in a rabbit model. *Obstetrics and gynecology* 110, 1121-1129 (2007).
24. Devlieger, R., et al. Increased polymorphonuclear infiltration and iatrogenic amniotic band after closure of fetoscopic access sites with a bioactive membrane in the rabbit at midgestation. *American journal of obstetrics and gynecology* 188, 844-848 (2003).
25. Harmanli, O.H., Wapner, R.J. & Lontz, J.F. Efficacy of fibrin glue for in vitro sealing of human chorioamniotic membranes. *The Journal of reproductive medicine* 43, 986-990 (1998).

26. Louis-Sylvestre, C., Rand, J.H., Gordon, R.E., Salafia, C.M. & Berkowitz, R.L. In vitro studies of the interactions between platelets and amniotic membranes: a potential treatment for preterm premature rupture of the membranes. *American journal of obstetrics and gynecology* 178, 287-293 (1998).
27. Devlieger, R., Gratacos, E., Ardon, H., Vanstraelen, S. & Deprest, J. Factors influencing the flow rate through a surgical defect in human fetal membranes. *Prenatal diagnosis* 22, 201-205 (2002).
28. Petratos, P.B., Baergen, R.N., Bleustein, C.B., Felsen, D. & Poppas, D.P. Ex vivo evaluation of human fetal membrane closure. *Lasers in surgery and medicine* 30, 48-53 (2002).
29. Papadopoulos, N.A., et al. Fetal membrane closure techniques after hysteroamniotomy in the midgestational rabbit model. *American journal of obstetrics and gynecology* 178, 938-942 (1998).
30. Young, B.K., et al. Minimally invasive endoscopy in the treatment of preterm premature rupture of membranes by application of fibrin sealant. *Journal of perinatal medicine* 28, 326-330 (2000).
31. Young, B.K., et al. The closure of iatrogenic membrane defects after amniocentesis and endoscopic intrauterine procedures. *Fetal diagnosis and therapy* 19, 296-300 (2004).
32. Engels, A.C., et al. Collagen plug sealing of iatrogenic fetal membrane defects after fetoscopic surgery for congenital diaphragmatic hernia. *Ultrasound in obstetrics & gynecology : the official journal of the International Society of Ultrasound in Obstetrics and Gynecology* 43, 54-59 (2014).
33. Gratacos, E., et al. Successful sealing of fetoscopic access sites with collagen plugs in the rabbit model. *American journal of obstetrics and gynecology* 182, 142-146 (2000).
34. Lewi, L., et al. Successful patching of iatrogenic rupture of the fetal membranes. *Placenta* 25, 352-356 (2004).
35. Quintero, R.A., et al. Treatment of iatrogenic previable premature rupture of membranes with intra-amniotic injection of platelets and cryoprecipitate (amniopatch): preliminary experience. *American journal of obstetrics and gynecology* 181, 744-749 (1999).
36. Sener, T., Ozalp, S., Hassa, H., Yalcin, O.T. & Polay, S. Maternal blood clot patch therapy: a model for postamniocentesis amniorrhea. *American journal of obstetrics and gynecology* 177, 1535-1536 (1997).
37. Mahdavi, A., et al. A biodegradable and biocompatible gecko-inspired tissue adhesive. *Proc Natl Acad Sci U S A* 105, 2307-2312 (2008).
38. Lang, N., et al. A blood-resistant surgical glue for minimally invasive repair of vessels and heart defects. *Sci Transl Med* 6, 218ra216 (2014).
39. Brubaker, C.E., Kissler, H., Wang, L.J., Kaufman, D.B. & Messersmith, P.B. Biological performance of mussel-inspired adhesive in extrahepatic islet transplantation. *Biomaterials* 31, 420-427 (2010).
40. Lee, H., Scherer, N.F. & Messersmith, P.B. Single-molecule mechanics of mussel adhesion. *Proc Natl Acad Sci U S A* 103, 12999-13003 (2006).
41. Lee, H., Lee, B.P. & Messersmith, P.B. A reversible wet/dry adhesive inspired by mussels and geckos. *Nature* 448, 338-341 (2007).
42. Lee, B.P., Dalsin, J.L. & Messersmith, P.B. Synthesis and gelation of DOPA-modified poly(ethylene glycol) hydrogels. *Biomacromolecules* 3, 1038-1047 (2002).
43. Burke, S.A., Ritter-Jones, M., Lee, B.P. & Messersmith, P.B. Thermal gelation and tissue adhesion of biomimetic hydrogels. *Biomedical materials* 2, 203-210 (2007).
44. Bilic, G., et al. Injectable candidate sealants for fetal membrane repair: bonding and toxicity in vitro. *American journal of obstetrics and gynecology* 202, 85 e81-89 (2010).
45. Haller, C.M., et al. Mussel-mimetic tissue adhesive for fetal membrane repair: a standardized ex vivo evaluation using elastomeric membranes. *Prenatal diagnosis* 31, 654-660 (2011).
46. Kiveli, A., et al. Mussel mimetic tissue adhesive for fetal membrane repair: initial in vivo investigation in rabbits. *Eur J Obstet Gynecol Reprod Biol* 171, 240-245 (2013).
47. Haller, C.M., et al. Mussel-mimetic tissue adhesive for fetal membrane repair: an ex vivo evaluation. *Acta biomaterialia* 8, 4365-4370 (2012).
48. Knight, E. & Przyborski, S. Advances in 3D cell culture technologies enabling tissue-like structures to be created in vitro. *J Anat* 227, 746-756 (2015).
49. Pampaloni, F., Reynaud, E.G. & Stelzer, E.H.K. The third dimension bridges the gap between cell culture and live tissue. *Nat Rev Mol Cell Bio* 8, 839-845 (2007).
50. Lutolf, M.P. & Hubbell, J.A. Synthetic biomaterials as instructive extracellular microenvironments for morphogenesis in tissue engineering. *Nat Biotech* 23, 47-55 (2005).
51. Cushing, M.C. & Anseth, K.S. Materials science. Hydrogel cell cultures. *Science* 316, 1133-1134 (2007).
52. Zhu, J. Bioactive modification of poly(ethylene glycol) hydrogels for tissue engineering. *Biomaterials* 31, 4639-4656 (2010).
53. Tibbitt, M.W. & Anseth, K.S. Dynamic microenvironments: the fourth dimension. *Sci Transl Med* 4, 160ps124 (2012).

54. Sarrazin, S., Lamanna, W.C. & Esko, J.D. Heparan sulfate proteoglycans. *Cold Spring Harb Perspect Biol* 3(2011).
55. Ramirez, F. & Rifkin, D.B. Extracellular microfibrils: contextual platforms for TGF β and BMP signaling. *Curr Opin Cell Biol* 21, 616-622 (2009).
56. Guilak, F., et al. Control of Stem Cell Fate by Physical Interactions with the Extracellular Matrix. *Cell Stem Cell* 5, 17-26 (2009).
57. Kubow, K.E., et al. Crosslinking of cell-derived 3D scaffolds up-regulates the stretching and unfolding of new extracellular matrix assembled by reseeded cells. *Integr Biol (Camb)* 1, 635-648 (2009).
58. Lin, F., et al. Fibronectin growth factor-binding domains are required for fibroblast survival. *J Invest Dermatol* 131, 84-98 (2011).
59. Singh, P. & Schwarzbauer, J.E. Fibronectin and stem cell differentiation - lessons from chondrogenesis. *J Cell Sci* 125, 3703-3712 (2012).
60. Wijelath, E.S., et al. Heparin-II domain of fibronectin is a vascular endothelial growth factor-binding domain: enhancement of VEGF biological activity by a singular growth factor/matrix protein synergism. *Circ Res* 99, 853-860 (2006).
61. Yamada, Y., Hozumi, K. & Nomizu, M. Construction and Activity of a Synthetic Basement Membrane with Active Laminin Peptides and Polysaccharides. *Chem-Eur J* 17, 10500-10508 (2011).
62. Imitola, J.A. & Massague, J. Type beta transforming growth factor controls the adipogenic differentiation of 3T3 fibroblasts. *Proc Natl Acad Sci U S A* 82, 8530-8534 (1985).
63. Arnold, U., Lindenhayn, K. & Perka, C. In vitro-cultivation of human periosteum derived cells in bioresorbable polymer-TCP-composites. *Biomaterials* 23, 2303-2310 (2002).
64. Imitola, J.A. & Massague, J. Transforming Growth-Factor-Beta Stimulates the Expression of Fibronectin and Collagen and Their Incorporation into the Extracellular-Matrix. *J Biol Chem* 261, 4337-4345 (1986).
65. Ehrbar, M., et al. Enzymatic formation of modular cell-instructive fibrin analogs for tissue engineering. *Biomaterials* 28, 3856-3866 (2007).
66. Ehrbar, M., et al. Biomolecular hydrogels formed and degraded via site-specific enzymatic reactions. *Biomacromolecules* 8, 3000-3007 (2007).
67. Ehrbar, M., et al. Elucidating the role of matrix stiffness in 3D cell migration and remodeling. *Biophysical Journal* 100, 284-293 (2011).
68. Lutolf, M.P., Gilbert, P.M. & Blau, H.M. Designing materials to direct stem-cell fate. *Nature* 462, 433-441 (2009).
69. Discher, D.E., Mooney, D.J. & Zandstra, P.W. Growth factors, matrices, and forces combine and control stem cells. *Science* 324, 1673-1677 (2009).
70. Prewitz, M., Seib, F.P., Pompe, T. & Werner, C. Polymeric biomaterials for stem cell bioengineering. *Macromolecular rapid communications* 33, 1420-1431 (2012).
71. Metzger, S., et al. Modular poly(ethylene glycol) matrices for the controlled 3D-localized osteogenic differentiation of mesenchymal stem cells. *Advanced healthcare materials* 4, 550-558 (2015).
72. Lienemann, P.S., et al. A versatile approach to engineering biomolecule-presenting cellular microenvironments. *Advanced healthcare materials* 2, 292-296 (2013).
73. Ljungberg, U.K., et al. The interaction between different domains of staphylococcal protein A and human polyclonal IgG, IgA, IgM and F(ab')₂: separation of affinity from specificity. *Mol Immunol* 30, 1279-1285 (1993).
74. Lienemann, P.S., Lutolf, M.P. & Ehrbar, M. Biomimetic hydrogels for controlled biomolecule delivery to augment bone regeneration. *Adv Drug Deliv Rev* 64, 1078-1089 (2012).
75. Milleret, V., Simona, B.R., Lienemann, P.S., Vörös, J. & Ehrbar, M. Electrochemical Control of the Enzymatic Polymerization of PEG Hydrogels: Formation of Spatially Controlled Biological Microenvironments. *Advanced healthcare materials*, n/a-n/a (2013).
76. Simona, B.R., et al. Density gradients at hydrogel interfaces for enhanced cell penetration. *Biomater Sci-Uk* 3, 586-591 (2015).
77. Martin, J.A., Hamilton, B.E., Osterman, M.J., Driscoll, A.K. & Mathews, T.J. Births: Final Data for 2015. *Natl Vital Stat Rep* 66, 1 (2017).
78. (US), I.O.M. in *Preterm Birth: Causes, Consequences, and Prevention* (eds. Behrman, R.E. & Butler, A.S.) (Washington (DC), 2007).
79. Akkermans, J., et al. A worldwide survey of laser surgery for twin-twin transfusion syndrome. *Ultrasound in obstetrics & gynecology : the official journal of the International Society of Ultrasound in Obstetrics and Gynecology* 45, 168-174 (2015).

CHAPTER 2 _ MINIMALLY INVASIVE SURGICAL DEVICE FOR PRECISE APPLICATION OF BIOADHESIVES TO PREVENT IPPROM

This chapter is the preprint version of the article submitted on October 27th 2017 to Fetal Diagnosis and Therapy.

The resulting work is the content of a patent submitted to the European Patent Office on February 6th 2017, serial number EP17154743

The results of this work was the base for the funding of a CTI grant (no. 27063.1 PFLS-LS)

AUTHORS

Yannick R. Devaud, Silvia Züger, Roland Zimmermann, Martin Ehrbar, Nicole Ochsenbein-Kölble

DOCTORAL CANDIDATE'S CONTRIBUTION

The totality of this work was accomplished by the doctoral candidate. The co-authors advised in the experimental designs and Silvia Züger helped in the data acquisition. The doctoral candidate also exclusively performed data analysis, figure drawing and writing, with feedbacks from the last authors.

2.1 _ ABSTRACT

The benefits of endoscopic fetal surgery are mitigated by the high risk of iatrogenic premature preterm rupture of fetal membrane (iPPROM). While previous studies have reported good sealing candidates to prevent membrane rupture, the delivery of these materials to the location of membrane puncture has not been addressed. We describe an approach to apply sealing materials onto the inside of the amnion through the same catheter used for the fetoscopy. We developed a device composed of an umbrella-shaped receptor and an applicator. The receptor is pushed through the catheter by the applicator and expands automatically when pushed into the amniotic cavity. The receptor is then positioned and glued against the amnion at the defect site. We tested the adhesion strength of multiple glues and tested the feasibility and reproducibility of this fetal membrane sealing approach on an ex vivo model. The receptor opened in all tests and its positioning showed no particular difficulties (n = 18). When applied via the minimal invasive procedure, receptors were glued efficiently onto the membrane and all of them completely covered the defect (n = 5). The mean time needed for the whole procedure was 3 minutes. This study attests of the feasibility of our method and presents a potential future solution for the precise local application of bioadhesives for the prevention of membrane rupture after fetal surgeries.

2.2 _ INTRODUCTION

With advances in fetal diagnosis and therapies, in specialized centers fetoscopy has become a real therapeutical option to treat potentially life-threatening diseases during pregnancy. However, this invasive intervention into the amniotic cavity is associated with a significant risk of preterm birth resulting in fetal morbidity and mortality.¹ Preterm birth is mainly due to the injury of the fetal membranes, which do not heal spontaneously after surgical injury.²⁻⁵ The risk of an iatrogenic preterm prelabor rupture of fetal membranes (iPPROM), which happens in up to 30% of all fetoscopies,¹ affect a significant number of pregnant women worldwide. Therefore, it is generally accepted that preventive sealing and stabilization of fetal membranes could significantly extend pregnancy and thus drastically improve fetal health and survival.

In opposition to reports indicating potential fetal membrane healing signals *in vitro*,⁶⁻⁸ *ex vivo* and *in vivo* investigations show a very limited success towards membrane healing. One approach showed by some studies has focused on the deposition of scaffolds to promote cell invasion and trigger wound healing. Decellularized amniotic membranes stimulated reepithelization on *in vivo* rabbit mid-gestational models when implanted alone⁹ or in combination with fibrin.¹⁰ The same results were observed when porcine-derived bioactive membranes were used as carriers of soluble transforming growth factor beta (TGF β) or fibroblast growth factor 1 (FGF-1).¹¹ Another approach to seal fetal membranes consisted in inserting nature-derived materials. This was successfully done on animal models by applying ECM-mimicking materials such as MatrigelTM¹² or by placing sponges containing collagen¹² or gelatin.¹³ However, collagen plug insertion was also tested on humans but did not show any evidence of decreasing the risks of membrane rupture.¹⁴

Alternatively, biocompatible materials derived from the natural blood clotting mechanism were used to reproduce the coagulation process in wound healing and seal the defects. Previous *ex vivo* work reported fibrin glue¹⁵ and platelet concentrate¹⁶ as potential effective amniotic membrane sealants. Although animal models could not confirm the efficacy of fibrin glue,¹⁷ *in vivo* studies on humans reported a relative success for amniotic fluid leakage prevention when platelets were added in combination with cryoprecipitate^{18,19} or covered with industrially-available fibrin glue.^{20,21} Positive performances of platelets injection were accompanied with extensive platelet production and provoked fetal death in some reported cases.²²

More recently, the development of mussel-inspired adhesives working in wet environments brought new hopes for the efficient closure of the fetal membrane.²³⁻²⁵ Indeed, this glue showed good sealing potential *in vitro*,^{24,26} *ex vivo*²⁵ and on rabbit models *in vivo*.²³

Despite a multitude of candidate glues for membrane sealing, there is an obvious lack in a reliable method to deposit these sealants, which are applied in a liquid form, on the inside of the amniotic cavity at the exact site of injury. This study aims to establish a method to seal fetal membrane defects by accessing the wound through the catheter used during fetoscopy. To reach this aim, the focus was set on developing a minimally invasive device able to deliver a gluing material in a very controlled and localized manner at the site of fetal membrane puncture.

2.3 _ MATERIALS AND METHODS

Our approach to prevent iPPROM relied on the combination of three elements: i) a receptor for the gathering of adhesive materials, ii) an applicator to introduce the receptor and iii) an injection system to deliver the adhesive materials inside the receptor. All these elements were assembled in one single device enabling to carry out the sealing procedure in five short steps. The idea was to insert the receptor through the fetoscopy catheter, deploy it inside the amniotic cavity, bring it back to the inside wall of the fetal membrane and glue the umbrella onto the fetal membrane. The catheter is removed while the umbrella is left glued to the membrane until it comes out with the baby's birth. This method enables the sealing of the defect without detachment of the fetal membrane from the decidua and avoids the puncture of an additional hole for the application of the adhesive.

2.3.1 _ DEVICE COMPONENTS FOR THE PREVENTIVE SEALING OF FETAL MEMBRANES

UMBRELLA-SHAPED RECEPTOR FOR THE GATHERING OF SEALING MATERIALS

The receptor is responsible to gather the sealing materials at the site of puncture and is glued against the fetal membrane until delivery. It was composed of two elements: a nitinol backbone and a membrane covering that backbone in order to gather the adhesives. Nitinol is a very elastic FDA approved metallic alloy that possesses unique shape memory properties.²⁷ The nitinol stripes thickness was set at 200 μ m and the umbrella-shaped height at 3mm. The receptor was composed of 8 identical oval struts, each connected to the neighboring one, forming a circular shape. This circular design directed the tight folding of the umbrella into a shape smaller than the 10 French catheter (Figure 2.2A). They were produced by laser cutting followed by temperature-based shape setting.

As for the membrane covering the nitinol backbone, Degrapol®, a polyesterurethane polymer, was the material of choice given its high elasticity.²⁸ Besides its ideal mechanical characteristics, it has previously shown good biocompatibility and capacity to integrate into rabbit fetal membranes and promote reepithelialization.⁹ To make those membranes, we first produced 150 μ m thick Degrapol® sheets. To do so, 600mg of lyophilized Degrapol® was dissolved in 3.52g of Chloroform and 0.88g of Hexafluoroisopropanol to make 5g of 12% Degrapol® mix. The solution was left at room temperature overnight and 2 ml of this solution was electro-spun at a rate of 1ml per hour on 12 glass slides rotating on the collector. The distance between the syringe needle and the collector was 10cm. The resulting Degrapol® sheets were removed from the glass slides by immersing in 30% ethanol. The nitinol backbone was inserted between two Degrapol® sheets that were pressed together to fuse them, covering the nitinol backbone.

APPLICATOR AND INJECTOR

A stainless-steel tube with an outer diameter of 2.9mm and inner diameter of 2.7mm was designed and manufactured (Figure 2.2C, Applicator). This tube slid freely in the 10 French catheter and was tight enough to push the receptor (Figure 2.2C, Receptor) through the catheter. A double chamber tube connected to its glue injector (Duplocath 180, Baxter AG, Volketswil, Switzerland) from the Tisseel® glue pack was inserted into the hollow tube from the proximal to the distal end to ensure that the two glue substrates only merge at the distal end of the tube into the receptor. The proximal end (Figure 2.2C, Glue Injector) permitted the separate injection of the two glue precursors.

The receptor must remain attached to the applicator in order to prevent the loss of it in the amniotic cavity upon deployment and to allow the pulling against the fetal membrane defect. To do so, we attached a thread to the umbrella-shaped receptor and connected it to a locking system at the distal part of the applicator. Upon unlocking of this system by the user, the thread is set free and the receptor detached from the applicator.

BIOADHESIVES

To test the fetal membrane sealing procedure Histoacryl® (B.Braun Surgical AG, Melsungen, Switzerland), fibrin glue (Tisseel®, Baxter AG, Volketswil, Switzerland), and mussel glue²⁹⁻³³ were employed. Histoacryl® is a cyanoacrylate-based, Federal Drug Administration (FDA) approved one component glue that polymerizes upon contact with hydroxyl ions present in wet environments. Due to its strong gluing ability, it is used for application such as net fixation for inguinal hernia.³⁴ Histoacryl® was directly transferred from its ampoule to a syringe tube before application. Fibrin is another commonly used tissue sealant that showed potentially good binding ability to fetal membranes.²⁶ Fibrin glue is composed of two human plasma derived precursors, sealer protein (mostly fibrinogen) and thrombin, which are injected simultaneously inside the two-chamber injector tube and polymerize within 5 seconds when gathered in the receptor. The mechanism of action replicates the wound healing process where thrombin activates the coagulation cascade. Mussel glue is a sealant that readily polymerizes upon mixing of the polymer precursor with its activator and was shown to have very good properties for the sealing fetal membranes under wet conditions.^{25,26} As previously described, the polymer substrate is dissolved in 2x PBS and mixed in a 1:1 volume ratio to 12mg/ml sodium periodate for a final mussel glue concentration of 150mg/ml.

HUMAN FETAL MEMBRANES

Human fetal membranes were collected from patients with written consent following the decision from the Ethical Committee of the District of Zürich (study Stv22/2006). Fetal membranes were harvested after caesarian section at term (between 37 and 39 weeks) and frozen at -80°C until usage. All of them were negatively selected for HIV, hepatitis B, diabetes mellitus, chlamydia, and streptococcus B.

2.3.2 _ MECHANICAL TESTING

MECHANICAL STABILITY OF THE RECEPTOR

The mechanical stability of the receptor was assessed by measuring the force needed to completely flatten the receptor. A thread was attached to the center culm of the receptor with its hollow part facing down. The thread was then pulled until the receptor was flattened and the force needed to do so was measured with a dynamometer (Pesola AG, Schindellegi, Switzerland, ref.DO29/FH27). Receptors with and without Degrapol® membrane were pulled on solid (Petri dish) and soft surfaces (1.5cm thick bovine muscle) (n=5).

ADHESION STRENGTH PROVIDED BY BIOADHESIVES TO GLUE THE RECEPTOR TO INTACT FETAL MEMBRANES

Intact, dry fetal membranes were flattened on a Petri dish with the amnion facing up. The receptors were placed on top of the membrane followed by the injection of 500µl of adhesives inside the receptors through a syringe and allowed to polymerize for 5 min. The adhesion strength between fetal membrane and receptors provided by the glues was measured with a dynamometer by pulling the receptors perpendicularly to the membrane surface (n=5 for each adhesive).

2.3.3 _ APPLICATION AND GLUING OF RECEPTOR ON PUNCTURED FETAL MEMBRANES

DRY EXPERIMENTAL CONDITIONS

A fetal membrane was mounted onto an empty plastic cup with the amnion facing downward to the interior of the cup. A very high bonding elastomeric membrane (3M AG, Rüschlikon, Switzerland) was punched with a 6mm diameter biopsy punch and deposited onto the fetal membrane on the plastic cup model. To quantify the mechanical stability, we measured the force needed to pull up the centre of the mounted fetal membrane by 1.5cm with a dynamometer.

COMPLETE EX VIVO FETAL MEMBRANE DEFECT MODEL

To simulate the intervention, we created a physiologically relevant ex vivo model. Porcine skin containing a small muscle layer with a total thickness of 0.5cm was chosen to mimic the upper abdominal wall. A bovine muscle of 1cm thickness and a human fetal membrane were added under the abdominal wall mimic to reproduce the uterus layer. Those two layers, together with the human fetal membranes, were put together, stretched, placed onto an 8cm diameter aluminum cylinder and tightly clamped by screwing a ring on top (Figure 2.1). A 5mm cut was made with a scalpel on the skin mimic to facilitate the access to underlying tissues. To quantify the mechanical stability, we measured the force needed to pull up the center of the model by

1.5cm with a dynamometer. The construct was watertight and had a transparent bottom for visualization purposes. Two inlets in the cylinder enabled the cylinder to be filled with solutions reproducing the amniotic fluid. Another inlet permitted the insertion of a video-intubation system (Acutronice Medical Systems AG, Switzerland) to enable visual control over the placement of the receptor. The time needed for each step of the procedure was measured.

DEFECT SEALING

A 10 French catheter (Check-Flo Performer® Introducer, Cook Medical, Bloomington, IN, USA) was mounted on the obturator (Anklin AG, Switzerland) and inserted through the tissue mimic in a 45° angle. The obturator was removed and the catheter left in the defect. The receptor was tightly folded and inserted in the catheter before pushing it in the plastic cup or inside the cavity filled with saline solution. The receptor was pulled against the membrane and 500µl of mussel glue, fibrin glue or Histoacryl® (100µl corresponding to the dead volume of the double-chamber injection channel plus 400µl adhesive) was perfused through the injector into the receptor using syringes connected to the injection inlets. Polymerization was allowed for 1 minute while the receptor was held against the fetal membrane in its umbrella-shaped conformation. After the intervention, membranes were unmounted from the plastic cup or the aluminum and turned upside down. The umbrella was pulled perpendicularly to the membrane surface and the force needed to remove the receptor from the membrane was measured with a dynamometer.

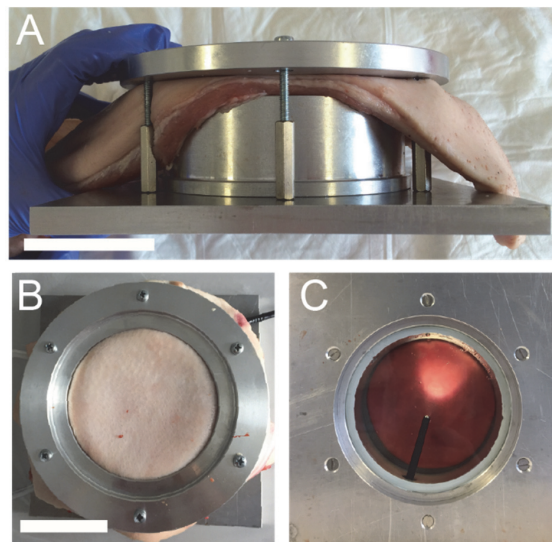


Figure 2.1. Ex vivo fetal membrane model. A) side view B) top view and C) bottom view of the tissue clamped in the aluminum cylinder. (Scale bars: 5cm)

2.4 _ RESULTS

2.4.1 _ DESIGN OF DEVICE FOR THE PREVENTIVE SEALING OF FETAL MEMBRANES

To prevent loss of sealing material in the amniotic cavity, which are initially liquid and become solid upon curing, we developed an umbrella-shaped glue receptor (Figure 2.2A, B and C Receptor) that ensures local gathering of gluing materials and a shielded environment for their adhesion. In addition, we designed and fabricated an applicator (Figure 2.2C, Applicator) facilitating the application of the umbrella and the injection of the adhesives (Figure 2.2C, Glue injector).

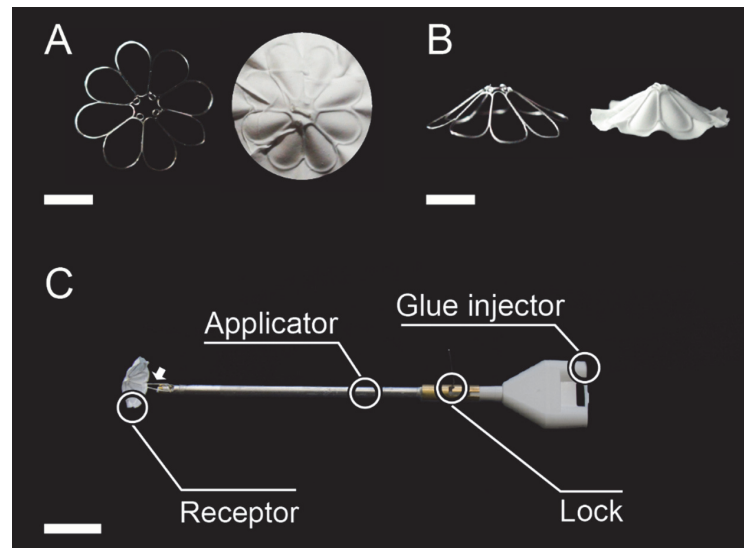


Figure 2.2. Photographs of the device's components. A) top and B) side view of the umbrella-shaped receptor without (left) and with (right) Degrapol® membrane coverage. (Scale bars: 5mm) C) Applicator device prototype in its open conformation. The Applicator is responsible to push the Umbrella inside the 10 French introducer (not shown). The Glue injector is the entry site for the glue, which is delivered to the Umbrella with the assistance of a double chambered tube placed inside the Applicator (Scale bar: 15mm). The release mechanism of the Umbrella is controlled by one small metallic wire going through the Applicator (Lock). When in the Locked position, the wire traps the suture wire connected to the umbrella. When in the Unlocked position, the suture wire is no longer trapped and the umbrella can be disconnected from the Applicator. (Scale bar: 2cm)

As the central part of the strategy explained here, the receptor was designed such that it fits through the catheter, deploys into a larger, predefined shape, gathers the adhesive at the site of defect and remains glued to the amnion until delivery. To this end, we adopted a circular structure made of nitinol (Figure 2.2A and B), whose form enables the tightly folding into the catheter and spontaneous deployment into the original shape upon exit of the catheter. This metallic backbone was integrated into an elastic Degrapol® membrane (Figure 2.2A and B, white membrane) to confine the adhesives inside the receptor and limit the exchange with the

amniotic fluid. Additionally, to enable the surgeon to feel a resistance before its flattening or even everting, the receptor was given a curvature of 3mm. The applicator, by which the receptor is pushed through the catheter into the amniotic cavity, is made of a tube with an outer diameter (3mm) and a length exceeding the catheter's size by 10mm. The applicator was shown to slide through the 10 French catheter with minimal force ($0.2\text{N} \pm 0.02\text{N}$) and access the inside of the amniotic cavity.

We compared the resistance of receptors with or without Degrapol® to evaluate the contribution of the membrane to the receptor's stability. In addition, we performed this assay on a plastic Petri dish or on a 1.5cm thick muscle layer, which aims to determine the impact of the support on which the receptor is measured. While the backbone on the stiff and the soft surface deformed at almost identical forces of $0.21 \pm 0.02 \text{ N}$ and $0.2 \pm 0.02 \text{ N}$, respectively, the resistance to deformation of the full umbrella was significantly increased on both soft and stiff substrates (Figure 2.3). The force for flattening was significantly higher on the solid substrate ($0.33 \pm 0.02\text{N}$) as compared to the soft substrate ($0.25 \pm 0.02\text{N}$). This indicates that the receptor needs to be tested with the membrane on a soft tissue to ensure the relevance of the assay for its in vivo application.

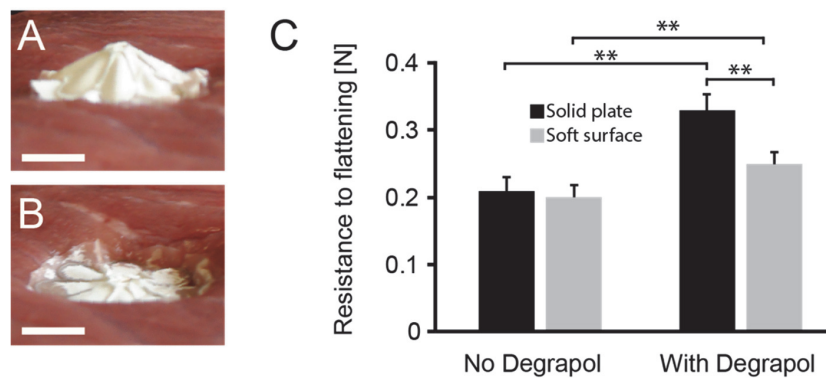


Figure 2.3. Shape stability of the receptor. A) Umbrella-shaped receptor with with Degrapol® membrane on porcine muscle (soft surface) before pulling test and B) during pulling test. (scale bar: 5mm) C) Forces needed to flatten the receptor. (n=5; **: $p < 0.02$)

2.4.2 _ ADHESION STRENGTH OF THE RECEPTOR TO INTACT FETAL MEMBRANES

In the first step, we evaluated the potential of three adhesive candidates to glue the Degrapol® coated receptors to dry, intact fetal membranes. The measured adhesion forces of the receptors to the fetal membranes showed that mussel glue reached similar gluing properties as Histoacryl® ($0.83 \pm 0.2\text{N}$ and $1.1 \pm 0.17\text{N}$ respectively, $n=5$), while Fibrin with $0.2 \pm 0.14\text{N}$ ($n=5$) exhibited very weak binding (Figure 2.4, black bars). As a drawback, Histoacryl® had the effect of drying out both the fetal and Degrapol® membranes.

2.4.3 _ APPLICATION AND GLUING OF THE RECEPTOR ON FETAL MEMBRANE DEFECTS UNDER DRY EXPERIMENTAL CONDITIONS

Next, we assessed the reliability of our method in dry experimental conditions in the plastic cup model. We used our device to insert the umbrella and deliver the adhesives to glue the receptor on the fetal membrane defect. In all the assays, the receptors adhered to the fetal membrane following adhesion and release. However, all the glues showed different strengths of adhesion. Histoacryl® resisted up to $0.96 \pm 0.38\text{N}$ (n=3) of pulling force until detachment, compared to $0.35 \pm 0.12\text{N}$ (n=5) and $0.17 \pm 0.18\text{N}$ (n=5) for mussel glue and fibrin respectively (Figure 2.4, grey bars). In all the cases (n=13), the umbrellas deployed to their initial shape, were placed tightly on the fetal membrane and no leakage of the glue was observed upon injection. In addition, the measure of mechanical stability of the model showed a force of 0.1N for a displacement of 1.5cm.

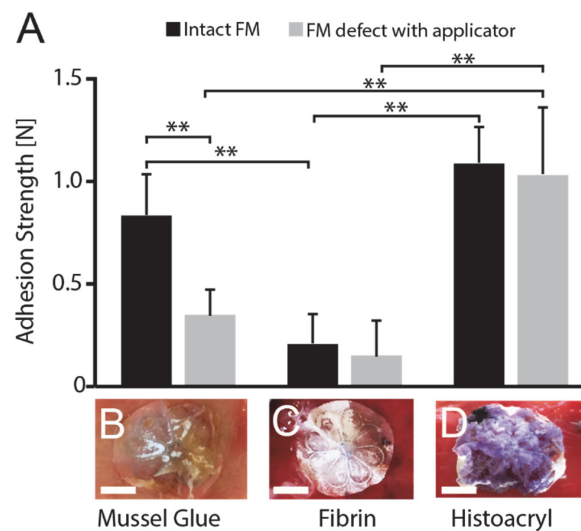


Figure 2.4. Gluing of umbrellas to fetal membranes. A) The histogram shows adhesion strengths of umbrellas glued to fetal membranes with B) Mussel glue (black n=5; grey n=5), C) Fibrin glue (black n=5; grey n=5) or D) Histoacryl® (black n=5; grey n=3). Black bars represent the cases where the receptors were directly glued on intact fetal membranes. Grey bars show the cases when the receptors were applied through the defect and glued on the fetal membrane under dry conditions. (**:p<0.02). The photos show representative images of umbrellas when glued to the fetal membrane defect model. (scale bars = 5mm)

2.4.4 _ FETAL MEMBRANE DEFECT SEALING PROCEDURE ON COMPLETE EX VIVO MODEL

DEFECT SEALING EX VIVO

To conclude the proof of feasibility of the approach, we simulated the defect sealing on a more clinically relevant model and observed the procedure from the inside of the cavity with an endoscopic camera (Figure 2.5). While the addition of saline solution simulated the amniotic fluid, the multiple layers improved anatomical resemblance and improved mechanical stability. Indeed, the displacement test assessing the mechanical stability showed a force of 1N required for the displacement of 1.5cm. Mussel glue was chosen due to its suited applicability in wet environments and its non-cytotoxicity. In all trials ($n = 5$), the receptor opened into its original shape and was properly placed onto the defect. The glue was well confined in all the umbrellas despite some observations of minimal leakage. These were mainly due to the slight permeability of the Degrapol® and to the excessive volume of adhesive injected. However, this never impaired the adhesion of the receptor to the fetal membranes. Indeed, all the receptors held onto the fetal membranes upon release and removal of the applicator. The adhesion strength gluing the receptor to the fetal membrane was in average $0.13 \pm 0.04\text{N}$.

TIME OF PROCEDURE

Time intervals needed for each part of the intervention are summarized in Table 2.1. Device application, which included tightly folding the receptor and placing it onto the fetal membrane, was the longest step of the procedure with an average of 1 minute and 28 ± 43 seconds. Glue injection time had a constant 1 minute polymerization period in all the tests, to which 27 ± 7 seconds was needed to place the syringes on the glue injection inlets and apply the glue. Finally, 13 ± 9 seconds were added to activate the locking system and release the receptor. In summary, the total average time for the whole procedure was 3 minutes and 08 seconds, which is insignificant compared to, for example, the 45 minutes needed for laser surgery in the case of TTTS.

	Time [min:sec]	Success rate
Device application	$1:28 \pm 0:43$	5/5 (100%)
Glue injection	$1:27 \pm 0:07$	5/5 (100%)
Umbrella release	$0:13 \pm 0:09$	5/5 (100%)

Table 2.1. Statistics of the fetal membrane sealing procedure on an ex vivo model.

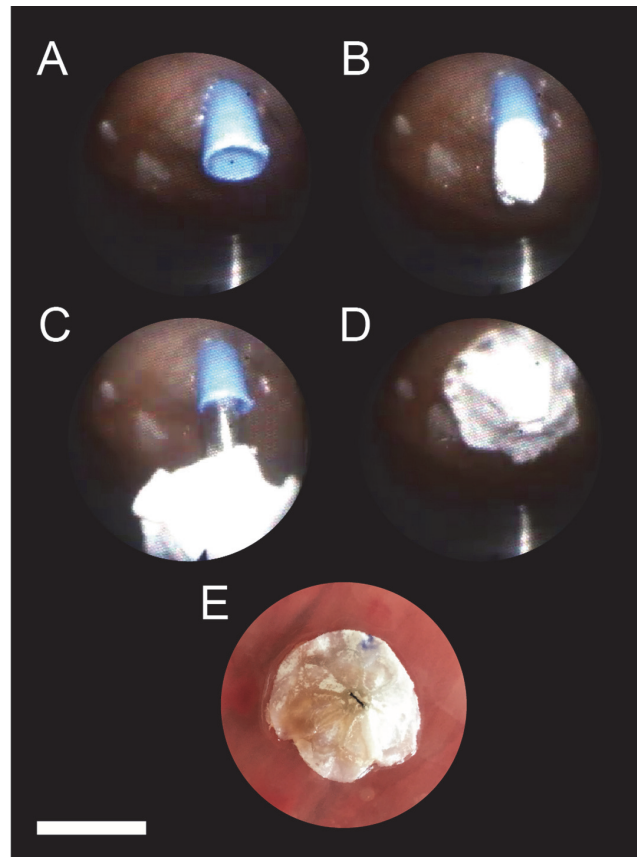


Figure 2.5. Ex vivo fetal membrane defect sealing procedure. A) to E) illustrate the procedure from inside of the cylinder, reproducing the view from the amniotic cavity. A) accession of the catheter (blue tube) right after punching through the construct to create the defect, B) the white element shows the umbrella in its crimped conformation being introduced, C) deployed and D) pulled against the fetal membrane. E) Mussel Glue was absorbed by the Degrapol®, changing its color to red. The figure shows the umbrella glued onto the fetal membrane after dismantling. (Scale bar: 5mm).

2.5 _ DISCUSSION

In this study, we developed a novel method to preventively seal fetal membrane defects by a minimal invasive procedure and succeeded in proving its feasibility. We demonstrated it by developing a model reproducing close to real anatomic conditions and by delivering gluing materials at the site of membrane puncture in a controlled manner, which is believed to be the key for efficient membrane sealing. Indeed, previous studies showing the deposition of hydrogel materials or blood coagulation-derived materials lacked a controlled method specifically designed for this matter.^{9,12,15-17,20,35} The deliberate choice of diverse sealing materials – two-component glues like fibrin or the promising mussel glue²³⁻²⁶ and Histoacryl® – was done to demonstrate the compatibility of our device with materials of different natures and to highlight the relevance of our method for the testing of those injectable candidates. As follows, we discuss more in detail the elements that make the device presented here a serious option to be considered for the application of sealing or even healing agents at the site of fetal membrane puncture.

RECEPTOR

The umbrella-shaped receptor was easily folded into the catheter, slid freely through the catheter and always deployed automatically into the defined shape. The mechanical stability assessed by the pulling test against a hard or a soft surface indicated that the nitinol backbone stability needs to be measured with the membrane covering the metallic structure and on a soft surface in order to have relevant data translatable to the *in vivo* situation. In addition, the relatively low resistance force (0.25N) suggests that structural changes might be needed to increase this value up to a palpable resistance (0.5-1N) but without impairing the folding capability of the receptor. The reason for that would be to enable the surgeons to feel the moment when applying the receptor onto the fetal membrane. This can be done by increasing the nitinol thickness and varying the number of struts.

As for the membrane covering the nitinol backbone, Degrapol® met the expectations for glue gathering but its use for further investigations is limited to non-cyanoacrylate glues. The use of an alternative solution to cover the nitinol backbone could potentially tackle this burden. For example, with expanded polytetrafluoroethylene (ePTFE), a FDA approved polymer used for example in hernia repair,³⁶ membranes with important elastic and non-permeable properties could be generated, corresponding to the functional requirements of our application. This polymer can also be electrospun and is already used to cover nitinol stents in some applications.³⁷ The clinical use of ePTFE has also been done in combination with Histoacryl® sealant for ePTFE graft fortification,³⁸ which speaks in favor of combining those materials in future investigations. In addition, Histoacryl® and other cyanoacrylate-based glues are routinely used *in vivo* for eyelid skin grafts without complications.³⁹ Similar to ePTFE, silicone can provide equal mechanical properties. Its use in combination with nitinol for thoraco-amniotic or vesicoamniotic shunts makes it a good candidate for our application.⁴⁰ However, further investigation is required to determine the best adhesive candidates to combine with silicone.

RECEPTOR ADHESION TO FETAL MEMBRANES

We first aimed to assess the inherent ability of different glues to bind the receptors to fetal membranes, which is the sine qua non for their successful use to prevent iPPROM. The glues used in this study showed different characteristics. Fibrin was not efficient in any test and barely any adhesive force was measurable. Mussel glue and Histoacryl® showed a very good performance when glued on intact fetal membrane, which confirms the potential of those glues to be used as sealants on fetal membranes. When applying the glues on the fetal membrane defect models with the device, fibrin glue and Histoacryl® showed similar values in contrary to mussel glue, which had a lower adhesion strength. This was probably due to the lower mechanical stability of the elastomeric membrane, which did not allow pressing the umbrella against the fetal membrane to form a thin glue layer. Similarly to previous studies,²⁶ Histoacryl® presented the strongest bonding efficiency throughout the study but the binding strength correlated with dissolution of Degrapol®, motivating once again its replacement with a more compatible material like silicone or ePTFE.

PROCEDURE SIMULATION ON AN EX VIVO MODEL

Finally, we chose the adhesive that was previously shown to have a significant potential to work in wet environment and did not have a destructive effect on Degrapol®. We increased the complexity of the assays by recreating the wet environment of the amniotic cavity inside the cylinder and recapitulated the abdominal and uterine wall with ex vivo tissues. This was necessary to increase by 10-fold the mechanical support provided by the whole tissue mimic compared to the elastomeric model (1N vs 0.1N), which granted the model with an increased physiological relevance.

All the receptors were well positioned and played their role of glue gathering successfully. The measure of the strength of attachment showed relatively low adhesion force of mussel glue ($0.13 \pm 0.04\text{N}$) but all stayed tight to the fetal membranes after receptor release. However, the data showing the adhesion strength of mussel glue on intact membranes in dry conditions indicates that mussel glue has the potential to confer strong adhesion. Different improvements might influence the adhesive strength. For example, a mixer could be added at the distal part of the applicator to pool the glue substrates better together. Alternatively, the optimization of the volume and/or viscosity of the adhesive could significantly help increase adhesion strength by improving fluid dynamics at the amnion and receptor surfaces.

TIME OF PROCEDURE

Furthermore, the whole procedure did take approximately 3 minutes, which is a determinant factor when adding up a step in the surgical procedure. This time span can be further decreased with training, experience and by starting the procedure with the receptor already tightly folded inside the tube, making the time factor a negligible element for the adoption of the method.

CONCLUSION

We fruitfully designed and produced a functioning device facilitating the controlled deposition of bioadhesives for prophylactic sealing of fetal membrane defect after fetoscopic interventions. Our data indicates that the application method can reliably be used to precisely inject gluing materials and seal the punctured amnion from the inside of the cavity. This study also highlighted the need of an alternative material for the receptor membrane and for stronger adhesives. We believe that those elements can be improved in a further step with alternative materials already existing in the industrial field. Regardless of the adhesives used, the results proved the feasibility of our method to successfully place an umbrella-shaped receptor that gathers bioadhesives for the closure of fetal membrane defects while respecting the geometrical requirements imposed by fetoscopic intervention instruments. We are thus convinced that this method has a future in the prevention of iPPROM and opens a new horizon in prenatal treatment.

2.6 _ REFERENCES

1. Beck, V., Lewi, P., Gucciardo, L. & Devlieger, R. Preterm prelabor rupture of membranes and fetal survival after minimally invasive fetal surgery: a systematic review of the literature. *Fetal diagnosis and therapy* 31, 1-9 (2012).
2. Gratacos, E., et al. A histological study of fetoscopic membrane defects to document membrane healing. *Placenta* 27, 452-456 (2006).
3. Devlieger, R., et al. Matrix metalloproteinases-2 and -9 and their endogenous tissue inhibitors in fetal membrane repair following fetoscopy in a rabbit model. *Mol Hum Reprod* 6, 479-485 (2000).
4. Devlieger, R., et al. Matrix metalloproteinases-2 and -9 and their endogenous tissue inhibitors in tissue remodeling after sealing of the fetal membranes in a sheep model of fetoscopic surgery. *J Soc Gynecol Investig* 9, 137-145 (2002).
5. Sopher, D. The response of rat fetal membranes to injury. *Annals of the Royal College of Surgeons of England* 51, 240-249 (1972).
6. Quintero, R.A., Carreno, C.A., Yelian, F. & Evans, M.I. Repair kinetics of amnion cells after microsurgical injury. *Fetal diagnosis and therapy* 11, 348-356 (1996).
7. Devlieger, R., Gratacos, E., Verbist, L., Pijnenborg, R. & Deprest, J. Gestational age-dependent repair kinetics of microsurgical defects in monolayers of human amniocytes. *Gynecol Obstet Invest* 69, 62-66 (2010).
8. Bilic, G., Ochsenbein-Kolble, N., Hall, H., Huch, R. & Zimmermann, R. In vitro lesion repair by human amnion epithelial and mesenchymal cells. *American journal of obstetrics and gynecology* 190, 87-92 (2004).
9. Ochsenbein-Kolble, N., et al. Enhancing sealing of fetal membrane defects using tissue engineered native amniotic scaffolds in the rabbit model. *American journal of obstetrics and gynecology* 196, 263 e261-267 (2007).
10. Mallik, A.S., et al. Fetoscopic closure of punctured fetal membranes with acellular human amnion plugs in a rabbit model. *Obstetrics and gynecology* 110, 1121-1129 (2007).
11. Devlieger, R., et al. Increased polymorphonuclear infiltration and iatrogenic amniotic band after closure of fetoscopic access sites with a bioactive membrane in the rabbit at midgestation. *American journal of obstetrics and gynecology* 188, 844-848 (2003).
12. Gratacos, E., et al. Successful sealing of fetoscopic access sites with collagen plugs in the rabbit model. *American journal of obstetrics and gynecology* 182, 142-146 (2000).
13. Luks, F.I., Deprest, J.A., Peers, K.H., Steegers, E.A. & van Der Wildt, B. Gelatin sponge plug to seal fetoscopy port sites: technique in ovine and primate models. *American journal of obstetrics and gynecology* 181, 995-996 (1999).
14. Engels, A.C., et al. Collagen plug sealing of iatrogenic fetal membrane defects after fetoscopic surgery for congenital diaphragmatic hernia. *Ultrasound in obstetrics & gynecology : the official journal of the International Society of Ultrasound in Obstetrics and Gynecology* 43, 54-59 (2014).
15. Harmanli, O.H., Wapner, R.J. & Lontz, J.F. Efficacy of fibrin glue for in vitro sealing of human chorioamniotic membranes. *The Journal of reproductive medicine* 43, 986-990 (1998).
16. Louis-Sylvestre, C., Rand, J.H., Gordon, R.E., Salafia, C.M. & Berkowitz, R.L. In vitro studies of the interactions between platelets and amniotic membranes: a potential treatment for preterm premature rupture of the membranes. *American journal of obstetrics and gynecology* 178, 287-293 (1998).
17. Papadopoulos, N.A., et al. Fetal membrane closure techniques after hysteroamniotomy in the midgestational rabbit model. *American journal of obstetrics and gynecology* 178, 938-942 (1998).
18. Quintero, R.A., et al. Treatment of iatrogenic previable premature rupture of membranes with intra-amniotic injection of platelets and cryoprecipitate (amniopatch): preliminary experience. *American journal of obstetrics and gynecology* 181, 744-749 (1999).
19. Lewi, L., et al. Successful patching of iatrogenic rupture of the fetal membranes. *Placenta* 25, 352-356 (2004).
20. Young, B.K., et al. Minimally invasive endoscopy in the treatment of preterm premature rupture of membranes by application of fibrin sealant. *Journal of perinatal medicine* 28, 326-330 (2000).
21. Young, B.K., et al. The closure of iatrogenic membrane defects after amniocentesis and endoscopic intrauterine procedures. *Fetal diagnosis and therapy* 19, 296-300 (2004).
22. Sener, T., Ozalp, S., Hassa, H., Yalcin, O.T. & Polay, S. Maternal blood clot patch therapy: a model for postamniocentesis amniorrhea. *American journal of obstetrics and gynecology* 177, 1535-1536 (1997).
23. Kivellio, A., et al. Mussel mimetic tissue adhesive for fetal membrane repair: initial in vivo investigation in rabbits. *Eur J Obstet Gynecol Reprod Biol* 171, 240-245 (2013).
24. Haller, C.M., et al. Mussel-mimetic tissue adhesive for fetal membrane repair: a standardized ex vivo evaluation using elastomeric membranes. *Prenatal diagnosis* 31, 654-660 (2011).

25. Haller, C.M., *et al.* Mussel-mimetic tissue adhesive for fetal membrane repair: an ex vivo evaluation. *Acta biomaterialia* 8, 4365-4370 (2012).
26. Bilic, G., *et al.* Injectable candidate sealants for fetal membrane repair: bonding and toxicity in vitro. *American journal of obstetrics and gynecology* 202, 85 e81-89 (2010).
27. Melton, K.N. & Mercier, O. The Mechanical-Properties of Niti-Based Shape Memory Alloys. *Acta Metall Mater* 29, 393-398 (1981).
28. Riboldi, S.A., Sampaolesi, M., Neuenschwander, P., Cossu, G. & Mantero, S. Electrospun degradable polyesterurethane membranes: potential scaffolds for skeletal muscle tissue engineering. *Biomaterials* 26, 4606-4615 (2005).
29. Brubaker, C.E., Kissler, H., Wang, L.J., Kaufman, D.B. & Messersmith, P.B. Biological performance of mussel-inspired adhesive in extrahepatic islet transplantation. *Biomaterials* 31, 420-427 (2010).
30. Burke, S.A., Ritter-Jones, M., Lee, B.P. & Messersmith, P.B. Thermal gelation and tissue adhesion of biomimetic hydrogels. *Biomedical materials* 2, 203-210 (2007).
31. Lee, B.P., Dalsin, J.L. & Messersmith, P.B. Synthesis and gelation of DOPA-modified poly(ethylene glycol) hydrogels. *Biomacromolecules* 3, 1038-1047 (2002).
32. Lee, H., Lee, B.P. & Messersmith, P.B. A reversible wet/dry adhesive inspired by mussels and geckos. *Nature* 448, 338-341 (2007).
33. Lee, H., Scherer, N.F. & Messersmith, P.B. Single-molecule mechanics of mussel adhesion. *Proc Natl Acad Sci U S A* 103, 12999-13003 (2006).
34. Dilege, E., *et al.* N-butyl cyanoacrylate versus conventional suturing for fixation of meshes in an incisional hernia model. *J Invest Surg* 23, 262-266 (2010).
35. Devlieger, R., Gratacos, E., Ardon, H., Vanstraelen, S. & Deprest, J. Factors influencing the flow rate through a surgical defect in human fetal membranes. *Prenatal diagnosis* 22, 201-205 (2002).
36. Bilsel, Y. & Abci, I. The search for ideal hernia repair; mesh materials and types. *Int J Surg* 10, 317-321 (2012).
37. Van Steenberghe, W. The first prospective endoscopic experience with the ePTFE-covered Viabil stent in patients with a distal malignant biliary stenosis. *Acta Gastroenterol Belg* 73, 18-24 (2010).
38. Saygun, O., *et al.* Reinforcement of the suture line with an ePTFE graft attached with histoacryl glue in duodenal trauma. *Can J Surg* 49, 107-112 (2006).
39. Shorr, N., Cohen, M.S. & Lessner, A. Histoacryl closure of eyelid skin grafts. *Ophthal Plast Reconstr Surg* 7, 190-193 (1991).
40. Hellmund, A., *et al.* Prenatal Diagnosis and Evaluation of Sonographic Predictors for Intervention and Adverse Outcome in Congenital Pulmonary Airway Malformation. *PLoS One* 11, e0150474 (2016).

CHAPTER 3 _ LOCALLY CONTROLLING MESENCHYMAL STEM CELL MORPHOGENESIS BY 3D PDGF-BB GRADIENTS TOWARDS THE ESTABLISHMENT OF AN IN VITRO PERIVASCULAR NICHE

This chapter is the postprint version of the article published in *Integrative Biology*, 7, 101-111, in 2015.

DOI: 10.1039/C4IB00152D

AUTHORS

Yannick R. Devaud,^{ab} Philipp S. Lienemann,^{ab} Raphael Reuten,^c Benjamin R. Simona,^d Maria Karlsson,^e Wilfried Weber,^e Manuel Koch,^c Matthias P. Lütolf,^b Vincent Milleret,^a and Martin Ehrbar^a

DOCTORAL CANDIDATE'S CONTRIBUTION

The two first authors shared main authorship in this published paper due to their equal scientific contribution to the realisation of the project. The doctoral candidate was responsible to develop the PDMS frames to enable the formation of channels in PEG hydrogels. He studied the channel formation to obtain a reproducible tool for reliable study. He characterized molecule diffusion from the channel into the gel to establish protein gradients and studied cell spreading and migration in contact to PDGF-BB. He also contributed to the paper by analysing cell proliferation, spreading and migration in single cell assay. Figures 3.3, 3.5 and 3.6 were the result of this work. The layout of those figures was done by Philipp S. Lienemann.

Besides this active contribution, the candidate helped in the development of the code used for microtissue migration assay and mastered cell culture, PEG hydrogels preparation, microtissue formation, encapsulation of single cells and microtissues and cell labelling, which were necessary for all parts of the project.

^a Laboratory for Cell and Tissue Engineering, Department of Obstetrics, University Hospital Zurich, Schmelzbergstr. 12, 8091 Zurich, Switzerland

^b Institute of Bioengineering, Ecole Polytechnique Fédérale de Lausanne (EPFL), Station 15, Bld AI 1109, 1015 Lausanne, Switzerland

^c Institute for Dental Research and Oral Musculoskeletal Biology, Center for Biochemistry, University of Cologne, 50931 Cologne, Germany

^d Laboratory of Biosensors and Bioelectronics, Institute for Biomedical Engineering, University and ETH Zurich, F76 Gloriastr. 35, 8092 Zurich, Switzerland

^e Faculty of Biology and BIOS Centre for Biological Signalling Studies, University of Freiburg, Schänzlestr. 18, 79104 Freiburg, Germany

3.1 _ ABSTRACT

This study aimed to take advantage of the hydrogel system enabling the binding of biological cues to the gel backbone to increase the spatial complexity of a 3D cell culture environment. The objective was to establish a stable gradient of biological signals by their immobilization in hydrogels containing a homogeneous cell population and see the effect of this gradient depending on the spatial distribution of the biological cues. The perivascular niche was taken as an inspiration for the establishment of growth factor gradients given that they play a key role in the development of blood vessels by directing mesenchymal stem cells (MSCs) towards the stabilization of those blood vessels.

The perivascular niche is a complex microenvironment containing MSCs, among other perivascular cells, as well as temporally organized biochemical and biophysical gradients. Due to a lack of conclusive phenotypic markers, MSCs' identity, heterogeneity and function within their native niche remain poorly understood. The in vitro reconstruction of an artificial three-dimensional (3D) perivascular niche would offer a powerful alternative to study MSC behavior under more defined conditions. To this end, we here present a poly(ethylene glycol)-based in vitro model that begins to mimic the spatiotemporally controlled presentation of biological cues within the in vivo perivascular niche, namely a stably localized platelet-derived growth factor B (PDGF-BB) gradient. We show that 3D-encapsulated MSCs respond to soluble PDGF-BB by proliferation, spreading, and migration in a dose-dependent manner. In contrast, the exposure of MSCs to 3D matrix-tethered PDGF-BB gradients resulted in locally restricted morphogenetic responses, much as would be expected in a native perivascular niche. Thus, the herein presented artificial perivascular niche model provides an important first step towards modelling the role of MSCs during tissue homeostasis and regeneration.

3.2 _ INTRODUCTION

Mesenchymal stem cells (MSCs) have recently been described to reside in perivascular niches of several human tissues.^{1,2} The *de novo* formation of these niches, which consist of an endothelium that is surrounded by perivascular cells, such as MSCs, relies on the spatiotemporal controlled presentation of biological cues.³ Whereas metabolic demand, low oxygen tension, or healing wounds control the sprouting of endothelial cells by an elevated expression of vascular endothelial growth factor (VEGF),⁴ the mobilization of perivascular cells and their stable retention has been described to rely on factors released and presented from endothelial cells.⁵ One of these biological cues is platelet derived growth factor-B (PDGF-BB), which has been shown to promote chemotaxis, proliferation, and spreading of various perivascular cells.⁶ Its secretion at relatively large quantity by endothelial tip cells during vascular sprouting is required for perivascular cells to spread and proliferate along the vascular wall, initiating the indispensable vessel stabilization.⁷ Moreover, the distribution of endothelial cell secreted PDGF-BB is spatiotemporally controlled through its interaction with heparin sulfate proteoglycans (HSPG) of the extracellular matrix (ECM). The affinity binding of PDGF-BB to ECM components results in an altered presentation of the molecule to MSCs, which will face matrix tethered growth factors rather than soluble factors. In addition, continuous ECM immobilization results in creation of a stable PDGF-BB gradient that descends from the vessel. This gradient is in turn sensed by perivascular cells and steers their localized assembly along the surface of the vessel (Figure 3.1A). MSCs are operatively defined by their potential to differentiate into cells of the osteogenic, adipogenic, and chondrogenic lineage after *in vitro* expansion. However, the complexity of their *in vivo* localization in the perivascular niche and the lack of MSC-specific markers hamper our further understanding of their identity, heterogeneity, and functional role in adult tissue homeostasis and regeneration.⁸ Therefore, there is great need for three dimensional (3D) *in vitro* models, which adequately recapitulate the *in vivo* arrangement of cells, ECM components and other biomolecules of the perivascular niche. Such models would allow for elucidation of biological processes that control the fate and localization of MSCs in the perivascular niche during vessel assembly, quiescence, or injury induced activation.

Recently, the systematic deconstruction of stem cell niches and their reconstruction under defined conditions has been proposed as a mean to understand individual parameters of complex niche signaling networks.⁹ Indeed, great progress has been made towards the development of ECM-mimicking synthetic matrices, potentially allowing for the *in vitro* emulation of stem cell niches by the generation of 3D microenvironments.⁹⁻¹¹ Such hydrogel matrices, as they are based on biologically inert materials such as poly(ethylene glycol) (PEG), can be formed with defined stiffness and degradability. We have described synthetic, transglutaminase cross-linked hydrogels (TG-PEG hydrogels), which are enzymatically degradable and contain the cell adhesion site RGD^{12,13} and at low stiffness allow 3D cell adhesion, spreading and migration.¹⁴ Their modular design, additionally to the flexible immobilization of engineered building blocks such as growth factors or enzymes,¹⁵ allowed the formation of structured hydrogels by locally controlling the enzymatic gel formation.¹⁶ Of note, such PEG-based matrices, in contrast to biologically

derived materials such as the widely used Matrigel™ or collagen, are highly defined and do not exert any biological response, allowing the studying of cell behavior on a blank canvas.¹⁷⁻¹⁹

Here, in order to elucidate MSC behavior during PDGF-controlled formation of the perivascular niche, we aimed at the creation of a 3D biomimetic model, which mimics the naturally occurring stable, matrix-immobilized PDGF-BB gradient, which is present in the perivascular niche. By placing MSCs within a 3D-structured TG-PEG hydrogel,¹³ we describe an *in vitro* bottom-up approach for the recapitulation of physical as well as PDGF-presenting properties of the perivascular niche (Figure 3.1B). In this model, we first confirmed the specific ability of soluble PDGF-

BB but not VEGF₁₂₁ to activate MSCs, leading to 3D morphogenetic processes such as cell proliferation, spreading, and migration. Furthermore, we assessed the activity of matrix tethered PDGF on MSCs and finally we created stable 3D PDGF-BB gradients, which resulted in spatiotemporal control of MSC spreading and motility, as was described during the naturally occurring investment of endothelium with perivascular cells. The herein described biomimetic niche model is a promising first step to study the role of MSCs during vascular morphogenesis, tissue healing and regeneration *in vitro*.

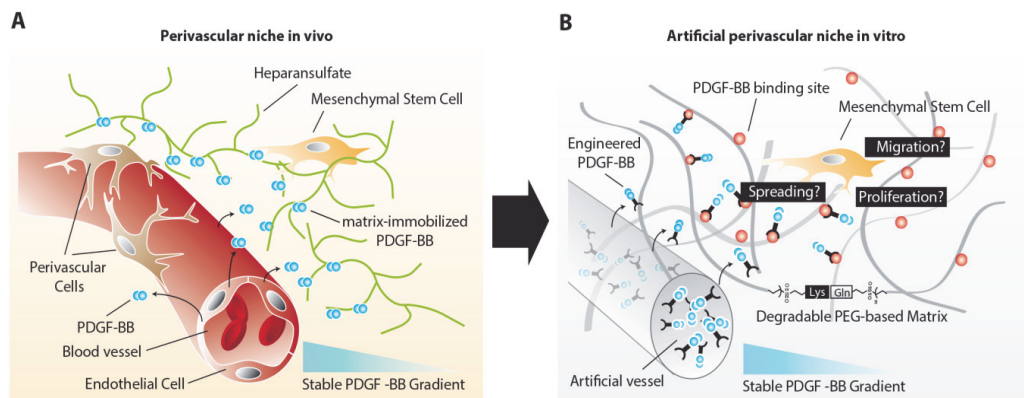


Figure 3.1. Schematic representation of the perivascular niche. A) Native perivascular niche. The native perivascular niche is composed of endothelial cells, perivascular cells (pericytes and SMCs), MSCs and ECM matrix containing matrix associated and soluble cues. Endothelial cell derived PDGF-BB binds with high affinity to heparane sulfate proteoglycane components (HSPG) of the ECM and thereby form a stable localized gradient. B) Engineered perivascular niche. The engineered perivascular niche, analogous to its *in vivo* counterpart, consists of an artificial vessel, a proteolytically degradable matrix with integrin binding sites, and a stable gradient of PDGF-BB. The fate of MSCs can be evaluated within the defined, positional microenvironments.

3.3 _ MATERIALS AND METHODS

CELL CULTURE

Bone marrow aspirates were obtained from healthy donors (average age 28 y.o.) after informed consent during orthopaedic surgical procedures in accordance with the local ethical committee (University Hospital Basel; Prof. Dr. Kummer; approval data 26/03/2007 Ref Number 78/07). Cells were isolated as described previously^{12,13}. Human bone marrow MSCs were cultured in minimal essential medium alpha (MEMalpha, Gibco Life Technologies, cat. no. 22571-020) supplemented with 10% (v/v) fetal calf serum (FCS, Gibco Life Technologies, cat. no. 10500), 1% (v/v) penicillin/streptomycin solution (Gibco Life Technologies, cat. no. 15140-122) and 5 ng/ml FGF-2 (Peprotech, cat. no. 100-18B). For experiments, MSCs were cultured in serum-free DMEM/F-12 + GlutaMAX™ (Gibco Life Technologies, cat. no. 31331-028) supplemented with 1% (v/v) penicillin/streptomycin solution. MSCs between passages 2 and 4 were used for all of the experiments.

PREPARATION OF TG-PEG HYDROGELS

Matrix metalloproteinase (MMP)-sensitive TG-PEG hydrogels were prepared as described previously.²¹ In brief, eight-arm PEG precursors containing the pending factor XIIIa substrate peptides glutamine acceptor (n-PEG-Gln) or lysine donor with an additional MMP-sensitive linker (n-PEG-MMP_{sensitive}-Lys) were mixed stoichiometrically (final dry mass content 1.5%) in Tris-Buffer (50 mM Tris, pH 7.6) containing 50 mM calcium chloride. 50 µM Gln-RGD peptide and indicated amounts of Gln-ZZ were added to the precursor solution prior to initiation of cross-linking by 10 U/ml thrombin-activated factor XIIIa and vigorous mixing.

MICROTISSUE FORMATION

For microtissue formation, indicated cell suspensions (final. conc. 25'000 cells/ml) were suspended in the respective medium for the experiment and supplemented with 0.2% (w/v) methyl cellulose (Sigma-Aldrich, cat. no. M0512). Droplets of 30 µl were placed in non-adhesive cell culture dishes (Greiner bio-one, cat. no. 633180) and cultured overnight as hanging drops. The resulting spheroids (approx. 750 cells) were harvested in cell culture medium and washed once with cell culture medium.

ENCAPSULATION OF SINGLE CELLS AND MICROTISSUES IN TG-PEG HYDROGELS

For encapsulating single dispersed cells or microtissues in TG-PEG gels, cell or microtissue suspensions were diluted in the respective medium and added to the complete TG-PEG solution. To form disc shaped hydrogels of approximately 5 mm diameter, 20 µl of this mixture were then sandwiched between sterile hydrophobic glass microscopy slides (obtained by treatment with SigmaCote, Sigmacote, Sigma-Aldrich, cat. no. SL2) separated by spacers (ca. 1 mm thickness) and clamped with binder clips. To prevent sedimentation of cells or microtissues, the forming

matrices were slowly rotated at room temperature (RT) until the onset of gelation and then incubated for additional 30 min. at 37°C. The hydrogels were thereafter released and transferred into a 24-well plate. Finally, the plates with the gels were incubated in 500 μ l of the respective medium at 37°C and 5% CO₂ in a humidified atmosphere.

CELL LABELING

After the experiments, the samples were fixed with 4% paraformaldehyde. After stopping the reaction with 0.1 M Glycine in PBS (phosphate buffered saline, pH 7.2), the samples were washed twice with PBS. Permeabilization was performed for 20 min at RT with 0.2% Triton X-100 (Sigma-Aldrich, cat. no. T-8787) in PBS followed by 2 washing steps with PBS. For F-actin staining, the samples were incubated over night at 4°C with rhodamine-labeled phalloidin (Life technologies, cat. no. R415). Afterwards, the samples were washed 3 times with PBS and stained for cell nuclei using Hoechst (1:1000, Life technologies, cat. no. H3570). Subsequently, the samples were washed again 3 times with PBS before analysis with either confocal laser scanning microscopy or fluorescent microscopy.

MICROTISSUE MIGRATION ASSAY

MSC microtissues were encapsulated in TG-PEG hydrogels (final conc.: approx. 250 microtissues ml⁻¹) and cultured for 20 hours. The samples were fixed and stained for F-actin. Z-stack images of microtissues were acquired at 10 x magnification using a confocal microscope (Leica TCS SP5). Cell migration was quantified by an automated image analysis script written in MATLAB (R2013a, MathWorks Inc, USA) that measures the distance of stained pixels from the microtissue center. Data is displayed as histogram depicting the amount of pixels relative to the migration distance. Pixels with a distance larger than 100 μ m from the spheroid center were considered in the statistical analysis.

SINGLE CELL PROLIFERATION, SPREADING, AND MIGRATION ASSAYS

MSCs were embedded in TG-PEG hydrogels (final conc.: 0.5 x 10⁶ ml⁻¹) and cultured for 5 days. For migration assays, three random positions were selected using an inverted microscope (Leica DMI6000 B) equipped with a motorized focus and stage. Cell migration was followed for 22.5 hours using the manual tracking plugin in ImageJ. For proliferation and spreading assays, after cell fixation, cells were stained for nuclei as well as F-actin and Z-stack images (total stack size: 500 μ m) were acquired at 10 x magnification using a confocal microscope (Leica TCS SP5). Cell proliferation was analyzed by measuring the numbers of 3D F-actin using the ImageJ plugin 'Object Counter3D'. For circularity ratio, a Z-stack projection from F-actin Z-stack images (total stack size: 150 μ m) was made and cell circularity ratio was calculated using ImageJ. Cell circularity ratio is the ratio between a cell's shape and a circle with the same perimeter. It therefore is a dimensionless number that is greater than 0 and less or equal to 1. The more elongated a cell is the closer the circularity ratio is to 0. Cells with a circularity ratio below 0.25 were considered as elongated.

PREPARATION OF THE PDMS FRAMES

Polydimethylsiloxane (PDMS) frames were made as described previously.¹⁶ In short, the silicon elastomer and the curing agent (Sylgard 184, Dow Corning Corporation, USA) were mixed (10:1 in mass) at 2000 rpm for 3 min in a ARE-250 mixer (Thinky Corporation, Japan). The mixture was subsequently poured into poly(methyl methacrylate) (PMMA) molds, where 500 μm in diameter stainless steel wires were positioned to create the holes for the future electrodes. The mixture was subsequently degassed for 30 min in a vacuum chamber and baked for 4 h at 60°C. The stainless steel wires and the PDMS forms were removed from the PMMA molds, rinsed with isopropanol (IPA), oxygen plasma cleaned (1 min at 300 W, Plasma-System 100, Technics Plasma GmbH, Germany) and finally pressed onto plasma cleaned microscope glass cover slips. Straightened Tungsten wires (W, 500 μm in diameter, Advent Research Materials Ltd, UK) were inserted in the PDMS forms and connected to a potentiostat-galvanostat in a two electrode setup (PGU-10V-1A-IMP-S and ECMwin computer interface, Elektroniklabor Peter Schrems, Germany).

RECOMBINANT PROTEINS

Untagged growth factors were purchased from Peprotech (VEGF₁₂₁, cat. no. 100-20A; PDGF-BB, cat. no. 100-14B). Linker protein Gln-ZZ was recombinantly produced in E.coli BL21 as described previously.²⁵ Fc tagged PDGF-BB (PDGF-BB_{FC}) and VEGF-A (VEGF-A_{FC}) were cloned, expressed and purified as follows: PDGF-B and VEGF-A from Homo sapiens (PDGF-B: NP_002599.1, aa: 21-190 and VEGF-A: NP_001020539.2, aa: 207-371) were cloned into a modified PCEP vector with an N-terminal double Strep- tag II fused followed by IgH protein from Mus musculus (AAH03435.1, aa: 245-463). A pool of HEK293 cells were stably transfected followed by screening for high level expression. Secreted PDGF-BB_{FC} and VEGF-A_{FC} were purified by Streptavidin beads (IBA). The purified PDGF-BB_{FC} and VEGF-A_{FC} were then dialyzed against 1 x phosphate buffer saline (PBS) pH 7.4. Labeling of PDGF-BB_{FC} was done using DyLight 550 Fluorophore (Thermo Fisher Scientific Inc.) following the manufacturer's instructions.

SOLID PHASE BINDING ASSAY BETWEEN GLN-ZZ AND PDGF-BB_{FC}

Gln-ZZ peptide was coated at 10 $\mu\text{g ml}^{-1}$ (500 ng well⁻¹) overnight at 4°C onto 96-well plates (Nunc Maxisorb). After washing with TBS, plates were blocked for 2 hours at RT with TBS containing 3% bovine serum albumin. Ligand (PDGF-BB_{FC}) was diluted to concentrations from 0.03 nM to 500 nM and incubated for 2 hours at room temperature. After extensive washing with TBS, bound ligands were detected with a streptavidin horseradish peroxidase (HRP)-conjugate (IBA) 1:5000. HRP was detected by Pierce TMB ELISA Substrate (Thermo Scientific™). Absorption was measured at 450 nm after stopping the reaction with 2 M sulfuric acid. A Blank value corresponding to BSA coated wells was automatically subtracted.

CHANNEL AND PDGF GRADIENT FORMATION IN TG-PEG HYDROGELS

Perfusable channels with a diameter of 500 μm were produced in TG-PEG hydrogels as described previously.¹⁶ Briefly, 60 μl of complete TG-PEG hydrogel mixture, if indicated, containing MSCs were poured before the onset of gelation into the PDMS frame accommodating a straightened Tungsten wire. The polymerization of the TG-PEG was allowed to progress during 6 minutes while the Tungsten wire was anodically polarized (2 V DC, versus a Platinum auxiliary electrode). Subsequent removal of the anodically polarized Tungsten wires lead to reproducible formation of regularly shaped channels within the TG-PEG gel. Stable or evolving PDGF gradients were formed by perfusing the channel with 1 μl PDGF-Fc or fluorescently labeled PDGF-Fc (180 ng μl^{-1}) in presence or absence of 20 μM Gln-ZZ in the surrounding TG-PEG gel, respectively. Images of fluorescently labeled PDGF-BB_{FC} gradients were taken after 0.5, 24, and 48 hours using an inverted fluorescence microscope (Leica DMI6000 B). Fluorescence intensity was measured on a line perpendicular to the channel using the PlotProfile function in ImageJ

ANALYSIS OF MSC SPREADING AND MIGRATION WITHIN PDGF-BB GRADIENTS

MSCs were encapsulated in TG-PEG hydrogels (final conc.: $0.5 \times 10^6 \text{ ml}^{-1}$) within the PDMS mold and cultured overnight. The day after, Tungsten wires were removed and indicated amounts of PDGF-BB_{FC} were loaded into the channel. For migration assays, two positions adjacent to the channel and two positions 3 mm away from the channel were selected using an inverted microscope (Leica DMI6000 B) equipped with a motorized focus and stage. Cell migration was followed for 22.5 hours using the manual tracking plugin in ImageJ. For spreading analysis, cells were fixed after 48 hours in culture. After F-actin staining, Z-stack images (total stack size: 150 μm) of the complete constructs were acquired at 10 x magnification using a confocal microscope (Leica SP5) equipped with a long distance 10 x objective. Z-stack projections were made thereof, stitched together and the image was divided into 8 equally sized segments each having a width of 0.5 mm. For quantification, cell circularity ratio was analyzed in each part using ImageJ.

STATISTICAL ANALYSIS

All mean values were compared by one-way analysis of variance (ANOVA) using MATLAB (R2013a, MathWorks Inc, USA) followed by a tukey-kramer post hoc test to judge statistical significance. Statistical significance was accepted for $p < 0.05$. One asterisks reports $p < 0.05$ and two asterisks $p < 0.01$.

3.4 _ RESULTS

3.4.1 _ PDGF-BB MODULATES 3D MSC FUNCTIONS IN VITRO

In order to study the role of PDGF-BB on MSC during morphogenesis in the perivascular space, we established a 3D microtissue-based *in vitro* assay.

MSC microtissues were embedded within a recently developed polyethylene glycol (PEG) hydrogel, termed 'TG-PEG hydrogel', that recapitulates biochemical and biophysical properties of the microenvironment MSCs face in their anatomical location.^{12, 13} This synthetic hydrogel was formulated to be matrix MMP-1-degradable, have low cross-link density (94 ± 25 Pa shear modulus)¹⁴ and provide cell adhesion sites ($50 \mu\text{M}$ RGD) in order to provide the MSCs a hydrated microenvironment in which proliferation, spreading and migration are possible. 4 hours after stimulation of the MSC microtissues with PDGF-BB already, MSCs started to migrate from the microtissues into the surrounding synthetic environment. Quantification of migration showed that in absence of PDGF-BB cells remained in a quiescent state within the microtissue, whereas upon 20 hours of exposure to PDGF-BB (10 nM) cells had invaded the artificial ECM up to $500 \mu\text{m}$ (Figure 3.2A and B). When MSC microtissues were treated with equal amounts of VEGF₁₂₁ no significant outgrowth was observed as compared to the controls. Taken together, this data confirmed that PDGF-BB specifically controls morphogenesis related functions of MSCs and that its role can be studied *in vitro* within the designed artificial environment.

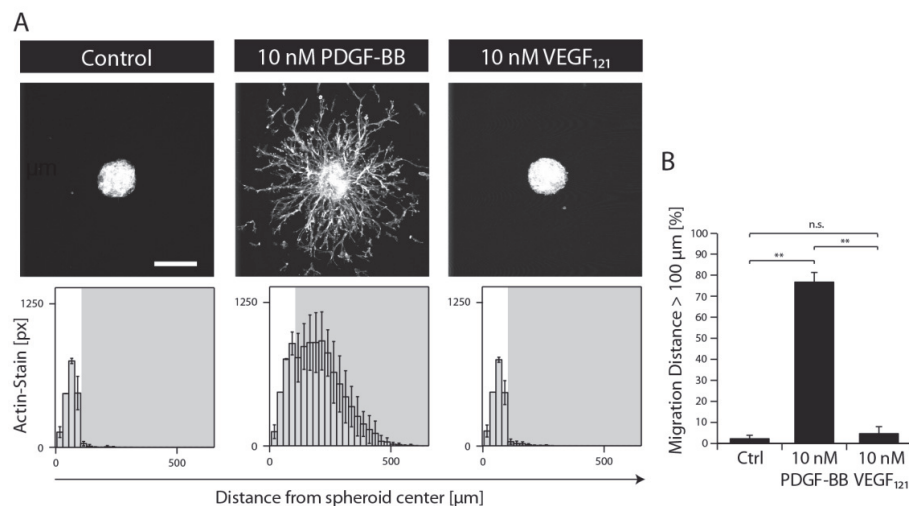


Figure 3.2 PDGF-BB induces 3D MSC morphogenesis in biomimetic microenvironment. MSC microtissues consisting of approx. 750 cells were embedded in synthetic matrices and stimulated with the indicated growth factor for 20 hours under serum-free conditions. A) Z-stack projections of F-actin stained MSCs (upper panels, scale bar = $200 \mu\text{m}$). Histograms showing the distribution of MSCs from microtissue center when stimulated with the respective growth factor (lower panels). B) Bar graph illustrating the percentage of actin-stained pixels being located at a distance larger than $100 \mu\text{m}$ from the centre of the microtissue. Data is depicted as mean \pm SD ($n \geq 4$, **, $p < 0.01$, n.s., not significant).

DISCRIMINATION OF 3D MORPHOGENETIC PROCESSES BY SINGLE CELL ASSAY

To elucidate the effect of PDGF-BB on individual cellular processes, single dispersed cells were embedded in TG-PEG hydrogels and cultured for several days in the absence or in the presence of 10 and 50nM PDGF-BB. Confocal images (z-stacks) of cytoskeleton stained cells after 5 days of culture revealed that presence of PDGF-BB had a dose dependent effect, which resulted in the formation of relatively dense cellular networks (Figure 3.3A). Automated quantification of confocal images was applied to analyze cell number, cell circularity ratio as a measure of cell elongation, and single cell migration. PDGF-BB enhanced MSC numbers on average by 45% (10nM PDGF-BB) and 81% (50nM PDGF-BB) (Figure 3.3B). Moreover, MSC Population's cell elongation was shifted towards more spread cells with a smaller cell circularity ratio after treatment with PDGF-BB (Figure 3.3C). Based on the evaluation of the cell populations' circularity ratio histograms, a cell that had a circularity ratio below 0.25 was considered as elongated. In the untreated cell population only $13 \pm 4\%$ of the cells were elongated whereas in the PDGF-BB treated conditions $32 \pm 9\%$ (10 nM PDGF-BB) and $63 \pm 5\%$ (50 nM PDGF-BB) of the cells were elongated (Figure 3.3D). Also, cell motility was increased in a dose dependent manner as found by tracking cells for 22.5 hours (Figure 3.3E). Whereas the mean distance that cells migrated during this time in the control sample was $47 \pm 11 \mu\text{m}$, cells that were exposed to 10 nM or 50 nM PDGF-BB migrated $173 \pm 20 \mu\text{m}$ or $246 \pm 14 \mu\text{m}$, respectively. Taken together, this data indicates that PDGF-BB is an important player in influencing multiple facets of MSC morphogenesis.

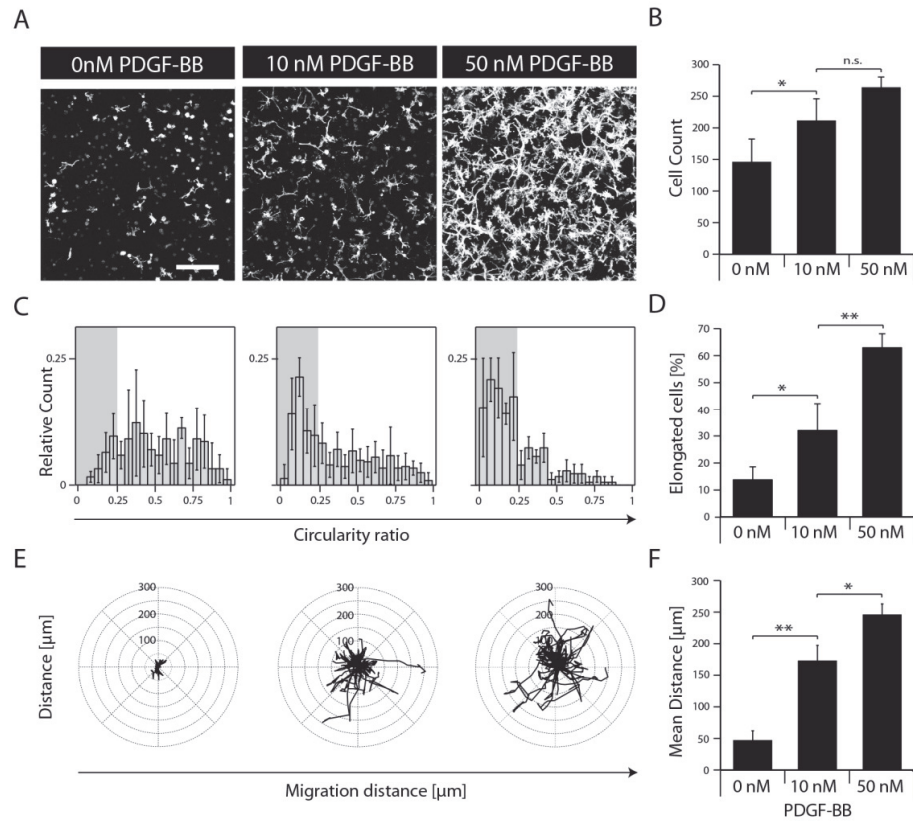


Figure 3.3 PDGF-BB induces proliferation, spreading and migration of 3D encapsulated MSCs. MSCs were encapsulated in TG-PEG hydrogels (0.5×10^6 cells ml^{-1}) and cultured under serum-free conditions in presence of the indicate amounts of PDGF-BB A) Z-stack projections (total stack size 500 μm) of F-actin stained MSCs after 5 days of culture (scale bar = 200 μm). B) MSC numbers as analysed by counting connected F-actin objects in 3D by an automated image analysis script as described in materials and methods. C) Histogram depicting the MSC population's circularity ratio ($4\pi \times (\text{cell area}) / (\text{cell perimeter}^2)$). D) Bar graph depicting percentage of elongated cells. Cells with a circularity ratio below 0.25 were considered as elongated. E) Cell tracks of MSCs were acquired and overlaid with a common starting point. The tracks represent a period of 22.5 hours (18 x 75 min) starting 24 hours after first growth factor exposure. F) Bar graph depicting mean migration distance. Data is depicted as mean \pm SD ($n \geq 4$, *, $p < 0.05$, **, $p < 0.01$, n.s., not significant).

MATRIX-MEDIATED PRESENTATION OF PDGF-BB

In order to mimic the naturally occurring interactions between the ECM and PDGF-BB and to control the spatiotemporal distribution of PDGF-BB within the *in vitro* niche model, a PDGF-BB variant (PDGF-BB_{FC}) was genetically engineered such that it contains the fragment crystallizable (Fc) region of antibodies at its N-terminus. When combined with a recently developed bifunctional linker protein (Gln-ZZ)¹⁵ this allows for mimicking the affinity interaction that is occurring *in vivo* between heparin sulfates of the ECM and PDGF-BB. Gln-ZZ can be incorporated into the TG-PEG hydrogel backbone via its C-terminal domain (Gln) and has high affinity for Fc-tagged proteins through its N-terminal Z domains. PDGF-BB_{FC} binding to Gln-ZZ and biological activity as well as specificity was confirmed in a solid-phase binding assay and microtissue morphogenesis assay, respectively.

In order to show that matrix-immobilized PDGF-BB_{FC} is biologically active, microtissues were embedded in TG-PEG gels containing 0 μM or 20 μM Gln-ZZ linker as well as 0, 10 or 50 nM PDGF-

BB_{FC}. The large excess of Gln-ZZ molecules present in the hydrogels assures that the majority of PDGF-BB_{FC} molecules are present in their matrix immobilized form. As for the soluble variant, the matrix-immobilized PDGF-BB_{FC} triggered MSC morphogenesis related functions, which can be modulated in a dose dependent manner (Figure 3.4A). MSCs exposed to hydrogels containing 20 μ M Gln-ZZ linker fully remained in the microtissue, with as little as 3% of actin stained areas (pixels) belonging to cells that had left the microtissue. On the other hand, cells that were exposed to hydrogels containing 20 μ M Gln-ZZ linker and 10 nM and 50 nM PDGF-BB_{FC} showed respectively 41% and 67% of actin stained pixels detached from the microtissue (Figure 3.4B). 10 nM PDGF-BB_{FC} admixed to the Gln-ZZ free hydrogel showed similar activity as 10 nM ZZ-immobilized PDGF-BB_{FC}.

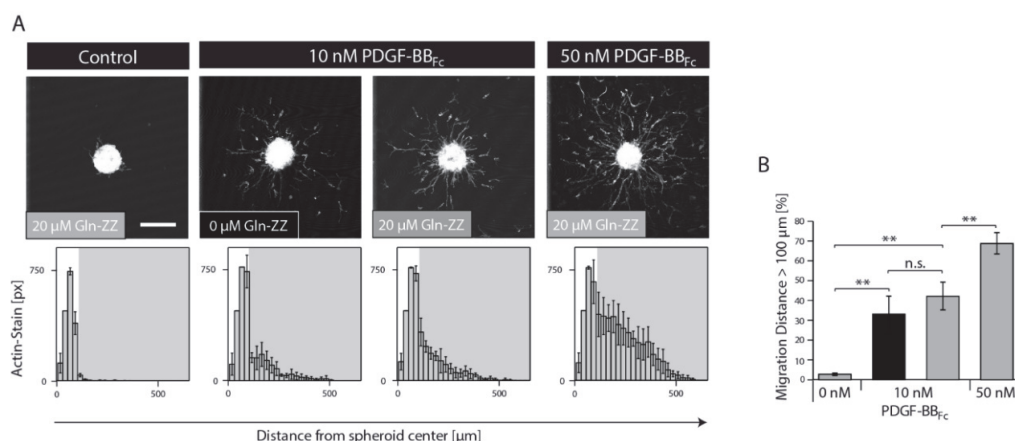


Figure 3.4 MSC migration in synthetic PDGF-BB-presenting cell-instructive matrices. MSC microtissues consisting of approx. 750 cells were encapsulated in TG-PEG hydrogels containing 0 μ M (black) or 20 μ M (grey) Gln-ZZ and 0, 10, or 50nM PDGF-BB_{FC}. A) Representative CLSM Z-stack projections of F-actin stained MSCs cultured for 20 hours under serum-free conditions. (scale bar = 200 μ m). B) Histograms showing the distribution of MSCs from microtissue center when embedded within the indicated matrix. C) Bar graph shows the percentage of actin-stained pixels being located at a distance larger than 100 μ m from the centre of the microtissue. Data is depicted as mean \pm SD ($n \geq 3$, **, $p < 0.01$).

3.4.2 _ MICROFLUIDIC APPROACH FOR THE CREATION OF 3D PDGF-BB GRADIENTS IN PEG HYDROGELS

As opposed to traditional cell culture assays, biomolecules within the body are not present in uniform concentrations, but rather in concentration gradients that descend from the site of biomolecule expression.²¹ In order to mimic *in vitro* the 3D PDGF-BB gradient that occurs in the perivascular niche around blood vessels, we applied a recently developed electrochemistry-based technique to form artificial vessels in the middle of the hydrogel by spatially inhibiting hydrogel polymerization.¹⁶ Such channels were loaded with controlled amounts of PDGF-BB_{FC}, which could freely diffuse from the channel into the surrounding hydrogel and reach the MSCs (Figure 3.5A). To monitor PDGF-BB diffusion into MSC containing hydrogels, fluorescently labeled PDGF-BB_{FC} was loaded in a channel and its distribution in the gel was analysed. After 48 hours the PDGF-BB_{FC} gradient had leveled out and PDGF-BB_{FC} was almost homogenously distributed within the hydrogel (Figure 3.5B). In order to fabricate a more sophisticated model that takes into account the interaction of PDGF-BB with the ECM, we made channels in Gln-ZZ containing hydrogels.

To test if the before described interaction between PDGF-BB_{FC} and Gln-ZZ would indeed lead to the establishment of the graded 3D immobilization of PDGF-BB, we perfused the fluorescently labeled PDGF-BB_{FC} through the channel into the Gln-ZZ presenting and MSC containing hydrogel (Figure 3.5C). 48 hours after perfusion, a stable 3D PDGF-BB_{FC} gradient originated from the channel into the hydrogel, indicating a stable interaction between PDGF-BB_{FC} and the matrix in presence of MSCs (Figure 3.5D). 1.5 mm from the channel the level of fluorescently labelled PDGF-BB_{FC} had decreased to background level.

MSC MORPHOGENESIS IN EVOLVING VERSUS STABLE 3D PDGF-BB GRADIENTS

In order to elucidate MSCs' morphogenetic response to being exposed to evolving and stable gradients of PDGF-BB_{FC}, MSCs were encapsulated in TG-PEG hydrogels containing an artificial vessel for biomolecule perfusion. As expected, perfusion of the channel with control medium without PDGF-BB_{FC} did not lead to a morphogenetic response as shown by measuring the cellular circularity ratio two days after perfusion within 3 consecutive segments each spanning 1.5 mm. Percentage of cells that were elongated (circularity ratio < 0.25) remained around 10% in all segments. This coincides with the value that was previously observed for the control in the static condition (Figure 3.3C and D). On the other hand, perfusion of 4 μ M PDGF-BB_{FC}, which created a short-term-evolving gradient of PDGF-BB_{FC} as shown before (Figure 3.5B), lead to cell spreading (decrease in circularity ratio) similarly to the previous static experiments (Figure 3.3C and D). After 2 days, however, only minor spatial differences in cell spreading were observed due to the levelling out of the soluble PDGF-BB_{FC} concentrations throughout the sample (Figure 3.6A). Percentage of cells that were elongated (circularity ratio < 0.25) was roughly between 20% and 40% (Figure 3.6C), which correlated with the elongation that was seen in the static condition in presence of 10 nM PDGF-BB (Figure 3.3C and D).

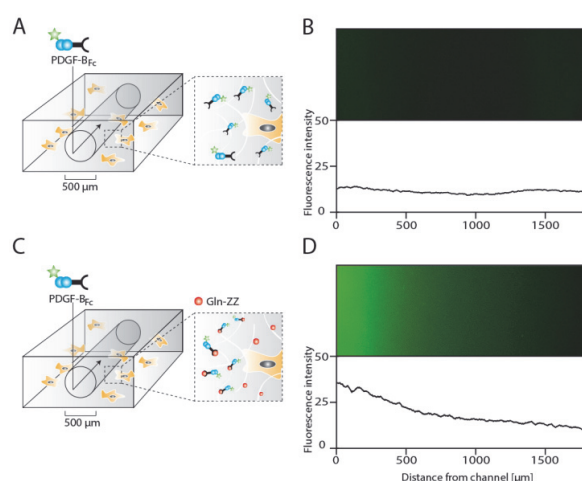


Figure 3.5. Hydrogel microfluidics for creation of evolving and stable PDGF-BB gradients in presence of cells. Scheme of PDGF-BB_{FC} delivery to 3D encapsulated MSCs using a perfusable channel in standard (A) and Gln-ZZ modified (C) TG-PEG hydrogels. Hydrogel channels were formed by electrochemical inhibition of hydrogel polymerization as described previously.¹⁶ B and D) Fluorescent microscopy images showing the area around the respective hydrogel channels 48 hours after perfusion with DyLight 550-labeled PDGF-BB_{FC} (upper panel) and the corresponding grey value histograms.

In contrast, if a stable PDGF-BB gradient was formed by perfusion of Gln-ZZ (20 μM) modified TG-PEG hydrogels with 4 μM PDGF-BB_{FC} the morphogenetic response of encapsulated MSCs was locally restricted to the vicinity (0 - 1500 μm) of the artificial vessel (Figure 3.6B). Due to the stable retention of PDGF-BB_{FC} only in the first segment 20% of the cells were elongated (circularity ratio < 0.25) whereas cells further away were not affected by the growth factor presence (Figure 3.6C). Moreover, the bound growth factor was locally inducing MSC motility as shown by the cell tracks of cells at 0 - 1 mm versus 2.5 - 3.5 mm distance from the channel (Figure 3.6B). These results emphasize the role of biomolecules within complex *in vitro* models and even more so the importance of controlling them spatiotemporally by mimicking the processes occurring in nature.

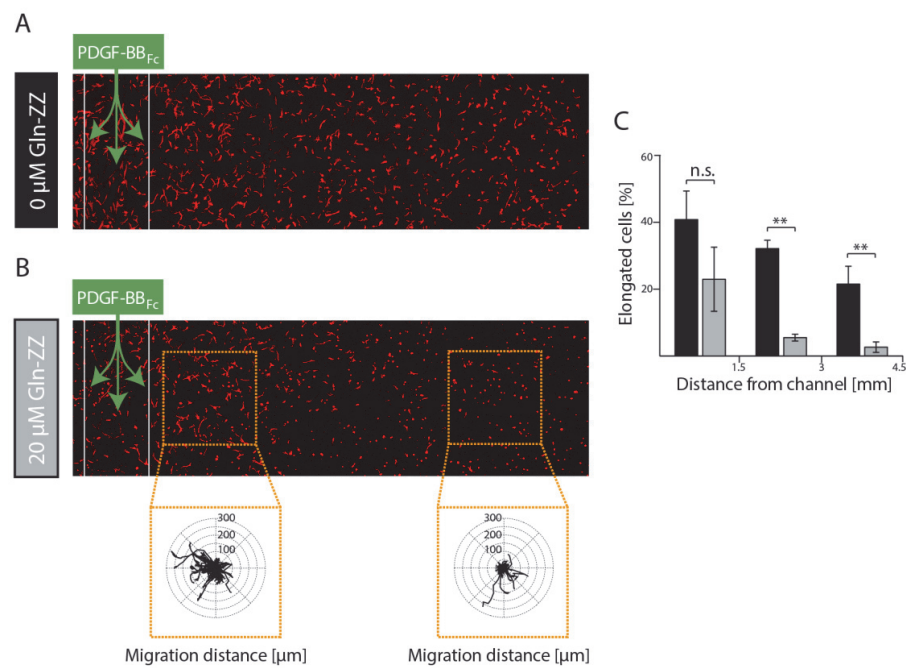


Figure 3.6. Evaluation of MSCs in a perivascular niche microenvironment mimicking evolving and stable PDGF-BB gradients. MSCs were encapsulated (0.25×10^6 cells ml^{-1}) in TG-PEG hydrogels and channels for biomolecule perfusion were formed by electrochemical inhibition of hydrogel polymerization. Data is shown for both conditions after 48 hours of culture as representative Z-stack images (total stack size 500 μm) of F-actin stained MSCs (Scale bar = 500 μm). Channels in unaltered (A) and 20 μM Gln-ZZ containing (B) TG-PEG hydrogel were perfused with 4 μM PDGF-BB_{FC}. Insets display overlaid tracks of migrating MSCs at the indicated positions of the sample. The tracks represent a period of 22.5 hours (18 x 75 min) starting 24 hours after PDGF-BB_{FC} perfusion. C) Histogram depicting percentage of cells with a circularity ratio below 0.25 relative to distance to channel in gels with 0 μM (black) or 20 μM Gln-ZZ (grey). Statistical comparison is made between the two groups of each region. Data is depicted as mean \pm SD ($n \geq 4$, n.s., not significant, **, $p < 0.01$).

3.5 _ DISCUSSION

A prevalent limitation to 2D and 3D cell culture assays has long been the lack of spatial and temporal control over the presentation of biomolecules, which especially for the engineering of complex milieus such as the stem cell niche is an evident prerequisite. We here present a biomimetic approach that recapitulates the localized ECM immobilization of PDGF-BB in the perivascular niche. By combining an electrochemistry-based hydrogel patterning approach¹⁶ with engineering of growth factor matrix interactions and diffusion controlled establishment of 3D gradients, human MSCs can readily be exposed to selected micro-environmental conditions as would be expected to occur in the surrounding of a blood vessel. This experimental setup offers several advantages to existing models: *i)* it is based on engineered ECM with defined and tunable physical, chemical and biological properties *ii)* growth factors can be promiscuously immobilized via affinity interactions and thus can be loaded independently of hydrogel formation and cell encapsulation *iii)* the use of channels allows the sequential loading of multiple engineered and native growth factors *iv)* due to the transparent character of the hydrogel system, cell behavior can be monitored throughout the length of the experiment so that morphogenetic parameters can be followed and independently evaluated.

Despite the fact that great efforts were devoted towards the development of models for studying cell fates in stable growth factor gradients *in vitro*, described approaches either do not take into account the three dimensionality of the microenvironment that surrounds cells *in vivo*²²⁻²⁶ or employ matrices with inherent biological properties²⁷⁻²⁹.

To the best of our knowledge, this is the first report on the implementation of a stable growth factor gradient within a fully defined synthetic hydrogel matrix. Moreover, as opposed to other studies²⁷⁻²⁹ that show stable 3D growth factor gradients, we here describe a method that allows for gradient formation in presence of cells, which is not only more closely mimicking the situation in nature, but as well omitting material interface problems that result from pre-fabrication of the gradient and post-hoc seeding of the cells onto the gradient.

VEGFs and PDGFs are known to be jointly involved in the assembly and stabilization of new vessels⁵. This was illustrated by the elimination of either VEGF signaling in endothelial cell or PDGF signaling in pericytes or by the deletion of either the ligands or the receptors, which has resulted in a largely defective development and function of vessels, leading to embryonic lethality.³⁰⁻³³ *In vitro* PDGFs promote the migration of multiple mesenchymal cell types such as fibroblasts, smooth muscle cells, and MSCs. However their role in controlling cell behavior during vessel stabilization has not been characterized in detail. As opposed to other studies,³⁴ we demonstrate the specific *in vitro* induction of morphogenetic processes in hydrogel encapsulated MSC microtissues by soluble PDGF-BB but not VEGF.

Importantly, the majority of expressed VEGF and PDGF molecules contain a positively charged C-terminal domain, which has been described to bind HSPGs of the extracellular matrix.³⁵ *In vivo* this affinity of growth factors to the ECM limits their diffusion away from the site of production and likely results in the formation of relatively stable positional cues. The consequence of such ECM immobilized cues for the formation of functional, properly structured vascular networks has been impressively shown by transgenic mice which either express only VEGF-variants that lack the C-

terminal heparin binding domain (VEGF₁₂₁) or only have high affinity for heparin (VEGF₁₈₉)^{36, 37}. While in the first case due to loss of directionality during branching, resulting vessels were large in diameter and less branched in the latter case extensive filopodia formation, highly branched and thin vessels were observed.³⁸ Similarly, the deletion of the C-terminal heparin binding motif of PDGF-BB resulted in abnormal coverage of pericytes, and their partial detachment from the vessel wall which for example manifests in defective vessels and consequently in retinal deterioration, or proteinuria.^{3, 39} These data indicate a role for the ECM immobilization of PDGF-BB in the assembly of functional blood vessels. The C-terminal binding motif of PDGFs largely restricts its distribution and availability *in vivo* near to the site of productions, which in the case of vessels is in the perivascular zone.³ In the presented *in vitro* model, a synthetic protein linker was applied to mimic this natural PDGF-BB ECM interaction. Additionally, fabrication of a perfusable channel in the hydrogel allowed for controlling the PDGF-BB source and thereby creation of evolving as well as, in the case of matrix-interacting PDGF-BB, stable 3D PDGF-BB gradients. Stable PDGF-BB gradients restricted PDGF-BB-induced spreading and migration to the vicinity of the growth factor source. In contrast, the freely diffusible growth factor led to a transient gradient rapidly leveling out throughout the gel. Similar observations were made by Nguyen et al.,⁴⁰ who recently described that a gradient formed in a hydrogel from a channel, initially spans over 300 μm and covers over 900 μm after 1h only. This short-term gradient of the growth factor lead to homogenous biological response throughout the entire model. These data indicate that the native perivascular organization of cells can be recapitulated *in vitro* by appropriate presentation of PDGF gradients. In 2D setups, soluble PDGF gradients were shown to induce fibroblast polarization and chemotaxis.^{41, 42} However, in the herein presented 3D setup, both soluble PDGF and the gradient of matrix-immobilized PDGF stimulated a chemokinesis related (stochastic) migration process. From these experiments it remains unclear whether during the formation of the gradient a short-term exposure of the MSCs to soluble PDGF, residual non-bound PDGF, or trace amounts of released PDGF were sufficient to induce non-directed migration or whether PDGF generally induces a migration process resembling chemokinesis. The high binding affinity of the ZZ-tag to Fc-domains ($K_d = 4.8 \cdot 10^{-8}/\text{M}$)⁴³ would suggest, that the release of the growth factor would be mainly be due to the very slow (not yet carefully characterized) degradation of the PEG-based matrix by cell-mediated cleavage of built-in MMP-sensitive linker sequences^{14, 44}. This indicates that although MSC migration might not occur in a highly directional fashion the sum of the PDGF-mediated processes leads to the assembly and stabilization of a perivascular niche. A further limitation of the current study is that in this simplified model the direct contact of MSCs with the vascular basement membrane, which is a known regulator of various stem cells, is not reproduced^{45, 46}. Together, these observations indicate that our *in vitro* model recapitulates some of the dynamics that are assumed to be present during vessel formation, including the diffusion of trace amounts of PDGF from the site of production before the capturing by the glycosaminoglycan components of the ECM. Enzymatic remodeling of the ECM by mobilized cells is also represented by the slow MMP-dependent degradation of the PEG-matrix and the consequent release of PDGF.

The steepness of the gradient and the protease-mediated release of PDGF from gradients can have a large influence on the amount of factor seen by a cell. As in this study these parameters were kept constant we cannot exclude that chemotactic migration would preferentially occur

in steeper gradients or upon cell-mediated promotion of release. Based on the observed slow degradability and thus the low availability for cells under evaluated cell culture conditions it is tempting to speculate that the graded PDGF reservoir is only very slowly exploited during the observed culture period. Both faster release kinetics and longer observations could thus clearly reinforce MSC function and even lead to improved tissue morphogenesis.

This study was restricted to the description of the isolated mesenchymal compartment of the perivascular niche. Earlier in vitro studies have described models, which use both mesenchymal, and endothelial cells to create a perivascular niche^{47, 48}. One approach which integrated microfluidic channels and 3D fibrin encapsulation of endothelial cells and MSCs revealed an important function of laminin to control the perivascular location of MSCs in an $\alpha_6\beta_1$ integrin mediated manner⁴⁸. This finding correlates well with studies showing the perivascular location of neuronal stem cells^{46, 49} and the critical function of vascular basal membrane laminin to control MSC function by $\alpha_6\beta_1$ integrin and PDGF-BB signaling^{48, 50}. The integration of endothelial cells with herein described perivascular niche model consisting of MSCs which are exposed to stable growth factor gradients might provide a promising platform for the studying of stem cells in their perivascular niche while varying individual cellular, matrix associated or soluble bio-molecular factors.

CONCLUSION

By combining advanced biomaterials with microfluidic technology we here present the creation of a spatially-defined tissue model recapitulating mechanical properties and stable PDGF gradients of the perivascular niche. We believe that this model and its further development by the incorporation of endothelial cells will help increase our understanding of the role of MSCs in vascular function as well as the cell extrinsic cues that control their fate.

3.6 _ REFERENCES

1. Crisan, M., *et al.* Perivascular multipotent progenitor cells in human organs. *Ann N Y Acad Sci* 1176, 118-123 (2009).
2. Sacchetti, B., *et al.* Self-renewing osteoprogenitors in bone marrow sinusoids can organize a hematopoietic microenvironment. *Cell* 131, 324-336 (2007).
3. Armulik, A., Abramsson, A. & Betsholtz, C. Endothelial/pericyte interactions. *Circ Res* 97, 512-523 (2005).
4. Ferrara, N., Gerber, H.P. & LeCouter, J. The biology of VEGF and its receptors. *Nat Med* 9, 669-676 (2003).
5. Armulik, A., Genove, G. & Betsholtz, C. Pericytes: developmental, physiological, and pathological perspectives, problems, and promises. *Dev Cell* 21, 193-215 (2011).
6. Heldin, C.H. & Westermark, B. Mechanism of action and in vivo role of platelet-derived growth factor. *Physiol Rev* 79, 1283-1316 (1999).
7. Gerhardt, H. & Betsholtz, C. Endothelial-pericyte interactions in angiogenesis. *Cell Tissue Res* 314, 15-23 (2003).
8. Murray, I.R., *et al.* Natural history of mesenchymal stem cells, from vessel walls to culture vessels. *Cell Mol Life Sci* 71, 1353-1374 (2014).
9. Lutolf, M.P., Gilbert, P.M. & Blau, H.M. Designing materials to direct stem-cell fate. *Nature* 462, 433-441 (2009).
10. Discher, D.E., Mooney, D.J. & Zandstra, P.W. Growth factors, matrices, and forces combine and control stem cells. *Science* 324, 1673-1677 (2009).
11. Prewitz, M., Seib, F.P., Pompe, T. & Werner, C. Polymeric biomaterials for stem cell bioengineering. *Macromol Rapid Commun* 33, 1420-1431 (2012).
12. Ehrbar, M., *et al.* Enzymatic formation of modular cell-instructive fibrin analogs for tissue engineering. *Biomaterials* 28, 3856-3866 (2007).
13. Ehrbar, M., *et al.* Biomolecular hydrogels formed and degraded via site-specific enzymatic reactions. *Biomacromolecules* 8, 3000-3007 (2007).
14. Ehrbar, M., *et al.* Elucidating the role of matrix stiffness in 3D cell migration and remodeling. *Biophys J* 100, 284-293 (2011).
15. Lienemann, P.S., *et al.* A versatile approach to engineering biomolecule-presenting cellular microenvironments. *Adv Healthc Mater* 2, 292-296 (2013).
16. Milleret, V., Simona, B.R., Lienemann, P.S., Vörös, J. & Ehrbar, M. Electrochemical Control of the Enzymatic Polymerization of PEG Hydrogels: Formation of Spatially Controlled Biological Microenvironments. *Advanced Healthcare Materials*, n/a-n/a (2013).
17. Cushing, M.C. & Anseth, K.S. Materials science. Hydrogel cell cultures. *Science* 316, 1133-1134 (2007).
18. Tibbitt, M.W. & Anseth, K.S. Dynamic microenvironments: the fourth dimension. *Sci Transl Med* 4, 160ps124 (2012).
19. Zhu, J. Bioactive modification of poly(ethylene glycol) hydrogels for tissue engineering. *Biomaterials* 31, 4639-4656 (2010).
20. Papadimitropoulos, A., *et al.* Expansion of human mesenchymal stromal cells from fresh bone marrow in a 3D scaffold-based system under direct perfusion. *PLoS One* 9, e102359 (2014).
21. Keenan, T.M. & Folch, A. Biomolecular gradients in cell culture systems. *Lab Chip* 8, 34-57 (2008).
22. DeLong, S.A., Moon, J.J. & West, J.L. Covalently immobilized gradients of bFGF on hydrogel scaffolds for directed cell migration. *Biomaterials* 26, 3227-3234 (2005).
23. Kapur, T.A. & Shoichet, M.S. Chemically-bound nerve growth factor for neural tissue engineering applications. *J Biomater Sci Polym Ed* 14, 383-394 (2003).
24. Liu, L., Ratner, B.D., Sage, E.H. & Jiang, S. Endothelial cell migration on surface-density gradients of fibronectin, VEGF, or both proteins. *Langmuir* 23, 11168-11173 (2007).
25. Stefonek, T.J. & Masters, K.S. Immobilized gradients of epidermal growth factor promote accelerated and directed keratinocyte migration. *Wound Repair Regen* 15, 847-855 (2007).
26. Stefonek-Puccinelli, T.J. & Masters, K.S. Co-immobilization of gradient-patterned growth factors for directed cell migration. *Ann Biomed Eng* 36, 2121-2133 (2008).
27. Aizawa, Y. & Shoichet, M.S. The role of endothelial cells in the retinal stem and progenitor cell niche within a 3D engineered hydrogel matrix. *Biomaterials* 33, 5198-5205 (2012).
28. Aizawa, Y., Wylie, R. & Shoichet, M. Endothelial cell guidance in 3D patterned scaffolds. *Adv Mater* 22, 4831-4835 (2010).

29. Wylie, R.G., *et al.* Spatially controlled simultaneous patterning of multiple growth factors in three-dimensional hydrogels. *Nat Mater* 10, 799-806 (2011).
30. Ferrara, N., *et al.* Heterozygous embryonic lethality induced by targeted inactivation of the VEGF gene. *Nature* 380, 439-442 (1996).
31. Hellstrom, M., Kalen, M., Lindahl, P., Abramsson, A. & Betsholtz, C. Role of PDGF-B and PDGFR-beta in recruitment of vascular smooth muscle cells and pericytes during embryonic blood vessel formation in the mouse. *Development* 126, 3047-3055 (1999).
32. Lindahl, P., Johansson, B.R., Leveen, P. & Betsholtz, C. Pericyte loss and microaneurysm formation in PDGF-B-deficient mice. *Science* 277, 242-245 (1997).
33. Shalaby, F., *et al.* Failure of blood-island formation and vasculogenesis in Flk-1-deficient mice. *Nature* 376, 62-66 (1995).
34. Ball, S.G., Shuttleworth, C.A. & Kielty, C.M. Vascular endothelial growth factor can signal through platelet-derived growth factor receptors. *J Cell Biol* 177, 489-500 (2007).
35. Andrae, J., Gallini, R. & Betsholtz, C. Role of platelet-derived growth factors in physiology and medicine. *Genes Dev* 22, 1276-1312 (2008).
36. Carmeliet, P., *et al.* Impaired myocardial angiogenesis and ischemic cardiomyopathy in mice lacking the vascular endothelial growth factor isoforms VEGF164 and VEGF188. *Nat Med* 5, 495-502 (1999).
37. Stalmans, I., *et al.* Arteriolar and venular patterning in retinas of mice selectively expressing VEGF isoforms. *J Clin Invest* 109, 327-336 (2002).
38. Ruhrberg, C., *et al.* Spatially restricted patterning cues provided by heparin-binding VEGF-A control blood vessel branching morphogenesis. *Genes Dev* 16, 2684-2698 (2002).
39. Lindblom, P., *et al.* Endothelial PDGF-B retention is required for proper investment of pericytes in the microvessel wall. *Genes Dev* 17, 1835-1840 (2003).
40. Nguyen, D.H., *et al.* Biomimetic model to reconstitute angiogenic sprouting morphogenesis in vitro. *Proc Natl Acad Sci U S A* 110, 6712-6717 (2013).
41. Martins, M., *et al.* Activity of PLCepsilon contributes to chemotaxis of fibroblasts towards PDGF. *J Cell Sci* 125, 5758-5769 (2012).
42. Schneider, I.C. & Haugh, J.M. Quantitative elucidation of a distinct spatial gradient-sensing mechanism in fibroblasts. *J Cell Biol* 171, 883-892 (2005).
43. Ljungberg, U.K., *et al.* The interaction between different domains of staphylococcal protein A and human polyclonal IgG, IgA, IgM and F(ab')₂: separation of affinity from specificity. *Mol Immunol* 30, 1279-1285 (1993).
44. Sala, A., *et al.* Engineering 3D cell instructive microenvironments by rational assembly of artificial extracellular matrices and cell patterning. *Integr Biol (Camb)* 3, 1102-1111 (2011).
45. Carrion, B., Kong, Y.P., Kaigler, D. & Putnam, A.J. Bone marrow-derived mesenchymal stem cells enhance angiogenesis via their alpha6beta1 integrin receptor. *Exp Cell Res* 319, 2964-2976 (2013).
46. Shen, Q., *et al.* Adult SVZ stem cells lie in a vascular niche: a quantitative analysis of niche cell-cell interactions. *Cell Stem Cell* 3, 289-300 (2008).
47. Baker, B.M., Trappmann, B., Stapleton, S.C., Toro, E. & Chen, C.S. Microfluidics embedded within extracellular matrix to define vascular architectures and pattern diffusive gradients. *Lab Chip* 13, 3246-3252 (2013).
48. Carrion, B., *et al.* Recreating the perivascular niche ex vivo using a microfluidic approach. *Biotechnol Bioeng* 107, 1020-1028 (2010).
49. Tavazoie, M., *et al.* A specialized vascular niche for adult neural stem cells. *Cell Stem Cell* 3, 279-288 (2008).
50. Lin, R.Z., *et al.* Human endothelial colony-forming cells serve as trophic mediators for mesenchymal stem cell engraftment via paracrine signaling. *Proc Natl Acad Sci U S A* 111, 10137-10142 (2014).

CHAPTER 4 _ IN VITRO PLATFORMS TO ASSESS THE RECRUITMENT POTENTIAL OF GROWTH FACTOR-DELIVERING HYDROGELS ON A WOUND HEALING MODEL

This chapter is the preprint version of a manuscript in preparation.

Part of the resulting work resulted in the filing of a patent application submitted to the European Patent Office on December 22nd 2016, serial number EP16206283.

AUTHORS

Yannick R. Devaud, Vincent Milleret, Matthias P. Lütolf and Martin Ehrbar

DOCTORAL CANDIDATE'S CONTRIBUTION

The doctoral candidate accomplished the totality of this work, including experimental design, data acquisition, evaluation, figure creation and writing. Vincent Milleret contributed in the fabrication of the hydrogel gradients. Matthias Lütolf and Martin Ehrbar were the principal investigators.

4.1 _ ABSTRACT

Synthetic hydrogels are excellent materials for the presentation and delivery of growth factors (GFs), which guide cell functions and promote tissue regeneration. Currently, novel GF-functionalized hydrogels are used to test the effect of those GF on embedded microtissues and single dispersed cells. However, despite the extended use of these assays, they fail in isolating the effect of the bound and soluble factors due to the simultaneous gel formation, GF immobilization and cell embedding. Additionally, those assays are very limited in throughput, which restricts the number of simultaneous tests. Here, we use hydrogel casting methods to decouple gel formation, growth factor exposure and 3D cell encapsulation, which permits the GF loading before cell exposure and the testing of a large number of samples at the same time for an increased throughput. In this preliminary study, we first took advantage of hydrogels that were formed with surface gradients to show a correlation of cell invasion into the hydrogels with increasing amounts of soluble platelet-derived growth factor (PDGF). In a more complex wound model, we created a channel in a tissue mimic and filled it with a PDGF-loaded healing hydrogel. In this wound model, we observed the dramatic increase in cell recruitment into the PDGF-releasing healing hydrogel. While this preliminary work did not include GF immobilization, it was an essential step for the establishment of healing models that can be used to determine the nature and optimize the concentration of biological cues towards wound healing.

4.2 _ INTRODUCTION

Development of bioengineered materials in the tissue engineering and regenerative medicine field has been a topic of intense research interest in the past decades. Advances in materials science and biotechnology have led to the possibility to cultivate cells in hydrogels deprived from any biological signal.^{1,2} The properties of those biomaterials and their compatibility to a large amount of cell types make them particularly suitable for in vitro models. While 3D cell cultures have partially replaced conventional 2D assays, more work needs to be done to increase the architectural complexity of 3D cell culture models and to the further development of relevant models for the understanding of cell behaviour in vitro.

In this study, we take advantage of the properties conferred by Poly(ethylene) glycol (PEG)-hydrogels to reproduce a tissue defect and simulate its healing by the delivery of biological cues. To do so, we employed platelet-derived growth factor (PDGF), which is a strong activator of blood clot formation and wound healing process. This growth factor promotes proliferation, recruitment and stimulation of mesenchymal cells, which are essential in tissue repair.³⁻⁶ PDGF also plays an important role in the perivascular niche where it is secreted by endothelial cells, activates mesenchymal stem cells (MSCs) present in the surrounding, directs them towards the vasculature and by this contributes to the stabilization of blood vessels.⁷

The ultimate goal of an in vitro model is its use to predict in vivo functional patterns of cells or tissues. In our vision of simulating wound healing, we aim to reproduce both the wounded tissue and the material delivering the healing triggering biological cues. For in vivo applications, the binding of GF to healing materials may be of relevance as it prevents its washing out, limits its effects to the site of application, and facilitates the minimization of its concentration for efficient cell stimulation.⁸⁻¹¹ Current techniques like hydrogel encapsulation of microtissues or homogeneous 3D cell cultures have an important drawback when it comes to testing the effect of bound factors. Indeed, to discard the soluble fraction of the signals, GF attachment should be followed by extensive washing steps before cell encapsulation. This is not possible in these methods where cells are encapsulated before or simultaneously to GF attachment. Other studies show invasion of cells in gels casted prior to cell seeding. However, they use native-derived materials like hyaluronic acid¹² or collagen,¹³ which might have inherent bioactive effects on the cells.

In this work, we use a gel formation method that confers physical properties enabling cells to be seeded in 3D even after hydrogel polymerization.^{14,15} This characteristic has the advantage of decoupling gel fabrication, GF binding and cell exposure, making it a perfect tool for evaluating the effect of bound GF only. However, before investigating the effect of GF attachment, it is important to validate this cell culture platform as a quantification method for cell activity. A previous study showed the use of this gel formation technique for cultivating multiple cell types and the sequential seeding of cell populations.¹⁶ This is realized by the local inhibition of PEG polymerization at the surface of the gel, making the gel surface very soft, which enables cells to infiltrate the gel even after the gel polymerized.

Here we highlight the potential to use this platform as a tool to measure growth factor activity by quantifying cell invasion into the gels at different soluble GF concentrations. We took advantage of the rapid simultaneous fabrication of 96 gels and developed and optimized scripts to automatize image acquisition and data processing to minimize the time of experiments.

Finally, based on the same technology of polymerization inhibition, we developed a platform enabling the reproducible formation of channels in PEG hydrogels as a wound model. This channel, mimicking a wound, was then filled with another hydrogel carrying biological cues promoting wound healing. We then assessed the rate of cell recruitment and colonization inside the loaded healing gel, which can be used to quantify the capacity of bioactive candidates for promoting wound healing.

4.3 _ MATERIALS AND METHODS

CELL CULTURE

Bone marrow aspirates were obtained from healthy donors (average age 28 y.o.) after informed consent during orthopaedic surgical procedures in accordance with the local ethical committee (University Hospital Basel; Prof. Dr. Kummer; approval data 26/03/2007 Ref Number 78/07). Cells were isolated as described previously.^{17,18} Human bone marrow MSCs were cultured in minimal essential medium alpha (MEMalpha, Gibco Life Technologies, cat. no. 22571-020) supplemented with 10% (v/v) fetal calf serum (FCS, Gibco Life Technologies, cat. no. 10500), 1% (v/v) penicillin/streptomycin solution (Gibco Life Technologies, cat. no. 15140-122) and 5 ng ml⁻¹ FGF-2 (Peprotech, cat. no. 100-18B). For experiments, MSCs were cultured in the same medium without FGF-2. MSCs between passages 1 and 3 were used for all of the experiments.

PREPARATION OF PEG HYDROGEL-GRADIENT 96-WELL PLATES

Matrix metalloproteinase (MMP)-sensitive TG-PEG hydrogels functionalized with RGD were prepared based on previously described transglutaminase cross-linked PEG hydrogels.^{17,18} In brief, eight-arm PEG precursors containing the pending factor XIIIa substrate peptides glutamine acceptor (n-PEG-Gln) or lysine donor with an additional MMP-sensitive linker (n-PEG-MMP_{sensitive}-Lys) were mixed stoichiometrically (final dry mass content 1.5%) in Tris-Buffer (50 mM Tris, pH 7.6) containing 50 mM calcium chloride. 50 µM Gln-RGD peptide were added to the precursor solution prior to initiation of cross-linking by 10 U ml⁻¹ thrombin-activated factor XIIIa and vigorous mixing.

20 µl of the precursor solution was added in each of the 96-wells and electrochemical process was applied on top of the gels to inhibit the polymerization at the surface of the gel. This resulted in the simultaneous production of 96 hydrogels with cross-linking gradient. This characteristic property, more precisely described in a previous study¹⁶, makes the gels adequate for cultivating cells in 3D after gel formation.

CELL INVASION IN HYDROGEL GRADIENT

In every well, 15'000 MSCs were seeded on the hydrogel gradients in 50 µl minimal essential medium alpha supplemented with 10% FCS and 1% penicillin/streptomycin and left to adhere to the gel surface for 30 minutes. 50 µl of the same medium, complemented with growth factor (GF), was added to each well. The samples were fixed with 4% paraformaldehyde after 3 days of culture. The reaction was stopped with 0.1M glycine in phosphate-buffered saline (PBS) and the samples were washed 3 times for 5 minutes with PBS. The cells were permeabilized with 0.2% TritonX 100 in PBS for 30 minutes followed by 3 times of 5 minute washing steps with PBS. Rhodamin-phalloidin (1:300, Invitrogen, Carlsbad, CA, USA) and 4',6-diamidino-2-phenylindole (DAPI, 1 ng/ml, Sigma Aldrich, St Louis, MO, USA) in PBS were added overnight at 4°C and rinsed 3 times for 15 minutes in PBS.

Cell imaging was done using an inverted confocal microscope (Leica TCS SP5) to acquire 500µm stacks. Images were taken at 10x magnification with a 6µm step size. Cell nuclei and actin cytoskeleton signals were acquired in an automated manner for the whole plate.

Imaris® 7.7.2 (Bitplane AG, Zurich, Switzerland) was used for image processing. DAPI signal were reconstructed using the dots surpassing tool (XYZ diameter estimates = 15, 15, 25µm; Quality above 5). Statistics of those dots (XYZ position) were exported as .xls file into a self-developed MATLAB script for data analysis.

PREPARATION OF THE PDMS FRAMES

Polydimethylsiloxane (PDMS) frames were made as described previously.¹⁵ In short, the silicon elastomer and the curing agent (Sylgard 184, Dow Corning Corporation, USA) were mixed (10:1 in mass) at 2000 rpm for 3 minutes in a ARE-250 mixer (Thinky Corporation, Japan). The mixture was subsequently poured into poly(methyl methacrylate) (PMMA) molds, where 500 µm in diameter stainless steel wires were positioned to create the holes for the future electrodes. The mixture was subsequently degassed for 30 minutes in a vacuum chamber and baked for 4 h at 60°C. The stainless steel wires and the PDMS forms were removed from the PMMA molds, rinsed with isopropanol (IPA), oxygen plasma cleaned (1min at 300 W, Plasma-System 100, Technics Plasma GmbH, Germany) and finally, pressed onto plasma cleaned microscope glass cover slips.

CELL INVASION INTO WOUND HEALING MODEL

Perfusable channels with a diameter of 500µm were produced in TG-PEG hydrogels (1.7% dry mass) as described previously.¹⁵ Briefly, straightened Tungsten wires (W, 500 µm in diameter, Advent Research Materials Ltd, UK) were inserted in the PDMS forms and connected to a potentio-galvanostat in a two electrode setup (PGU-10V-1A-IMP-S and ECMwin computer interface, Elektroniklabor Peter Schrems, Germany). 60µl of complete TG-PEG hydrogel mixture containing MSCs were poured before the onset of gelation into the PDMS frame (Figure 4.3A). The polymerization of the TG-PEG was allowed to progress for 10 minutes while the Tungsten wire was anodically polarized (2 V DC, versus a Platinum auxiliary electrode). The gels were covered with 100 µl cell culture media (MEM alpha, 10% FCS, 1% P/S) and left in the incubator at 37°C overnight. 8µl of TG-PEG gel precursor solution containing 20µM of TG-DyLight™550 with or without GF, called here the "healing hydrogel", was added in the PDMS injection chamber. After 1 minute of polymerization, the Tungsten wires were removed, leading to the suction of the healing hydrogel into the channel. Another wire was inserted in the opposite side of the channel to seal the system. Cell culture media (100ul MEM alpha, 10% FCS, 1% P/S) was added only 10 minutes later to enable polymerization of the healing hydrogel in the channel. The samples were incubated for 3 days at 37°C and 5% CO₂ in a humidified atmosphere.

Cells were fixed and stained as described in the previous paragraph. Confocal microscopy was used to image 500µm gel stacks. DAPI and actin filaments were imaged to visualize the cells and DyLight550™ to localize the channel. Imaris® was used for reconstruction and image processing. The healing hydrogel was reconstructed using the surface surpassing tool on the DyLight550

signal (Surface Grain Size = $10\mu\text{m}$; Diameter of Largest Sphere = $22.7\mu\text{m}$; Manual Treshold Value = $21.7853\mu\text{m}$; Manual Treshold Value B = $58.85\mu\text{m}$; "Number of Voxels" above $8.56\text{e}5$) and DAPI signal was surpassed with the dots reconstruction tool similarly as described in the previous paragraph. DAPI signal outside of the channel reconstruction was set to zero to keep only the nuclei inside of the healing hydrogel. The recruitment index was defined as the concentration of dots inside this healing material.

4.4 _ RESULTS

4.4.1 _ HYDROGEL GRADIENTS FOR CELL ACTIVATION ASSESSMENT

The invasion of stem/progenitor cells into the wound is a critical step in the healing process.¹⁹ Thus, healing materials injected into wounds need to have the capacity to promote cell migration. Gradient hydrogels were used to establish a model to quantify cell invasion (Figure 4.1). Thanks to the simultaneous fabrication of these PEG hydrogels in a 96-well format, different PDGF concentrations could be tested at the same time under very reproducible conditions in a significant number of replicates. After 3 days of culture time, image acquisition, processing and data analysis were all implemented in a self-made program to automate the process and minimize time.

INVASION INDEX AS A PARAMETER FOR MSCs RESPONSE TO GF

First of all, we focused on the establishment of an algorithm counting the spots dispersed in the hydrogel and measured the invasion index by calculating the ratio of non-invading cells to invading cells. To discriminate between non-invading and invading cells, we defined cells present within 50µm of the surface of the gel as non-invading and the ones beneath as invading (Figure 4.1). However, due to irregularities caused during the fabrication of the 96-well plate, the hydrogels did not present a perfectly flat surface, making it impossible to define the surface coordinates. In order to tackle this problem, we subdivided each stack into 16 x 16 (=256) sub-stacks in the surface plane (Figure 4.1B). In each stack, we defined the coordinate of the sub-surface as being the average position of the first cell starting from the top of the gel. The invasion indexes were calculated for each sub-stack and added up to get the invasion index of the whole sample. We compared this method to a method without subdivision. In this case, 256 (16x16) times more cells were taken to define the surface of the whole sample. In addition, to assess the influence of the cells needed to define the surface coordinates, 4 times more cells were chosen for each method. The data in Figure 4.1C shows that the invasion indexes vary considerably depending on the method used. Without subdividing the sample, 79% and 64% were considered to be invading the hydrogel, while this index dropped to 43% and 41% when subdividing the sample. Interestingly, the number of cells taken to define the surface had a bigger impact when considering the whole sample. In this case, increasing 4 times the number of cells made the invasion index drop by 15% while this drop was only 2% in the subdivision method. Hence, the subdivision method, which is a more representative method of the local topographic variations of the gel surface, proved to bring a significant improvement in the measurements of cell invasion. It was thus validated as the method of choice for the assessment of the level of invasion on hydrogel gradients in vitro.

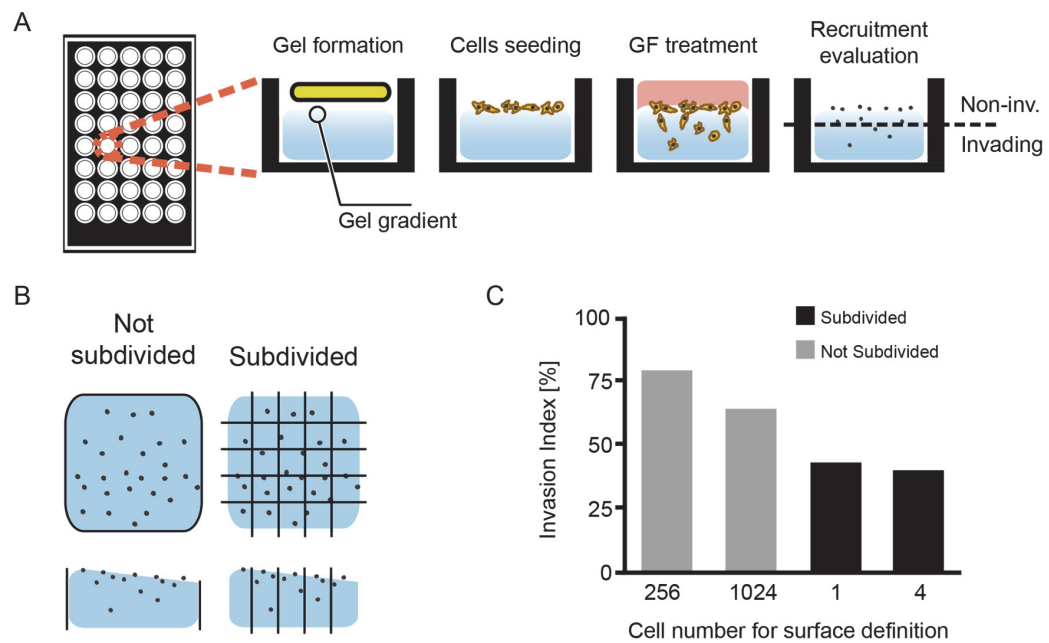


Figure 4.1. Schematic representation of the cell invasion assay on gel gradient. 96 gel gradients are formed simultaneously by electrochemistry mediated inhibition of polymerization. Cells are seeded on the gels and media with or without treatment is added to the wells. Images are acquired and numerical reconstruction is made to measure the position of cell nuclei. Data is analyzed and invasion index calculated following threshold parameters defining if cells are considered non-invading (within 50 μ m of the surface) or invading (below 50 μ m).

GF CONCENTRATION DEPENDENCE OF BM-MSCs INVASION INDEX

Next, we used this platform and the algorithm to quantify invasion dependency to GF concentration. Human BM-MSCs (15'000 cells) were seeded on each hydrogel and PDGF was added in the culture media. After 3 days in culture, in the absence of GF, only 8% of the cells invaded the gel (Figure 4.2). In opposition, the results showed a significant increase in cell invasion into the gels with higher PDGF concentrations. The invasion index raised to 20%, 29% and 32 % for 25, 50 and 100ng/ml PDGF respectively. Thanks to the hydrogel formation method and the image acquisition and data analysis, we could generate those results in a very limited amount of time for an important number of samples simultaneously. In addition, the GF concentration dependency of invasion index supported the potential of this method to measure activation potential of GF.

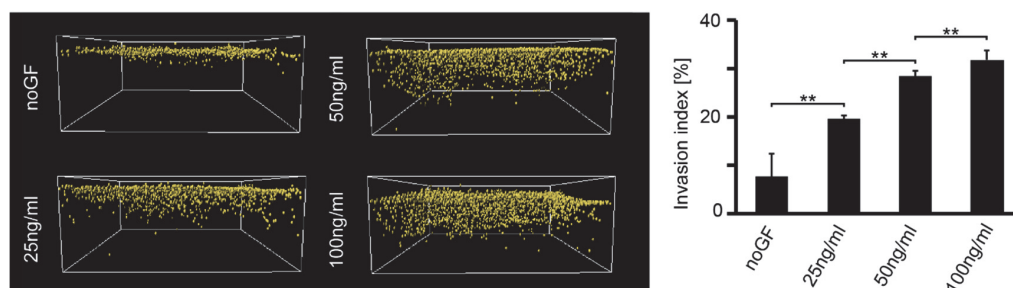


Figure 4.2. Invasion of BM-MSCs in hydrogel gradients depending on PDGF concentration. Images of the numerical reconstructions of DAPI signal by the dots surpassing tool in Imaris® depending on soluble PDGF concentration present in the medium. The white boxes represent the image stack acquired and the dense cell line is the surface of each gel gradient. Cells migrated downwards into the gel mass. The histogram shows the quantification of the invasion index for each group (n=5, **:p<0.02).

4.4.2_ HYDROGEL WOUND MODEL TO QUANTIFY HEALING POTENTIAL OF GFS

ESTABLISHMENT OF A WOUND MODEL IN PEG

While the method above was established to assess the activation potential of bioactive cues on a large number of samples in parallel, a more complex model composed of a wound mimic in a tissue model shall provide a more realistic tool to evaluate the healing potential of materials. Our approach consists cultivating cells in a hydrogel to mimic a tissue and creating a channel inside of this gel to simulate a wound, in which another hydrogel is injected as healing promoter. The way this was done is shown in Figure 4.3C-F where the steps of the procedures are schematized sequentially. First, electrochemistry is applied on a conductive rod during the polymerization of the tissue mimic. This method enables the reproducible formation of channels in hydrogels.¹⁵ The healing hydrogel (Figure 4.3C-F, red) is then placed in an injection chamber and sucked into the channel by pulling out the rod once the first signs of polymerization appear. Another rod was then added in the opposite side of the channel to confine the healing gel.

Injection of synthetic hydrogel into a pre-cultivated, cell-containing synthetic hydrogel depended on the reliable formation of the channel and the proper timing of gel perfusion and polymerization. To do so, the design and geometry of the mold showed in Figure 4.3A was carefully defined and optimized. PDMS was chosen as a support for the model because of its inert biological properties and its facile production into desired shapes. First, it contains a bottom well (Figure 4.3B, Gel-filled well) where the hydrogel tissue mimic is casted. This bottom well was designed with a small edge to prevent hydrogel adherence to the mold's walls and consequent meniscus formation and gel deformation. A second, wider well was formed on top to limit media volume to a maximum of 250 μ l (Figure 4.3B, Culture media well). Next, an injection chamber was added to the mold as inlet for the healing material (Figure 4.3B, Injection chamber). The design of this chamber contributed to the efficiency of the wound model. Indeed, the column pressure generated by the height of it contributed to the efficient suction of the healing gel into the wound mimic. The reduction of this height resulted in poor reproducibility of suction (data not shown). The injection chamber inlet was also deliberately high to keep the inlet away from the cell culture media, preventing any media residues to be mixed with the healing hydrogel precursor. Finally, the PDMS mold was mounted on a cover slip glass to enable imaging of the hydrogels. Figure 4.3B shows a cross-section of a confocal image resulting from the injection of a healing hydrogel (red) into an empty, previously formed gel (white). The image was acquired 3 days after its formation proving that the injected hydrogel polymerized and was stable inside the pre-cultivated gel. This was only reliably done thanks to the higher column of the injection chamber and when suction was done once the healing hydrogel started polymerizing. Early suction resulted in diffusion of the gel precursors and bad polymerization (data not shown).

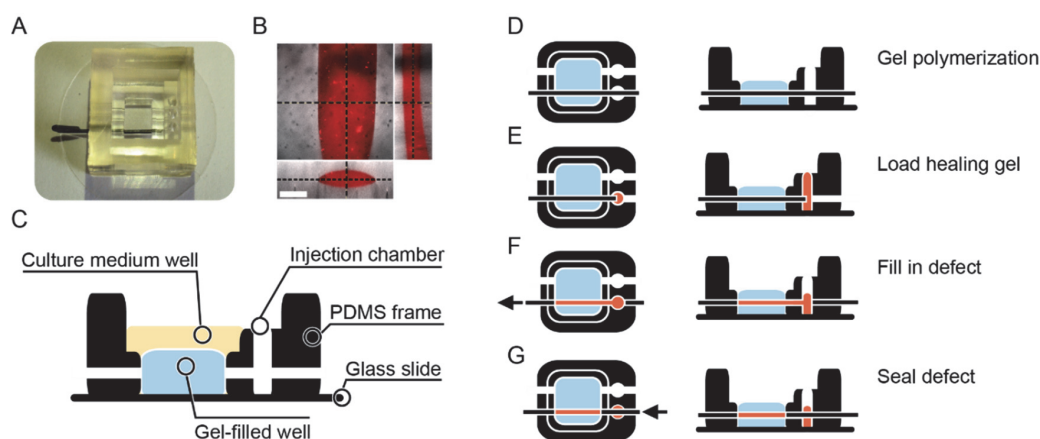


Figure 4.3. Wound healing model. A) Photo of the PDMS mold. B) Orthogonal cuts of a stack imaging acquired by confocal microscopy. In white the bulk hydrogel and in red the healing hydrogel in the channel. The fluorescent tags were covalently bound to both hydrogels during polymerization. (scale bar: 250 μ m). C) Schematic representation of the PDMS mold. D)-G) The tissue mimic (blue) is casted into the PDMS frame (black) while a current is applied on the tungsten wire (black line) during polymerization. The healing gel (red) is loaded in the loading well and polymerizes for 1 minute. Another wire is added at the open side to close the opposite access site. The tungsten wire is pushed back to suck the healing gel in and fill in the channel (i.e. wound). The opposite wire is pushed in towards the channel to seal it. (mold width = 1.5cm)

CELL RECRUITMENT POTENTIAL OF PEG HYDROGELS DELIVERING PDGF IN A WOUND MODEL

The injected gel enables the cells to be recruited from the surrounding tissue mimic into the healing hydrogel and imaging methods can then be used to quantify the level of cell recruitment. This way, one can test the potential of biological signals to promote tissue regeneration and find best candidates for wound healing. Here we inject healing hydrogels containing no or 1 ng/ μ l PDGF in a pre-cultivated tissue mimic containing 2×10^6 cells/ml. After 3 days of culture, we compared the concentration of cells present in the healing hydrogels depending on whether or not PDGF was delivered by that healing material. To do so, we used the “surpassing” method in Imaris® to reconstruct DAPI signals into spots and reconstructed the DyLight™550 signal into the healing hydrogel. We measured the recruitment concentration by counting the dots present within the reconstructed healing hydrogel and dividing by its volume. Figure 4.4A-D shows the images of the sample where no GF was delivered and Figure 4.4E-H when PDGF was delivered by the healing hydrogel. Figure 4.4A and E shows the raw image stack in a 3D projection with, in red, the DyLight™550 signal bound to the healing hydrogel and in yellow the DAPI signal from the cell nuclei. Figure 4.4B-D and 4.4F-H show the reconstructed images after exclusion of the DAPI signal not present within the healing hydrogel. The histogram in Figure 4.4 shows a significant increase in cell concentration in the presence of PDGF. The concentration was 714 ± 215 cells/mm³ when PDGF was present and 193 ± 164 cells/mm³ when an empty gel was injected. By confirming the differential activation patterns with or without PDGF, these observations attest of the feasibility and utility of our wound model as a quantification method for the recruitment potential of growth factors.

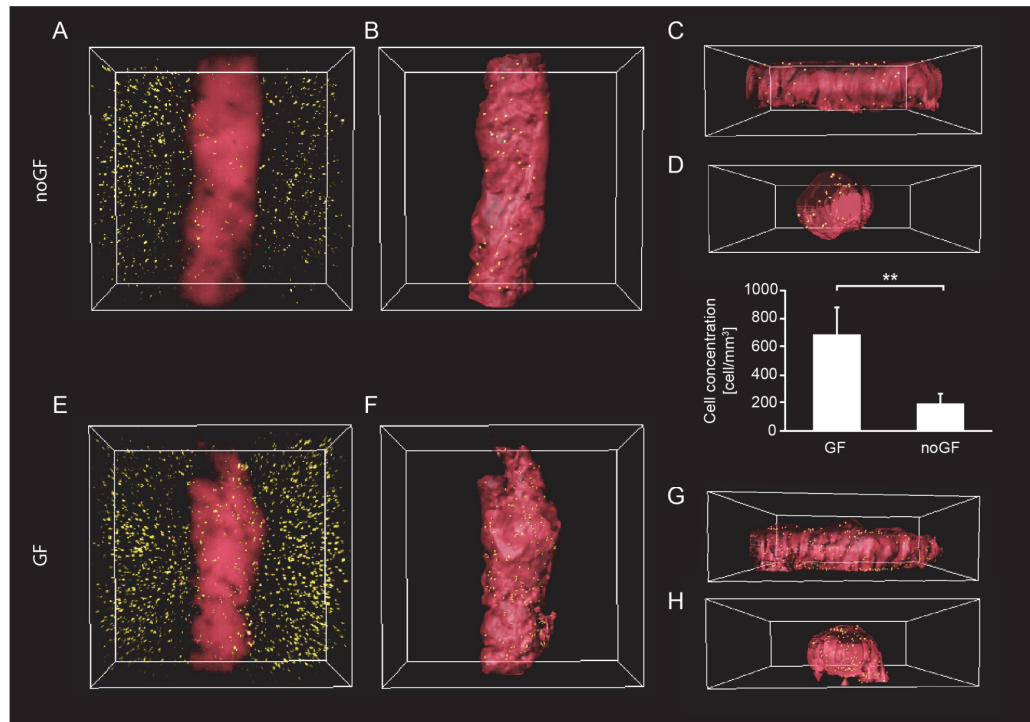


Figure 4.4. Cell recruitment into a healing hydrogel containing PDGF. A) and E) show a 500 μ m thick confocal imaging stack with the raw signals of DAPI (yellow) for cell nuclei and DyLight™550 (red) for the healing hydrogel. B) and F) are the numerical reconstruction using surface surpassing for the DyLight™550 signal and spots surpassing for the DAPI. Only the DAPI signal co-localizing with the DyLight™550 reconstruction was surpassed by spots. C) and G) represent the side view of this reconstruction. D) and H) are the front view of those stacks. A) to D) are the images of a representative sample where no GF was added, while E) to H) had 1 ng/ μ l GF loaded in the healing material. The histogram shows the cell concentration in the healing hydrogel when loaded with or without GF. (n = 6 for the GF group and n = 4 for the noGF group), mold size is 1.5x1.5mm, **:p<0.02).

4.5 _ DISCUSSION

In this study, we established two different models that succeeded in showing their efficiency in quantifying the influence of GF treatment on cell activation. PDGF concentration dependency of BM-MSC activity was used to validate our platforms by corroborating our results with the existing observations.⁴ There is no doubt about the relevance of using such platforms in tissue engineering and regenerative medicine. In a wound-healing context, the evaluation of the influence of biological cues on cell behaviour is of prime interest.

HYDROGEL GRADIENTS FOR CELL ACTIVATION ASSESSMENT

Measuring the invasion index provides to the experimenter a direct read-out on how those biological cues can affect cell migration. The data showed the potential of the gel gradient well plates to reliably quantify GF influence by correlating GF concentration and invasion index. In addition, the automation of manufacturing, image acquisition and data processing provided the ability to run a large number of samples in a limited amount of time. Indeed, 96-well gel formations were completed in 10 minutes, image acquisition ran automatically for 1 hour and data analysis occurred in a couple of seconds. This automation is extremely valuable when testing multiple bioactive cues in a statistically relevant number of replicates for a screening assay. We also showed that the data gained value by the use of our subdivision method. Indeed, without this correction, the invasion index was greatly influenced by the number of cells taken to define the overall surface and did not consider possible variation in surface topography or overall surface tilt. In this case, some cells underneath the overall surface threshold were considered as invading even though they were on the gel surface, leading to significantly higher invasion index without the subdivision method. Redefining smaller stacks helped correcting local irregularities and showed more representative results.

A significant advantage of the gel gradients resides in their characteristic uncoupling of gel formation and cell seeding. This unique feature permits the production of gels prior to cell seeding without losing the 3D cell culture property. The most logical future experimental assay would be the assessment of the influence of GF binding to the hydrogel backbone. Indeed, it is known that GF activity varies if bound to the hydrogel. The method presented could allow gel formation with covalently and/or affinity bound GF to the backbone followed by washing and cell exposure to GF. In this set-up, all non-bound GF would be discarded and the resulting cell migration would only be the consequence of the bound portion. This could be of major interest for the design of materials aiming to deliver bioactive cues at wounded sites, define their range of working concentrations and possibly tune and/or combine GF releasing kinetics for optimal cell response.

HYDROGEL WOUND MODEL TO QUANTIFY HEALING POTENTIAL OF GFs

A further step in this work consisted in combining the findings of the migration triggered by the GF treatment with a model of wound. A pre-cultivated hydrogel containing a homogeneous population of MSCs was taken as a tissue model in which a channel was formed to mimic a wound. Electrochemistry showed to be an efficient and reliable method to form those channels and enabled the suction of another PEG gel aiming to heal the wound mimic by delivering GF. The data showed that this PEG-PEG hybrid model can be a representative model for mimicking tissues, their wound and the delivery of a potential healing material. The presence of cells in the healing material attests that the cells constituting the tissue model were actively recruited by the inserted hydrogel. This data corroborated with the gel gradient model where cells invaded the gel only in the presence of GF.

This model makes possible more extensive investigation of the effect multiple GFs delivery. The combination of multiple GFs can be of relevance to mimic biological process where GF are not exposed alone, as for example shown in previous studies about blood vessel homeostasis.^{20,21} In addition, the biochemical properties of PEG hydrogels enable the binding of biological cues and the engineering of cleavage sites with different kinetic properties. This can be used as a tool to attach different GF with different binding affinities to different cleavage sites, making possible a time-dependent GF release. This could be integrated in the wound healing model presented here to assess the effect of sequential GF exposure and bring one relevant method for the fast developing trend of 4D biomaterial engineering.²²

CONCLUSION

This work succeeded in showing the potential use of the gel gradient platform for in vitro evaluation of the influence of biological cues in 3D. The possibility to run a large number of experiments in parallel pushes further the barrier of experimental design. Multiplexing, combining and repeating is now made easier even in 3D, with the advantage of being able to dissociate gel formation and cell exposure. In addition, we developed a wound model and showed the relevance of its method to simulate the delivery of biological cues at a wounded site. Both models are complementary to each other and we firmly believe that they carry serious potential for tissue engineering, regenerative medicine as well as drug screening purposes in 3D and, in the near future, in 4D.

4.6 _ REFERENCES

1. Knight, E. & Przyborski, S. Advances in 3D cell culture technologies enabling tissue-like structures to be created in vitro. *J Anat* 227, 746-756 (2015).
2. Pampaloni, F., Reynaud, E.G. & Stelzer, E.H.K. The third dimension bridges the gap between cell culture and live tissue. *Nat Rev Mol Cell Bio* 8, 839-845 (2007).
3. Kivelio, A., Ochsenbein-Koelble, N., Zimmermann, R. & Ehrbar, M. Engineered cell instructive matrices for fetal membrane healing. *Acta biomaterialia* 15, 1-10 (2015).
4. Lienemann, P.S., et al. Locally controlling mesenchymal stem cell morphogenesis by 3D PDGF-BB gradients towards the establishment of an in vitro perivascular niche. *Integr Biol-Uk* 7, 101-111 (2015).
5. Murphy, M.B., et al. Adult and umbilical cord blood-derived platelet-rich plasma for mesenchymal stem cell proliferation, chemotaxis, and cryo-preservation. *Biomaterials* 33, 5308-5316 (2012).
6. Ponte, A.L., et al. The in vitro migration capacity of human bone marrow mesenchymal stem cells: Comparison of chemokine and growth factor chemotactic activities. *Stem Cells* 25, 1737-1745 (2007).
7. Cao, R., et al. Angiogenic synergism, vascular stability and improvement of hind-limb ischemia by a combination of PDGF-BB and FGF-2. *Nat Med* 9, 604-613 (2003).
8. Macri, L., Silverstein, D. & Clark, R.A.F. Growth factor binding to the pericellular matrix and its importance in tissue engineering. *Adv Drug Deliver Rev* 59, 1366-1381 (2007).
9. Schultz, G.S. & Wysocki, A. Interactions between extracellular matrix and growth factors in wound healing. *Wound Repair Regen* 17, 153-162 (2009).
10. Fan, V.H., et al. Tethered epidermal growth factor provides a survival advantage to mesenchymal stem cells. *Stem Cells* 25, 1241-1251 (2007).
11. Martino, M.M., et al. Growth Factors Engineered for Super-Affinity to the Extracellular Matrix Enhance Tissue Healing. *Science* 343, 885-888 (2014).
12. Fisher, S.A., Anandakumaran, P.N., Owen, S.C. & Shoichet, M.S. Tuning the Microenvironment: Click-Crosslinked Hyaluronic Acid-Based Hydrogels Provide a Platform for Studying Breast Cancer Cell Invasion. *Adv Funct Mater* 25, 7163-7172 (2015).
13. Davis, G.E., Black, S.M. & Bayless, K.J. Capillary morphogenesis during human endothelial cell invasion of three-dimensional collagen matrices. *In Vitro Cell Dev Biol Anim* 36, 513-519 (2000).
14. Simona, B.R., et al. Density gradients at hydrogel interfaces for enhanced cell penetration. *Biomater Sci-Uk* 3, 586-591 (2015).
15. Milleret, V., Simona, B.R., Lienemann, P.S., Vörös, J. & Ehrbar, M. Electrochemical Control of the Enzymatic Polymerization of PEG Hydrogels: Formation of Spatially Controlled Biological Microenvironments. *Advanced healthcare materials*, n/a-n/a (2013).
16. Zhang, N., et al. Soft Hydrogels Featuring In-Depth Surface Density Gradients for the Simple Establishment of 3D Tissue Models for Screening Applications. *Slas Discov* 22, 635-644 (2017).
17. Ehrbar, M., et al. Enzymatic formation of modular cell-instructive fibrin analogs for tissue engineering. *Biomaterials* 28, 3856-3866 (2007).
18. Ehrbar, M., et al. Biomolecular hydrogels formed and degraded via site-specific enzymatic reactions. *Biomacromolecules* 8, 3000-3007 (2007).
19. Robson, M.C., Steed, D.L. & Franz, M.G. Wound healing: biologic features and approaches to maximize healing trajectories. *Curr Probl Surg* 38, 72-140 (2001).
20. Conway, E.M., Collen, D. & Carmeliet, P. Molecular mechanisms of blood vessel growth. *Cardiovasc Res* 49, 507-521 (2001).
21. Yancopoulos, G.D., et al. Vascular-specific growth factors and blood vessel formation. *Nature* 407, 242-248 (2000).
22. Tibbitt, M.W. & Anseth, K.S. Dynamic microenvironments: the fourth dimension. *Sci Transl Med* 4, 160ps124 (2012).

CHAPTER 5 _ LABEL FREE QUANTIFICATION PROTEOMICS FOR THE IDENTIFICATION OF MESENCHYMAL STEM CELL MATRISOME INSIDE 3D POLY-ETHYLENE GLYCOL HYDROGELS

This chapter is the preprint version of an article to be submitted in December 2017 to Biomaterials

AUTHORS

Yannick R. Devaud, Christian Trachsel,^f Jonas Grossmann,^f Matthias P. Lütolf, Martin Ehrbar

DOCTORAL CANDIDATE'S CONTRIBUTION

The doctoral candidate accomplished the totality of this work, comprising experimental design, data acquisition, evaluation, figure creation and writing. He benefited from the teaching, support and expertise of Christian Trachsel and Jonas Grossmann, who were responsible for the parts involving the mass spectrometer and the analysis software. They also wrote the materials and methods chapters corresponding to those two elements.

^f Functional Genomics Center Zürich, ETH Zürich, Winterthurerstrasse 190, 8057 Zürich, Switzerland

5.1 _ ABSTRACT

Synthetic hydrogels have been extensively used to recreate cellular microenvironments and to engineer tissues, yet the contribution of the cell-secreted extracellular matrix in these applications is insufficiently investigated. Cells grown in those hydrogels deposit their own extracellular matrix (ECM), providing a structural and functional environment of specific composition. Dissection of the exact composition of those engineered tissue mimics can be of importance to verify the fidelity of those in vitro models depending on the treatment provided to the cells. Here we chose a tandem mass spectrometry method (LC-MS/MS) to analyze the matrix deposited by bone marrow mesenchymal stem cells (BM-MSCs) embedded in 3D poly-ethylene glycol (PEG) hydrogel. We used a label free quantification method to determine the matrix composition following treatment with different growth factors (GFs). This study proved that LC-MS/MS is an efficient method to selectively identify the proteins deposited in 3D synthetic hydrogels. Results indicate a direct influence of GF treatment on matrix protein deposition. The protein abundance also varied significantly depending on the sequence in which the GFs were administered, raising the importance of GF choice and sequence to obtain the protein composition wanted, which is most crucial in tissue engineering applications.

5.2 _ INTRODUCTION

The extracellular matrix (ECM) is a complex network of proteins forming the environment in which the cells reside. Cells use their transmembrane proteins to adhere to this ECM, which gives them a 3D architectural support.¹⁻⁵ The attachment of the cells to ECM proteins triggers signaling pathways that are at least as important as soluble cues in influencing cell behavior and biological processes.⁶ Indeed, these proteins play an important role in cell survival, proliferation, migration and fate.⁷⁻¹³ In addition, ECM proteins can bind a number of growth factors, thereby inhibiting or increasing their activity.¹⁴⁻¹⁸ Deregulation in this tight controlled dynamic between ECM and cells has been directly linked to pathologies like marfan syndrome or cancer, which highlights the importance of a specific ECM protein composition for cell regulation and organ function.^{6,19-21} Previous studies have focused on identifying the proteins forming the ECM, also called matrisome, and classified them into two categories, the core matrisome and the matrisome associated proteins.^{22,23} The core matrisome constitutes the architectural blocks of the ECM and is split into three categories: the collagens, the glycoproteins and the proteoglycans. The collagens are mainly responsible for the tensile strength and the elasticity of the tissue.^{3,24-26} The glycoproteins play an important role in cell adhesion, signaling and GF binding. And the proteoglycans, which are glycoproteins with attached glycosaminoglycans (GAGs), help retain water in the tissue and are also known to bind growth factors.⁶

One of the goal of tissue engineering is to create 3D tissue replicates to study cell response to biological cues and to develop novel treatment approaches under controlled in vitro conditions.^{27,28} Since ECM composition has a direct influence on cell functions, gaining knowledge about the exact composition of the ECM produced by cells in 3D can be crucial for the relevance of the in vitro model. Poly-ethylene glycol (PEG) hydrogels are an example of synthetic materials developed for 3D cell culture. They have been designed to enable the experimenter to tune the cellular environment to direct cell behavior. For example, small peptides like the cell adhesion motif RGD or matrix metalloproteinase (MMP)-sensitive sites can be added to provide an ECM-like support and enable cell survival, spreading and migration without triggering any cell response.²⁹⁻³¹ One of the main advantages of PEG over other hydrogels used for 3D cell culture like Matrigel™ or collagen is its blank and biologically inert backbone. This makes PEG particularly adapted for the identification of ECM proteins in response to biological cues. Indeed, because of the absence of proteins in PEG hydrogels, the presence of proteins in the hydrogel can be attributed to the sole cell origin and allows to assign protein variation to the specific biological stimuli added to the cell cultures.^{12,30,32} Natural substrates like Matrigel™ or collagens are protein-based materials, thus, the presence of protein signals originating from the cells cannot be distinguished from the protein signals originating from the hydrogel itself. More than just in vitro platforms, hydrogels have recently been used as cell carriers for the initiation of tissue repair in vivo. One of the reason for the low success rate of those cellular therapies is caused by the low cell survival rate in the hydrogel implants.³³ This can be partly explained by the inappropriate composition of the carrier matrix. Precise definition and

reconstruction of the native cell microenvironment before implantation could thus provide those implants with a significant advantage and improve the success rate of cell therapy.

Currently, the identification of the proteins composing the cell's own ECM relies mainly on immunohistochemistry and next-generation RNA sequencing for transcriptome analysis.³⁴ The first method has the advantage of enabling visualization of intact structures in the spatial configuration of the tissue in a sensitive manner. However, it requires the targeting of specific proteins whose antibodies are available, which is an important limitation to the identification of an unknown set of proteins. In addition, fluorescent imaging is not adapted for multiplexing due to the limited number of color channels and imaging of 3D hydrogels does not allow reliable quantification of protein level variations. In opposite, transcriptome analysis has a greater sensitivity due to its amplification steps that increases signal intensity. However, the detection and quantification focuses on the messenger RNA and does not take into consideration the translation efficiency and post-transcriptional protein stability. Hence, it does not necessarily represent the real amount of proteins produced and deposited.³⁵

In recent 2D in vitro studies, tandem mass-spectrometry and label free quantification proteomics have been used to analyze the ECM produced by stem cells in a multitude of different culture conditions.³⁶⁻⁴⁰ More commonly, proteomics has also been used on native or decellularized organs to characterize the ECM composition and understand tissue organization and physiology.⁴¹⁻⁴⁸ In such studies, comparison of healthy control to "diseased" samples (e.g. aging, cancer) allow the identification of different ECM composition. This knowledge can then be used to identify new drug targets and/or therapies.^{37,38,49-53} While those experiments on native tissues have made the best use of proteomics tools, there is a lack of studies identifying and quantifying the ECM proteins present in synthetic hydrogels.

In this study, we present a label-free quantification proteomic approach to identify and quantify the ECM composition on a direct protein level. Opposed to recent work where only the culture medium was analyzed,^{54,55} we studied the ECM proteins produced and deposited by bone marrow mesenchymal stem cell (BM-MSC) inside the PEG hydrogels. We tested various culture conditions with different GF stimuli at different time points. One stimulus was transforming growth factor beta1 (TGFβ1), which is responsible for the stimulation of BM-MSCs differentiation into chondrocytes, for the inhibition of adipogenic differentiation and for modulating tissue remodeling during repair processes.^{56,57} Additionally, TGFβ1 has been reported to have a stimulating effect in ECM protein deposition in particular collagen and fibronectin.⁵⁸⁻⁶⁰ The other GF stimulus was the combination of platelet-derived growth factor (PDGF) and epidermal growth factor (EGF). Those GFs are strong metabolic activators and trigger migration and proliferation.^{56,60-63}

By deciphering the matrisome components, we could identify the building blocks of the environment created by the cells on a plain canvas and illustrate a way to influence their composition. This information is of crucial use in tissue engineering and regenerative medicine, where the fidelity of the in vitro models to the native tissue is determinant for the quality of the investigations.

5.3 _ MATERIALS AND METHODS

CELL CULTURE

Human BM-MSCs were obtained from healthy donors during orthopedic surgical procedures after informed consent and in accordance with the local ethical committee (University Hospital Basel; Prof. Dr. Kummer; approval data 26/03/2007 Ref Number 78/07). The cells were cultured in minimal essential medium α (MEM α , Gibco Life Technologies, cat. no. 22571-020) with 10% (v/v) fetal bovine serum supplement (FBS, Gibco Life Technologies, cat. no. 10500), 1% (v/v) penicillin/streptomycin (Gibco Life Technologies, cat. no. 15140-122) and 5 ng ml⁻¹ FGF-2 (Peprotech, cat. no. 100-18B). BM-MSCs at passage 2 were used for all experiments at a maximum confluence of 90%.

SINGLE CELLS ENCAPSULATION IN TG-PEG HYDROGELS

We prepared TG-PEG hydrogels as described previously.^{29,31} In brief, the two eight-arm PEG macromers (n-PEG-Gln and n-PEG-MMPsensitive-Lys) were mixed stoichiometrically for a final dry mass of 1.7% in Tris buffer (50mM, pH7.6 with 50mM calcium chloride). The adhesion peptide Gln-RGD (50 μ M) was added to the solution. BM-MSCs in MEM α , 10% FBS and 1% penicillin/streptomycin were added for a final concentration of 1.5 Mio cells per milliliter of hydrogel. Factor XIIIa (10U ml⁻¹) was then added to initiate PEG polymerization. Drops of 16 μ l of the gel preparation were then deposited in 96 well plates and the plates were rotated every 30 seconds during 4 minutes to prevent sedimentation of cells during hydrogel polymerization. After 15 minutes, 200 μ l of MEM α , 1% penicillin/streptomycin without FBS was added and the plates placed in the incubator (37°C, 5% CO₂) for 30 minutes. This media was then replaced by media supplemented with growth factors according to different treatment groups.

GROWTH FACTOR TREATMENT

We added 100 μ l of media with the selected GFs in each well. Negative control consisted of basal medium for all the groups (MEM α , 1% penicillin/streptomycin without FBS). Ascorbic acid (50 μ g/ml) was added to all the treatment groups. Total treatment time was 20 days with medium renewal every 5 days. The treatments were composed of different GF stimuli. One stimulus was transforming growth factor beta1 (TGF β 1, 100 μ g/ml) and the other was the combination of platelet-derived growth factor (PDGF, 100 μ g/ml) and epidermal growth factor (EGF, 100 μ g/ml). At the end of the treatment time, 200 μ l basal medium was added for 30 minutes to wash the gel of its soluble components.

ECM RETRIEVAL

The basal medium used for washing was discarded and 45µl of 0.05% Trypsin-EDTA (Gibco Life Technologies, cat. no. 25300-062) was added to digest the hydrogel. We pooled together 3 wells and retrieved 170µl in separate 500µl Eppendorf vials. They were then centrifuged for 10 minutes at 5000 x g to separate the cells from the hydrogel digestion. 150µl of the supernatant was taken, to which 45µl Trypsin was added overnight at room temperature to further digest the ECM protein into peptides.

CYTOSOLIC PROTEINS RETRIEVAL

SDS lysis buffer (4%(w/v) SDS, 100 mM Tris/HCL pH 8.2, 0.1M DTT) was added to the cell pellets in a 1:10 sample to buffer ratio and sonicated for 10 min. Samples were boiled for 5min at 95°C followed by 10min sonification. 30µl of sample was mixed with 200µl of urea buffer (8M urea in 100mM Tris/HCl pH 8.2) and the loaded on to Microcon – 30 filters (Merck Millipore Ltd, cat. No. MRCF0R30) by centrifugation at 14'000 x g. All following centrifugation steps were performed at 14'000 x g. Samples were washed with 200µl of urea buffer and wash solution was removed by centrifugation. Modification of Cys residues was performed by adding 100µl of 0.05M iodoacetamide in urea buffer on the filter, incubation for 1min at 600rpm and 5min w/o mixing at room temperature. Reaction solution was removed by centrifugation and samples were washed three times with 100µl of urea buffer and two times with 0.5M NaCl solution. The flow through of all steps was discarded. Filters were transferred to fresh collection tubes and 120µl of 0.05 Triethylammoniumbicarbonat containing 4ng/µl sequencing grade trypsin (Promega, cat. No. V511A) was added. Digestion was performed over night at room temperature in a wet chamber. The reaction was stopped by adding 5% TFA to a final concentration of 0.5% TFA. Peptides were harvested by centrifugation and desalted prior to mass spectrometry analysis.

ECM PEPTIDE COLLECTION AND SAMPLE PREPARATION

ECM samples were acidified by adding 5% trifluoroacetic acid (TFA) solution to a final concentration of 0.5% TFA in the sample. 25µl of 3% acetonitrile (ACN), 0.1% TFA was added to each sample prior to desalting on self-packed C18 stage tips. All following steps were performed at 2000 x g. Stage tips were cleaned 1x with 150µl 100% methanol and 1x 150µl 60% ACN/0.1%TFA by centrifugation for 1min. The stage tips were equilibrated with 2x 150µl of 3%/0.1%TFA by centrifugation for 1min. The samples were loaded in the stage tips by centrifugation for 10min followed by washing 2x with 150µl of 3% ACN/0.1%TFA. Peptide were eluted and collected into a fresh tube with 150µl of 60% ACN/0.1% TFA and centrifugation until complete stage tip dryness. The samples were dried to completeness by vacuum centrifugation and re-suspended in 16µl 3% ACN/0.1% formic acid (FA). Prior to mass spectrometry analysis this sample solution was further diluted 20x in 3% ACN/0.1% FA.

ANALYSIS BY MASS SPECTROMETRY (LC-MS/MS)

For each sample we analyzed 4 µl on a LTQ-Orbitrap Fusion mass spectrometer (Thermo Scientific) coupled to an nanoEasy LC 100 (Thermo Scientific). Full scan MS spectra were acquired from 300-1500 m/z with an automatic gain control target of 4e5, an Orbitrap resolution of 120'000 (at 200 m/z) and a maximum injection time of 50 ms. Internal mass calibration was performed using the two lock mass 371.101 m/z and 445.1200 m/z. Precursor for ms2 scans were isolated with the quadrupole with a window of 1.6 Da, an automated gain control value of 2000 and a maximum injection time of 300 ms. HCD fragments were generated using a normalized collision energy of 30 and analyzed in the linear trap using the rapid scan mode. Fragment scan were recorded with a fixed first mass of 110 m/z. Only precursors with charge states 2-7 and a signal intensity over 5000 were selected. Already fragmented ions were put onto a dynamic exclusion list for 25 seconds with an exclusion width of 10 ppm. Monoisotopic precursor selection was activated and the instrument was operated in top speed mode with a cycle time of 3 seconds. Peptide separation was achieved by RP-HPLC on C18 column (150 mm x 75 µm, 1.9 µm, Reprosil pure C-18 AQ, 120 Å (Dr. Maisch GmbH)). Column temperature was 50°C. Samples were separated over 90 minutes with a mixture of solvent A (0.1% formic acid in H₂O), solvent B (0.1% formic acid in ACN) and a flow rate of 300 nl/min, applying the following gradient table: 5-22% solvent B in 79 min, 22-32% B in 11 min. Column was cleaned after the run by 32-95% B in 2 min, hold 95% for 10 min prior to re-equilibration with initial conditions.

LABEL-FREE QUANTIFICATION AND PROTEIN QUANTIFICATION USING PROGENESIS

The raw files from the mass spectrometer were loaded into ProgenesisQ1 for Proteomics (v.3.1). Before the automatic aligning, the loading and the wash phase of the gradient were masked for peak picking, the aligning reference was chosen as such where the most features could visually be seen. From each Progenesis peptide ion (default sensitivity in peak picking) a maximum of the top five tandem mass spectra were exported using charge deconvolution and deisotoping option at a maximum number of 200 peaks per MS/MS. The Mascot generic file (.mgf) was searched with Mascot Server v.2.5.1.3 (www.matrixscience.com) using the parameters 10ppm for precursor ion mass tolerance, 0.6 Da for fragment ion tolerance. Semi-Trypsin for the hydrogel portion of the sample and Trypsin for the cell lysate was used as the protein-cleaving enzyme, two missed cleavages were allowed. Carbamidomethylation of cysteine was specified as a fixed modification, and oxidation of methionine, and N-terminal acetylation of proteins were selected as variable modifications.

Searched was a forward and reversed human database (downloaded on 18/04/2013 from uniprot) concatenated to 260 known mass spectrometry contaminants in order to evaluate the false discovery rate using the target-decoy strategy.⁶⁴

The mascot result was loaded into Scaffold v4.2.1 and filtered for 5% FDR on peptide level and 10% FDR on protein level using protein cluster analysis. The Scaffold spectrum report was exported and loaded into ProgenesisQ1.

In the experimental design, we used a between group analysis where 10 relevant experimental designs were generated. The four treatment groups were all compared to the negative control (4 experimental designs) and to each other (6 experimental designs). Each of the groups had four sample repetitions. The signal intensity was normalized by the FXIII signal, which was equally present in all the samples.

For quantification, we assessed all proteins identified with at least 2 features and calculated individually for each group the average of the normalized abundance from the 3 most intense peptide ions of each protein group.⁶⁵ This normalized quantitative protein abundance was further transformed using hyperbolic arcsine transformation prior to statistical testing with the parametric t-test. The visualization was done in R environment, where the libraries ggplot2 (v.2.2.1) and gplots (v.3.0.1) were used to generate the volcano plots and heatmaps.^{66,67}

Finally, an over-representation analysis (ORA) was done using WebGestalt 2017 on-line toolkit (Webgestalt.org) enabling the comparison of two sets of genes.⁶⁸⁻⁷⁰ Homo sapiens (hsapiens) was set as the organism of interest and geneontology as the functional database class.

5.4 _ RESULTS

5.4.1 _ PROTEOMICS TO DETECT ECM PROTEINS PRESENT IN 3D SYNTHETIC PEG HYDROGELS

OVEREXPRESSION OF MATRISOME PROTEINS IN HYDROGEL EXTRACT

3D cultured cells secrete their own ECM into a surrounding biomaterial, which results in the modification of their own microenvironment⁷¹. In this work, we aimed at investigating if cell-secreted ECM components can be directly analyzed from 3D cell cultures. Hence, we cultured BM-MSCs for two weeks in earlier described, fully defined synthetic PEG hydrogels (Figure 5.1).²⁹ After gel digestion by trypsin followed by separation of cells and residues by centrifugation, we compared the protein profiles of the separately analyzed cell lysates and hydrogel portions of the same culture.

All the data derived from Progenesis analysis. PEG hydrogels that underwent the same procedure but did not contain cells were taken as control condition for protein identification. Proteins passing our filter criteria described in the materials and methods part were considered for further analysis. Coagulation FXIII and Serum Albumin were the only proteins detected in gels without cells, originating from the culture media and the gel polymerization process.

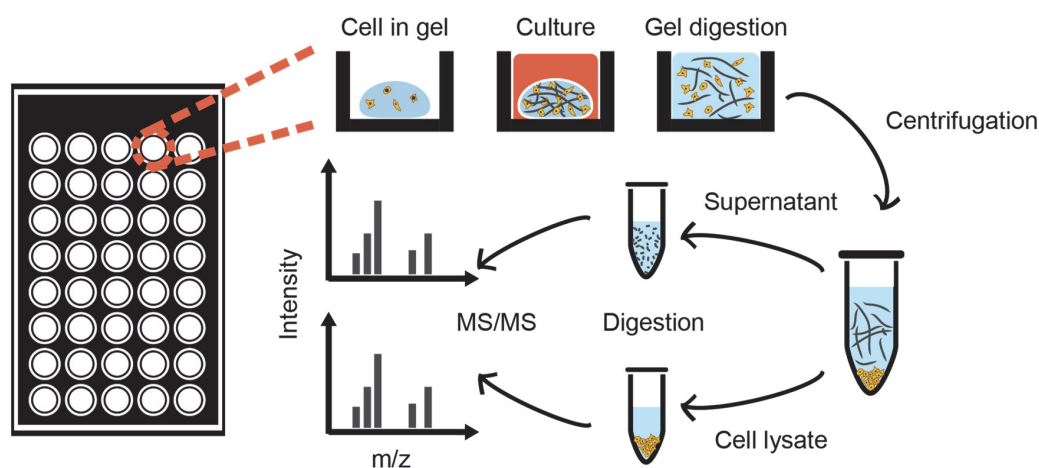


Figure 5.1. Schematic of the experimental procedure. The cells are encapsulated in a PEG gel, which is polymerized in a 96-well plate. Cell culture media with or without treatment is added to the well for the time of the experiment. At the end, the medium is replaced by Trypsin to digest the gel. Centrifugation permits the retrieval of the supernatant with the partly digested proteins fractions. Trypsin is added to the supernatant in order to obtain peptides. These are then prepared and run in the mass spectrometer. The cell fraction is lysated and protein digestion and mass spectrometry is also run on those samples.

The analysis identified 133 proteins in the gel embedding the BM-MSCs, with a protein false discovery rate (protFDR) estimated at zero because of the absence of decoy proteins. From those 133 proteins, 33 matrisome proteins were identified (24.7% of total protein count). 19 (14.2%) were core-matrisome and 14 (10.5%) were matrisome-associated proteins (Figure 5.2A). From the total signal volume detected, 37% and 13% were signal volume from the core-matrisome and matrisome-associated proteins (Figure 5.2B). Besides those matrisome proteins, proteins with cytoplasmic origin were detected as well. Their presence is the result of cell excretion and cell content leakage caused by a) apoptosis induced cell lysis during the cell culture process or b) cell lysis during sample preparation. In comparison, the analysis on the cell lysate identified 869 proteins, from which only 7% were core-matrisome (3%) or matrisome-associated (4%) proteins (Figure 5.2A). The same tendency was observed for the total signal volume where 17% and 5% originated from the total volume of matrisome proteins (Figure 5.2B).

In order to verify that the matrisome proteins found in the supernatant fraction was representative of the cell environment and not of the cell lysate, we performed an ORA analysis of the two data set. The ORA of the identified proteins against the total protein coding human genome showed a 8.79 fold enrichment over the expected value in extracellular structure organization in the hydrogel fraction. This was not the case in the cell lysate fraction where the GO term "Extracellular structure organization" was not present in top 10 enriched categories. In summary, cell lysate and hydrogel fraction show significant different protein profiles. The hydrogel fractions are highly enriched in matrisome and matrisome-associated proteins in contrast to cell lysates, which indicates that this technique can be used reliably to identify the proteins produced by BM-MSCs cultured in PEG hydrogels.

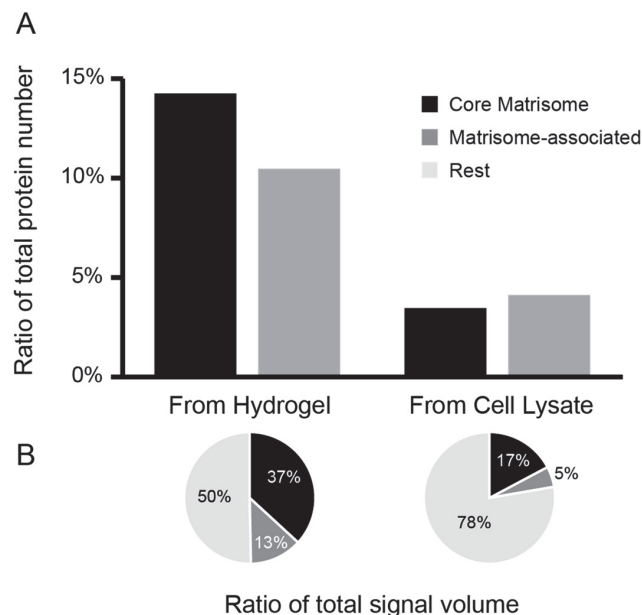


Figure 5.2. Number of proteins and ratio of total signal volume for each protein group depending on the origine (hydrogel or cell lysate digest). In black, the core matrisome proteins, in grey the matrisome-associated ones and in light grey the rest. A) Ratio of the number of core matrisome, and matrisome-associated proteins to the total amount of proteins detected. B) The ratio of the protein signal volume compared to the total signal volume.

BM-MSCs ECM SIGNATURE IN PEG HYDROGELS

From a bioengineering point of view, the composition of the ECM deposited, which likely replaces and furnishes the PEG bulk, is of great interest. Since the ECM directs the behavior, the presence or absence of one or another ECM component could potentially modify bioactivity. We here list the core matrisome and matrisome-associated proteins found after 20 days in serum-free culture media independently of the treatment. The proteins are divided into the core matrisome formed by collagens, glycoproteins and proteoglycans and the matrisome-associated proteins excreted by the cells (Table 5.1). Only the proteins identified with more than 2 peptides were taken into account. None of those proteins were in the gels without cells, which ensures that the proteins detected did not originate from the cell culture media.

Gene symbol	Protein name
Collagens	
COL1A1	Collagen 1 α 1
COL1A2	Collagen 1 α 2
COL6A1	Collagen 6 α 1
COL6A2	Collagen 6 α 2
COL6A3	Collagen 6 α 3
COL11A1	Collagen 11 α 1
COL12A1	Collagen 12 α 1
COL14A1	Collagen 14 α 1
Glycoproteins	
FN1	Fibronectin
FBLN1	Fibulin-1
TNC	Tenascin
THBS1	Thrombospondin-1
THBS2	Thrombospondin-2
POSTN	Periostin
TGFB1	Transforming growth factor- β -induced protein ig-h3
AEBP1	Adipocyte enhancer-binding protein 1
LRG1	Leucine-rich α -2-glycoprotein
Proteoglycans	
HSPG2	Heparan sulfate proteoglycan 2
VCAN	Versican
Matrisome-associated	
MMP2	72 kDa type IV collagenase
A2M	Alpha-2-macroglobulin
ANXA1	Annexin A1
ANXA2	Annexin A2
ANXA5	Annexin A5
ANXA6	Annexin A6
F13A1	Coagulation factor XIII A chain
F13B	Coagulation factor XIII B chain
LGALS1	Galectin-1
HPX	Hemopexin
LOXL1	Lysyl oxidase homolog 1
P4HA2	Prolyl 4-hydroxylase subunit α -2
HTRA1	Serine protease HTRA1
SERPINH1	Serpin H1

Table 5.1. Core matrisome and Matrisome-associated proteins expressed by BM-MSCs and identified in the hydrogel portion.

5.4.2 _ INFLUENCE OF GROWTH FACTOR EXPOSURE ON ECM DEPOSITION

A major advantage of the approach presented here resides not only in the identification of the proteins composing the ECM but also in the possibility to quantify their relative abundance. This data is exploited in this study by investigating the influence of growth factor treatments in the differential production of ECM proteins by BM-MSCs in 3D PEG hydrogels. The GFs of choice were administered separately either throughout the total 20 days of the assay or exposed sequentially during the first and then the last 10 days of the experiment. Figure 5.3 shows the two stimuli for the 4 treatments of choice in addition to the negative control. Two treatments had either TGF β 1 or PDGF/EGF throughout the 20 days of culture. The two other treatments exposed TGF β 1 and PDGF/EGF stimuli sequentially, in different orders. Due to the distinct nature of the stimuli delivered, the ECM composition pattern is expected to vary with the different treatments.

The heatmap in Figure 5.3 represents the protein abundance as an inverse hyperbolic sine transformation of the protein signal intensity. It shows the intensity for all four replicates of each group. The 33 matrisome proteins were present in all the groups. Unsupervised clustering allows clear distinction between treated and untreated samples, which is clearly visible on the heatmap. Clustering also shows a separation in the second hierarchy of the dendrogram, attesting of a difference between the groups exposed either to PDGF/EGF or to TGF β 1 in the first 10 days. Furthermore, all the treatments are grouped, besides one exception where one sample of TGF β 1 - PDGF/EGF is grouped with the TGF β 1 - TGF β 1 treatment. This indicates low variance within the treatments, which means good reproducibility of the experiments.

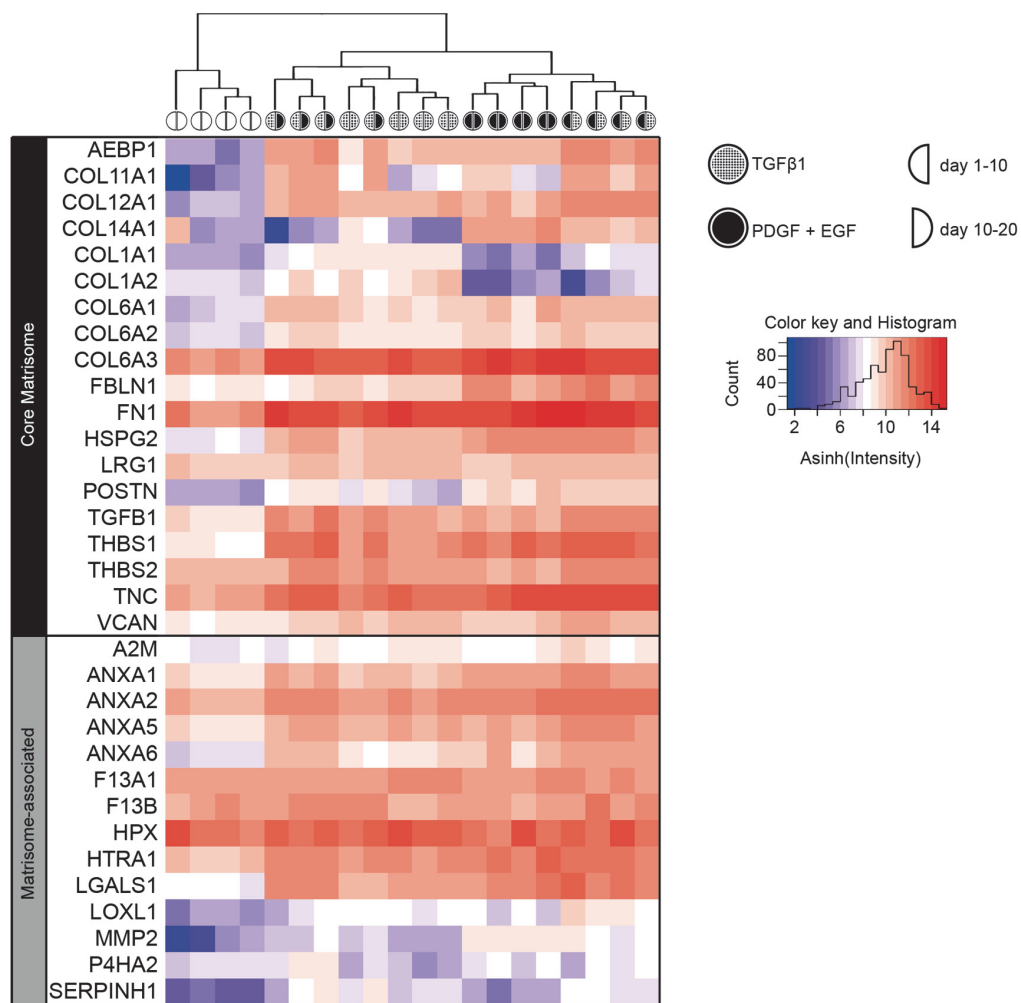


Figure 5.3. Heatmap representing asinh (signal intensity) for every matrisome protein detected. The dendrogram shows clustering of the groups by the signal intensity of the protein set. The color key and histogram represents the color assigned for each intensity level and the number of events for each of those intensities. The treatment groups are represented by a dotted filling for TGFβ1 (100ng/ml) a black filling for PDGF and EGF (100ng/ml each) and white for no treatment. Each group is composed of two sequential treatments represented by a left half-circle for the first 10 days and a right half-circle for the last 10 days of treatment.

INFLUENCE OF GROWTH FACTOR TREATMENT VERSUS NO TREATMENT

Our results clearly show that the protein abundance of cells grown without GF stimuli is much lower in comparison to cells treated with GF. A deeper statistical analysis comparing each treatment group to the negative control can quantify the increase or decrease of specific protein abundances, which could be a valuable tool to favor one treatment over another depending on the ECM composition wished. The heatmap in Figure 5.4A represents the base two logarithmic fold change in protein expression from each treatment compared to the non-treatment group. Figure 5.4B represents all 33 matrisome and matrisome-associated proteins as a volcano plot of significance versus fold change for each of the treatments compared to the negative control. We considered an expression to be significantly different when the raw fold change exceeded 2 (i.e. $\text{Log}_2(\text{fold change}) > 1$) and if the p-value was smaller than 5% (i.e. $-\text{Log}_{10}(\text{p-value}) < 1.301$).

The first observation is that 29 out of the 33 proteins have at least one treatment providing significant difference compared to the negative control. Indeed, every protein is present at least once in the significant (above horizontal grey dotted line) and differential (left or right from vertical grey dotted lines) expression panels. The 4 exceptions are LRG1, HPX, F13A1 and F13B (Figure 5.4, white box with black borders) which have no treatment significantly influencing their abundance. Looking in more details, the results provide clear input on the effect of each treatment on every protein. In total, 17 proteins are significantly influenced by all the treatments. The 12 other proteins have specific treatments providing significant change in protein abundance compared to the negative control. These are COL12A1, COL1A1, COL1A2 (Figure 5.4, blue box), COL6A2, FBLN1, HSPG2, THBS2, VCAN and MMP2, which are influenced by 3 treatments; COL6A1, by 2 treatments and finally A2M (Figure 5.4, yellow box) and P4HA2 (Figure 5.4, blue box) by one treatment out of the 4.

Interestingly, growth factor exposure does not have only an upregulating effect on ECM production. Indeed, 3 proteins are present in lower abundance in some treatment cases compared to the negative control. Those proteins are marked with a blue box and their downregulation is shown by their presence on the left side of the vertical grey dotted line. All of these 3 proteins have a specific treatment downregulating their abundance. COL1A2 is downregulated when only PDGF/EGF is administered, while in the case of P4HA2, this happens when only TGF β 1 is present. Finally, COL14A1 (Figure 5.4, blue box) can also be downregulated by exposing cells to TGF β 1 in the first part of the experiment. Interestingly, this tendency is inverted and COL14A1 is upregulated in the two other treatments. Similarly, besides when treated only with PDGF/EGF, like mentioned before, the production of COL1A2 is boosted when adding TGF β 1 first. These observations highlight the importance of treatment choice for given proteins. The significant down- and upregulation of COL1A2 and COL14A1 depending on the treatment are proofs of the differential expression triggered by growth factors, which can be determinant in the fabrication and reproduction of cellular microenvironments.

PROTEIN ABUNDANCE DEPENDING ON THE TREATMENT

In addition to studying if growth factor treatments have stimulating or inhibiting effects in ECM production compared to no treatment at all, it might be of interest to analyze variations between those treatments. This could help experimenters to choose culture conditions favoring higher or lower amount of certain type of proteins and direct specific ECM production. A first valuable information is to find the treatment favoring the larger number of proteins. By counting the number of proteins, we observe that the treatment with PDGF/EGF followed by TGF β 1 stimuli results in a total of 26 proteins present in significantly higher abundance compared to the negative control. This number drops to 23 for the PDGF/EGF – only groups, 24 for the TGF β 1 – only group and 22 for TGF β 1 followed by PDGF/EGF. Hence, PDGF/EGF followed by TGF β 1 turned out to be the treatment stimulating the larger number of different proteins.

In our premises, we hypothesized that a combination of GF might optimize ECM protein deposition thank to the complementary effects of TGF β 1, PDGF and EGF. To verify this idea, we compared the two groups composed of one stimulus only (TGF β 1 or PDGF/EGF) with the two

groups alternating those stimuli. Quantitative analysis shows that 7 proteins (COL11A1, TGFBI, AEBP1, COL12A1, ANXA5, ANXA6, and LOXL1) are in significantly higher amount when alternating GFs than when giving any of the unique GF treatments. In contrary, COL1A2, COL14A1 and MMP2 deposition is at its maximum when using one GF only. This highlights one more time the effect of the treatment choice on whether or not a protein is in higher quantity than in the negative control.

To conclude, we compared the effect of the sequence of GF exposure in the two treatments where both stimuli were administered. It is interesting to notice that, when there was a significant difference between those two treatments, the choice of PDGF/EGF before TGF β 1 always resulted in higher protein amount. As an example, COL12A1 and LOXL1 (Figure 5.4, red box) have a significantly higher upregulation when exposing to PDGF/EGF stimuli than the opposite. This point the important role not only of the combination of diverse bioactive stimuli but also from the sequence in which they are exposed.

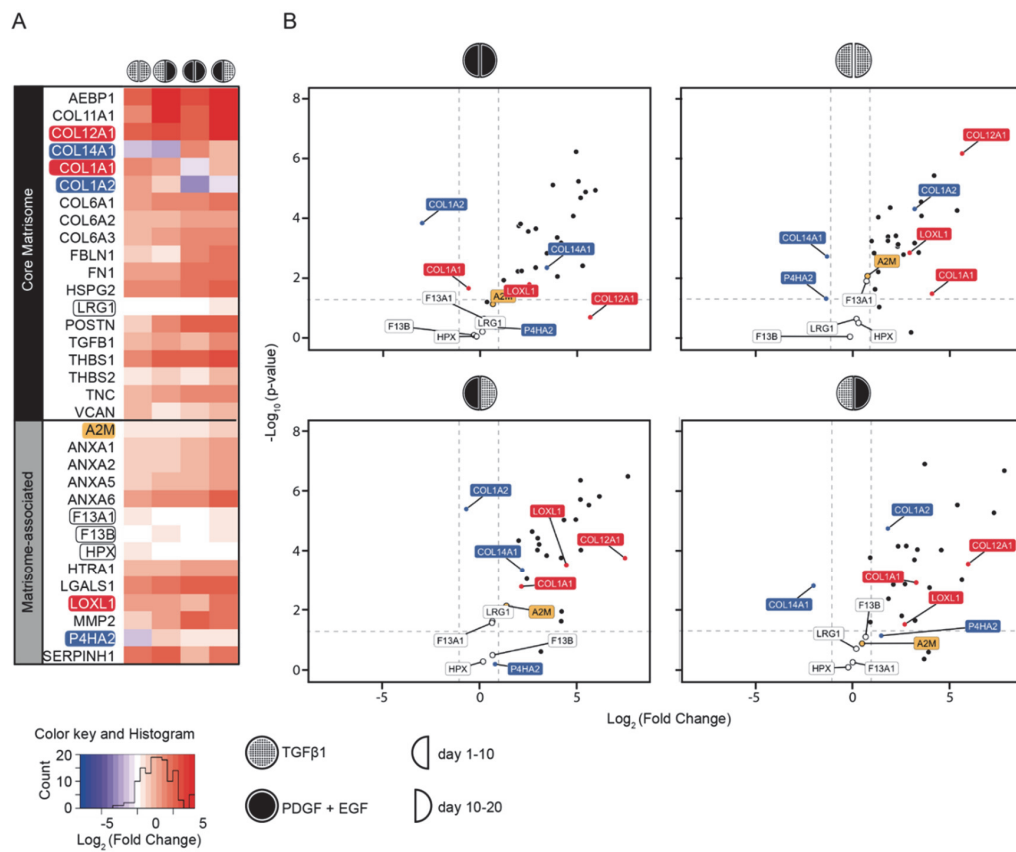


Figure 5.4. Comparative analysis of each treatment versus the negative control. A) Base 2 logarithmic fold change of protein expression for each group compared to the untreated group. The color key and histogram represents the color assigned for each change level and the number of events for each of those fold changes. B) Volcano plot to show the significance versus the fold-change in expression for the ECM proteins identified. The red horizontal line represents the threshold above which the expression is significantly different. The red vertical lines represent the threshold for 2 fold logarithmic over-(right) and under-(left) expression.

5.5 _ DISCUSSION

In this work, we successfully studied ECM deposition of cells immobilized in 3D synthetic hydrogels with an unbiased proteomics approach. This method enabled to tackle important limitations encountered with more classic approaches. A critical factor that contributed to the success of this study was the use of materials that did not generate background signal. The use of synthetic PEG hydrogels as cell carriers was perfectly suited to this application. The absence of protein, besides FXIII as the polymer linker enzyme, ensured no contribution of the cell carrier to the peptide signals detected by the mass spectrometer. In addition, the biologically inert characteristics of this material discarded the possibility of inherent cell stimulation. The use of alternative materials like for example Matrigel™ would completely jeopardize the possibility to detect proteins produced by cells. Indeed, Matrigel™ is a naturally derived material widely used in cell culture *in vitro* but has been shown to be made of hundreds of proteins.⁷² Proteomics analysis in these conditions is technically possible but the inherent presence of all these proteins would generate an important background signal originating from the gel itself as well as from the cell production stimulated by the proteins contained in the gel. In result, the peptides detected would be impossible to be assigned to the sole induction by the biological stimuli provided by the experimenter. Moreover, the use of FBS-free culture media prevented the contamination of the cell environment with proteins present in FBS. It also avoided the contribution of biological stimuli contained in the medium, which could have provoked alternative signals not originating from the treatment added.

To demonstrate our approach, we first proved that we could selectively analyze the environment created by the cells themselves in 3D synthetic hydrogel cultures. Indeed, the ORA and the signal distribution analysis showed a strong enrichment of ECM proteins when analyzing only the hydrogel component of the samples. This contrasted to the analysis of the cell lysate where ECM proteins were not overexpressed compared to theoretical expected expression rates. This did not only show that our samples contain mainly ECM proteins but also excluded the hypothesis that the proteins originate from the cell lysate residues.

The list of identified core-matrisome proteins was comparable to the results shown previously in 2D BM-MSC cultures, which supports the claim that our method can reliably be used in 3D.³⁶ The majority of the proteins were detected in all conditions with changing abundance. For example, FN1 was present in all conditions, including in the negative control. This protein is known to be present in almost all tissues and its deposition happens at very early stages in ECM production and plays a crucial role in the initiation of matrix assembly.⁷³ Its ability to bind growth factors, including PDGF and TGFβ1, could modulate the availability of those biological cues and possibly explain biological processes.¹⁴ The matrisome-associated protein excretion was mainly composed of proteases involved in tissue remodeling and wound healing (MMP2, HTRA1, ANXA), protease inhibitor (A2M), Collagen binding and/or catalysis (LOXL1, P4HA2, SERPINH1) and cell proliferation (LGALS1). As expected, coagulation factor XIII was also present since this enzyme was used for PEG polymerization.

Besides the identification of a relevant set of ECM proteins in all samples, we could also observe differential protein composition in the hydrogels as well as significant fold change variations in protein abundance depending on the treatment provided. This outcome suggests that the label-free quantification method can be of high relevance when aiming to reproduce an ECM with precise composition. For example, COL1A1 was only upregulated in the presence of TGF β 1 and the same tendency is observed for COL1A2, which is significantly downregulated in the absence of TGF β 1. This observation corroborates with previous observations in literature, which attributes the production of COL1 to the effect of TGF β 1⁵⁸⁻⁶⁰. Hence, the addition of this growth factor in cell culture media appears to be a requirement to maximize COL1A1 deposition. This can be of relevance when developing tendon, dermis, bone, cartilage or sclerotic tissue mimics, where COL1 is preferentially synthesized.⁷⁴

Another interesting observation resulting from this study is the opposite effect that some treatment have. This is the case for COL14A1, which was significantly upregulated in the cases where PDGF/EGF stimuli was delivered first and downregulated when TGF β 1 was given at the beginning. This protein is reported to act as a regulating protein in fibrin growth in developing tendon⁷⁵ and is present in most of the COL1 containing tissues.⁷⁶ This could indicate a possible interaction between those two proteins and speak in favor of a treatment promoting both proteins instead of just one. However, our results also suggests that some treatments have a stimulating effect on some proteins while having an inhibiting effect on others. Interestingly, this is the case for those two proteins mentioned above, COL14A1 and COL1. Our data show that a simultaneous upregulation of COL1A1, COL1A2 and COL14A1 cannot be done with the treatments administered. Treatments increasing COL1A1 and COL1A2 both inhibit the production of COL14A1. In opposition, upregulation of COL14A2 is accompanied by either downregulation of COL1A2 or upregulation of COL1A1. Hence, upregulation of the three proteins is, based on our results, not possible. Depending on the composition wanted, this could be a critical information towards the addition or not of a specific stimulus and to provide awareness about the compromises imposed by the choice of a treatment.

Finally, our analysis enabled to highlight the importance of the combination of growth factors and the sequence in which the cells are exposed to them. COL11A1, TGF β 1, AEBP1, COL12A1, ANXA5, ANXA6, and LOXL1 expression was upregulated when altering the treatments after 10 days and overall protein production was significantly increased when PDGF/EGF were administered first. This observation could be used in the future for approaches where the temporal control of signal presentation is addressed to explore the 4th dimension of tissue engineering. For example, click, clip and caging strategies enable to selectively bind, remove or make bioactive molecules available in a time-controlled manner.⁷⁷ Alternatively, the release of growth factors could be controlled by incorporating biological signals to the PEG backbone containing cleavage motifs with different cleavage kinetics. This way, growth factors are released by proteinases produced by the own cells and the release kinetics is controlled by the enzyme affinity of the cleavage motifs specific to each growth factor added.

CONCLUSION

The careful analysis of the protein level, depending on the treatment, enables the deciphering of the ECM replacing the PEG hydrogel scaffold, after a time in culture and provides a relevant method for building on-demand customized cellular environments. We showed that state of the art proteomics analysis tools could be used to analyze the complex environment deposited by the cells in relevant 3D platforms. This could be helpful for mimicking tissues as faithfully as possible for in vitro studies, drug screening and discovery platforms. Additionally, deciphering the native environment and directing the reproduction of it could provide in vivo implants with an environment that enhances the survival of the implanted cells and consequently improves their action on the host tissue.

5.6 _ REFERENCES

1. Engel, J. & Chiquet, M. *An Overview of Extracellular Matrix Structure and Function*, (Springer-Verlag Berlin, Heidelberger Platz 3, D-14197 Berlin, Germany, 2011).
2. Mager, M.D., LaPointe, V. & Stevens, M.M. Exploring and exploiting chemistry at the cell surface. *Nat Chem* 3, 582-589 (2011).
3. Rhodes, J.M. & Simons, M. The extracellular matrix and blood vessel formation: not just a scaffold. *J Cell Mol Med* 11, 176-205 (2007).
4. Stevens, M.M. & George, J.H. Exploring and engineering the cell surface interface. *Science* 310, 1135-1138 (2005).
5. Xu, J. & Mosher, D. *Fibronectin and Other Adhesive Glycoproteins*, (Springer-Verlag Berlin, Heidelberger Platz 3, D-14197 Berlin, Germany, 2011).
6. Hynes, R.O. The extracellular matrix: not just pretty fibrils. *Science* 326, 1216-1219 (2009).
7. Kubow, K.E., *et al.* Crosslinking of cell-derived 3D scaffolds up-regulates the stretching and unfolding of new extracellular matrix assembled by reseeded cells. *Integr Biol (Camb)* 1, 635-648 (2009).
8. Lin, F., *et al.* Fibronectin growth factor-binding domains are required for fibroblast survival. *J Invest Dermatol* 131, 84-98 (2011).
9. Singh, P. & Schwarzbauer, J.E. Fibronectin and stem cell differentiation - lessons from chondrogenesis. *J Cell Sci* 125, 3703-3712 (2012).
10. Wijelath, E.S., *et al.* Heparin-II domain of fibronectin is a vascular endothelial growth factor-binding domain: enhancement of VEGF biological activity by a singular growth factor/matrix protein synergism. *Circ Res* 99, 853-860 (2006).
11. Yamada, Y., Hozumi, K. & Nomizu, M. Construction and Activity of a Synthetic Basement Membrane with Active Laminin Peptides and Polysaccharides. *Chem-Eur J* 17, 10500-10508 (2011).
12. Zhu, J.M. Bioactive modification of poly(ethylene glycol) hydrogels for tissue engineering. *Biomaterials* 31, 4639-4656 (2010).
13. Guilak, F., *et al.* Control of Stem Cell Fate by Physical Interactions with the Extracellular Matrix. *Cell Stem Cell* 5, 17-26 (2009).
14. Martino, M.M. & Hubbell, J.A. The 12th-14th type III repeats of fibronectin function as a highly promiscuous growth factor-binding domain. *FASEB J* 24, 4711-4721 (2010).
15. Ramirez, F. & Rifkin, D.B. Extracellular microfibrils: contextual platforms for TGFbeta and BMP signaling. *Curr Opin Cell Biol* 21, 616-622 (2009).
16. Sarrazin, S., Lamanna, W.C. & Esko, J.D. Heparan sulfate proteoglycans. *Cold Spring Harb Perspect Biol* 3(2011).
17. Macri, L., Silverstein, D. & Clark, R.A.F. Growth factor binding to the pericellular matrix and its importance in tissue engineering. *Adv Drug Deliver Rev* 59, 1366-1381 (2007).
18. Schultz, G.S. & Wysocki, A. Interactions between extracellular matrix and growth factors in wound healing. *Wound Repair Regen* 17, 153-162 (2009).
19. Lu, P., Takai, K., Weaver, V.M. & Werb, Z. Extracellular matrix degradation and remodeling in development and disease. *Cold Spring Harb Perspect Biol* 3(2011).
20. Munger, J.S. & Sheppard, D. Cross Talk among TGF-beta Signaling Pathways, Integrins, and the Extracellular Matrix. *Csh Perspect Biol* 3(2011).
21. Yurchenco, P.D. Basement Membranes: Cell Scaffoldings and Signaling Platforms. *Csh Perspect Biol* 3(2011).
22. Naba, A., *et al.* The extracellular matrix: Tools and insights for the "omics" era. *Matrix Biol* 49, 10-24 (2016).
23. Hynes, R.O. & Naba, A. Overview of the Matrisome-An Inventory of Extracellular Matrix Constituents and Functions. *Csh Perspect Biol* 4(2012).
24. Kadler, K.E., Baldock, C., Bella, J. & Boot-Handford, R.P. Collagens at a glance. *Journal of Cell Science* 120, 1955-1958 (2007).
25. Birk, D.E. & Brueckner, P. *Collagens, Suprastructures, and Collagen Fibril Assembly*, (Springer-Verlag Berlin, Heidelberger Platz 3, D-14197 Berlin, Germany, 2011).
26. Kozel, B.A., Mecham, R.P. & Rosenbloom, J. *Elastin*, (Springer-Verlag Berlin, Heidelberger Platz 3, D-14197 Berlin, Germany, 2011).
27. Knight, E. & Przyborski, S. Advances in 3D cell culture technologies enabling tissue-like structures to be created in vitro. *J Anat* 227, 746-756 (2015).

28. Pampaloni, F., Reynaud, E.G. & Stelzer, E.H.K. The third dimension bridges the gap between cell culture and live tissue. *Nat Rev Mol Cell Bio* 8, 839-845 (2007).
29. Ehrbar, M., et al. Enzymatic formation of modular cell-instructive fibrin analogs for tissue engineering. *Biomaterials* 28, 3856-3866 (2007).
30. Lutolf, M.P. & Hubbell, J.A. Synthetic biomaterials as instructive extracellular microenvironments for morphogenesis in tissue engineering. *Nat Biotech* 23, 47-55 (2005).
31. Ehrbar, M., et al. Biomolecular hydrogels formed and degraded via site-specific enzymatic reactions. *Biomacromolecules* 8, 3000-3007 (2007).
32. Ehrbar, M., et al. Elucidating the Role of Matrix Stiffness in 3D Cell Migration and Remodeling. *Biophysical Journal* 100, 284-293 (2011).
33. Emgard, M., Karlsson, J., Hansson, O. & Brundin, P. Patterns of cell death and dopaminergic neuron survival in intrastriatal nigral grafts. *Exp Neurol* 160, 279-288 (1999).
34. Ren, J.Q., et al. Global transcriptome analysis of human bone marrow stromal cells (BMSC) reveals proliferative, mobile and interactive cells that produce abundant extracellular matrix proteins, some of which may affect BMSC potency. *Cytotherapy* 13, 661-674 (2011).
35. de Sousa Abreu, R., Penalva, L.O., Marcotte, E.M. & Vogel, C. Global signatures of protein and mRNA expression levels. *Mol Biosyst* 5, 1512-1526 (2009).
36. Ragelle, H., et al. Comprehensive proteomic characterization of stem cell-derived extracellular matrices. *Biomaterials* 128, 147-159 (2017).
37. Ji, Y.H., et al. Quantitative proteomics analysis of chondrogenic differentiation of C3H10T1/2 mesenchymal stem cells by iTRAQ labeling coupled with on-line two-dimensional LC/MS/MS. *Mol Cell Proteomics* 9, 550-564 (2010).
38. Georgi, N., et al. Differentiation of Mesenchymal Stem Cells under Hypoxia and Normoxia: Lipid Profiles Revealed by Time-of-Flight Secondary Ion Mass Spectrometry and Multivariate Analysis. *Anal Chem* 87, 3981-3988 (2015).
39. Brown, L.A., Sava, P., Garcia, C. & Gonzalez, A.L. Proteomic Analysis of the Pericyte Derived Extracellular Matrix. *Cell Mol Bioeng* 8, 349-363 (2015).
40. Harvey, A., Yen, T.Y., Aizman, I., Tate, C. & Case, C. Proteomic analysis of the extracellular matrix produced by mesenchymal stromal cells: implications for cell therapy mechanism. *PLoS One* 8, e79283 (2013).
41. Hill, R.C., Calle, E.A., Dzieciatkowska, M., Niklason, L.E. & Hansen, K.C. Quantification of Extracellular Matrix Proteins from a Rat Lung Scaffold to Provide a Molecular Readout for Tissue Engineering. *Molecular & Cellular Proteomics* 14, 961-973 (2015).
42. Calle, E.A., et al. Targeted proteomics effectively quantifies differences between native lung and detergent-decellularized lung extracellular matrices. *Acta biomaterialia* 46, 91-100 (2016).
43. Goddard, E.T., et al. Quantitative extracellular matrix proteomics to study mammary and liver tissue microenvironments. *Int J Biochem Cell B* 81, 223-232 (2016).
44. Johnson, T.D., et al. Quantification of decellularized human myocardial matrix: A comparison of six patients. *Proteom Clin Appl* 10, 75-83 (2016).
45. Li, Q.Y., et al. Proteomic analysis of naturally-sourced biological scaffolds. *Biomaterials* 75, 37-46 (2016).
46. Barallobre-Barreiro, J., et al. Proteomics Analysis of Cardiac Extracellular Matrix Remodeling in a Porcine Model of Ischemia/Reperfusion Injury. *Circulation* 125, 789-802 (2012).
47. Didangelos, A., et al. Proteomics Characterization of Extracellular Space Components in the Human Aorta. *Molecular & Cellular Proteomics* 9, 2048-2062 (2010).
48. Rizzo, D.G., Prentice, B.M., Moore, J.L., Norris, J.L. & Caprioli, R.M. Enhanced Spatially Resolved Proteomics Using On-Tissue Hydrogel Mediated Protein Digestion. *Anal Chem* 89, 2948-2955 (2017).
49. Naba, A., et al. The Matrisome: In Silico Definition and In Vivo Characterization by Proteomics of Normal and Tumor Extracellular Matrices. *Molecular & Cellular Proteomics* 11 (2012).
50. Huertas, A.C.M., Schmelzer, C.E.H., Hoehenwarter, W., Heyroth, F. & Heinz, A. Molecular-level insights into aging processes of skin elastin. *Biochimie* 128, 163-173 (2016).
51. Hakimi, O., Ternette, N., Murphy, R., Kessler, B.M. & Carr, A. A quantitative label-free analysis of the extracellular proteome of human supraspinatus tendon reveals damage to the pericellular and elastic fibre niches in torn and aged tissue. *Plos One* 12 (2017).
52. Peffers, M.J., et al. Proteomic Analysis Reveals Age-related Changes in Tendon Matrix Composition, with Age- and Injury-specific Matrix Fragmentation. *J Biol Chem* 289, 25867-25878 (2014).
53. Xiao, Z., Blonder, J., Zhou, M. & Veenstra, T.D. Proteomic analysis of extracellular matrix and vesicles. *J Proteomics* 72, 34-45 (2009).
54. Schneider, M.C., Barnes, C.A. & Bryant, S.J. Characterization of the chondrocyte secretome in photoclickable poly(ethylene glycol) hydrogels. *Biotechnol Bioeng* 114, 2096-2108 (2017).

55. Swartzlander, M.D., *et al.* Linking the foreign body response and protein adsorption to PEG-based hydrogels using proteomics. *Biomaterials* 41, 26-36 (2015).
56. Ng, F., *et al.* PDGF, TGF-beta, and FGF signaling is important for differentiation and growth of mesenchymal stem cells (MSCs): transcriptional profiling can identify markers and signaling pathways important in differentiation of MSCs into adipogenic, chondrogenic, and osteogenic lineages. *Blood* 112, 295-307 (2008).
57. Robson, M.C., Steed, D.L. & Franz, M.G. Wound healing: biologic features and approaches to maximize healing trajectories. *Curr Probl Surg* 38, 72-140 (2001).
58. Ignatz, R.A. & Massague, J. Transforming Growth-Factor-Beta Stimulates the Expression of Fibronectin and Collagen and Their Incorporation into the Extracellular-Matrix. *J Biol Chem* 261, 4337-4345 (1986).
59. Arnold, U., Lindenhayn, K. & Perka, C. In vitro-cultivation of human periosteum derived cells in bioresorbable polymer-TCP-composites. *Biomaterials* 23, 2303-2310 (2002).
60. Kivellio, A., Ochsenbein-Koelble, N., Zimmermann, R. & Ehrbar, M. Engineered cell instructive matrices for fetal membrane healing. *Acta biomaterialia* 15, 1-10 (2015).
61. Lienemann, P.S., *et al.* Locally controlling mesenchymal stem cell morphogenesis by 3D PDGF-BB gradients towards the establishment of an in vitro perivascular niche. *Integr Biol-Uk* 7, 101-111 (2015).
62. Ponte, A.L., *et al.* The in vitro migration capacity of human bone marrow mesenchymal stem cells: Comparison of chemokine and growth factor chemotactic activities. *Stem Cells* 25, 1737-1745 (2007).
63. Murphy, M.B., *et al.* Adult and umbilical cord blood-derived platelet-rich plasma for mesenchymal stem cell proliferation, chemotaxis, and cryo-preservation. *Biomaterials* 33, 5308-5316 (2012).
64. Kall, L., Storey, J.D., MacCoss, M.J. & Noble, W.S. Assigning significance to peptides identified by tandem mass spectrometry using decoy databases. *J Proteome Res* 7, 29-34 (2008).
65. Grossmann, J., *et al.* Implementation and evaluation of relative and absolute quantification in shotgun proteomics with label-free methods. *Journal of Proteomics* 73, 1740-1746 (2010).
66. Gregory R Warnes, B.B., Lodewijk Bronebakker, Bill Venables. gplots: Various R programming tools for plotting data. *R package version 2.4.1* (2009).
67. Team, R.C. R: A language and environment for statistical computing. *R Foundation for Statistical Computing, Vienna, Austria* (2013).
68. Wang, J., Duncan, D., Shi, Z. & Zhang, B. WEB-based GENE SeT Analysis Toolkit (WebGestalt): update 2013. *Nucleic Acids Res* 41, W77-W83 (2013).
69. Wang, J., Vasaikar, S., Shi, Z., Greer, M. & Zhang, B. WebGestalt 2017: a more comprehensive, powerful, flexible and interactive gene set enrichment analysis toolkit. *Nucleic Acids Res* 45, W130-W137 (2017).
70. Zhang, B., Kirov, S. & Snoddy, J. WebGestalt: an integrated system for exploring gene sets in various biological contexts. *Nucleic Acids Res* 33, W741-W748 (2005).
71. Bryant, S.J. & Anseth, K.S. Hydrogel properties influence ECM production by chondrocytes photoencapsulated in poly(ethylene glycol) hydrogels. *J Biomed Mater Res* 59, 63-72 (2002).
72. Hughes, C.S., Postovit, L.M. & Lajoie, G.A. Matrigel: A complex protein mixture required for optimal growth of cell culture. *Proteomics* 10, 1886-1890 (2010).
73. Schwarzbauer, J.E. & DeSimone, D.W. Fibronectins, Their Fibrillogenesis, and In Vivo Functions. *Csh Perspect Biol* 3(2011).
74. Karsenty, G. & Park, R.W. Regulation of type I collagen genes expression. *Int Rev Immunol* 12, 177-185 (1995).
75. Young, B.B., Gordon, M.K. & Birk, D.E. Expression of type XIV collagen in developing chicken tendons: association with assembly and growth of collagen fibrils. *Dev Dyn* 217, 430-439 (2000).
76. Walchli, C., Koch, M., Chiquet, M., Odermatt, B.F. & Trueb, B. Tissue-specific expression of the fibril-associated collagens XII and XIV. *J Cell Sci* 107 (Pt 2), 669-681 (1994).
77. Tibbitt, M.W. & Anseth, K.S. Dynamic microenvironments: the fourth dimension. *Sci Transl Med* 4, 160ps124 (2012).

CHAPTER 6 _ CONCLUSION

6.1 _ GENERAL DISCUSSION

The essence of this thesis was to develop a strategy for the healing of fetal membranes and prevent their rupture after fetoscopic interventions. To achieve that long-term goal, we worked on two very different aspects. On one hand, we developed a medical device for the minimal invasive delivery of injectable materials. On the other hand, we worked on the development of healing promoting materials as well as on methods that enable the assessment of their biological functions in a more basic research approach. In total, our work resulted in one peer reviewed publication, two manuscripts to be submitted in 2017, two patent applications and the funding of three grants.

6.1.1 _ DEVICE FOR PRECISE DELIVERY OF SEALING MATERIAL ON AN EX VIVO MODEL

The goal of objective 1 was to develop a minimally invasive implantable device and to test its functionality on a model reproducing fetal membrane injury ex vivo. This was described in Chapter 2. As a result, we managed to design and produce a prototype respecting all the requirements in terms of size and functionality to be compatible with the fetoscopic instruments used in the clinics. We showed that nitinol covered with a Degrapol® mesh could reliably be crimped into the accession catheter, pushed inside a cavity and deployed automatically into the shape configuration set. We then demonstrated that this umbrella-shaped receptor could efficiently be used as a tool for gathering any type of materials at the precise site of membrane defect. Indeed, the use of multiple glues (one component cyanoacrylate glue, two components fibrin and mussel glue), indicates that our device is adapted to materials of different natures. Our choice for testing mussel glue in wet conditions was motivated by recent evidence of its efficient adhesion ability.¹⁻⁴ Despite the low adhesion strength of mussel glue, its gluing ability was confirmed as it retained the receptor at the puncture site in the ex vivo model. However, the choice of adhesives is not limited to mussel glue. Alternative gluing materials, whose poor application efficiency was a limiting factor in previous studies,⁵⁻¹⁰ could take advantage of our device to be applied precisely at the defect site.

Next, we established an ex vivo replica with realistic physiological conditions, which enabled us to demonstrate the feasibility of our method on a clinically relevant model. The mechanical stability conferred by the multiple porcine and human tissue layers highlighted the importance of the quality of the model for a reliable assessment of our method. The watertight installation of the model enabled the recreation of a wet environment and allowed for an increase in fidelity towards the analogy with a real surgical set-up. In addition, we took advantage of our model system to add external inlets which enabled image retransmission from the inside of the amniotic cavity replicate for direct visual feedback.

As a result of our work, we submitted a European patent application on this technology on September 29th 2016. The potential of such technology was acknowledged by multiple instances confirming the potential translational impact that it could have on thousands of fetuses and families around the world. Indeed, a project proposal for further development was granted by the Commission for Technology and Innovation (CTI) and a Swiss National Science Foundation (SNF) grant was attributed in October 2016 based on the advances realized during this project. Further research will definitely help the domain of fetal surgery that suffers from the debilitating high rate of preterm birth and would open a new horizon in minimally invasive surgery by permitting interventions for indications which have been ignored until now.

6.1.2 _ HYDROGEL PLATFORMS TO STUDY HEALING INDUCING CUES IN VITRO

The specific objective of the second part of the project was to engineer healing promoting materials and to establish platforms that allow in vitro study of cellular response to biological cues.

STABLE 3D GROWTH FACTOR GRADIENTS

In the article presented in Chapter 3,¹¹ we reported MSC activation upon presentation of a gradient of immobilized PDGF. We first verified the activity of the GF on the cells in a microtissue assay and observed concentration dependency of migration, proliferation and morphology. Next, we took advantage of electrochemical inhibition of PEG polymerization to reproducibly create channels inside PEG hydrogels populated with MSCs.¹² We used these channels as a source of GF from which the biological cues diffused and bound by affinity to the surrounding PEG matrix. The PDGF gradient resulting from this process enabled us to create a synthetic platform with an organized 3D complexity and assess the spatially differential effects on MSC migration and morphology.¹¹ A large number of studies in 2D and 3D cell cultures focused on the formation of gradients in vitro.¹³⁻¹⁹ They have all been motivated by the interest in recreating a biological process present in nature and responsible for cellular regulation in developmental biology, wound healing and tissue homeostasis.^{20,21} In our work, we presented for the first time a stable gradient formed by growth factor immobilization in a synthetic 3D PEG environment.

SCREENING PLATFORM FOR CELL INVASION

In Chapter 4, we concentrated on the development of alternative platforms which allowed us to address the migration-inducing effect of those biological cues. As a matter of fact, migration is one of the first cellular processes in the wound healing mechanism,²² which, in the context of this thesis, is a characteristic required for a healing inducing material. Previous studies have shown how migration could be assessed using pre-casted collagen or hyaluronic acid gels.^{23,24} However, those materials have the disadvantage to carry signals inherent to their natural origin.

Here, we took once again advantage of the electrochemical inhibition of PEG polymerization to fabricate a whole 96-well plate of hydrogels possessing a stiffness gradient. Those gels had the property to be very soft at the surface, which enables hydrogel formation prior to cell seeding without losing the 3D aspect granted by PEG hydrogels. We report how this resulting platform can be used to quantify cell migration into the gel in response to biological cues in a 96-well plate. For that, we set our focus on developing scripts for the automation of confocal image acquisition of the 3D gel stack and data processing for the numerical conversion of signal into quantifiable input. In addition, we developed an algorithm enabling the correction of gel irregularities for reliable analysis of cell invasion. As a result, we succeeded in analysing a large number of samples in parallel in a very limited amount of time. This allowed us to test multiple growth factor concentrations in a statistically relevant number of replicates, which can be of importance for the use in larger scale studies aiming to address cell invasion level in synthetic hydrogels *in vitro*.

WOUND MODEL FOR CELL RECRUITMENT

Next, in Chapter 5, we developed a wound model by creating a channel in hydrogel cell culture and utilized it to test healing promoting materials. In this case, growth factor was delivered inside the wound mimic by the injection of a PEG hydrogel carrying biological cues inside the channel. This hydrogel played the role of a healing material and was designed to enable cell penetration inside of it. The recruitment potential of the growth factor was then evaluated by measuring the concentration of cells invading and colonizing the healing hydrogel. This platform confirmed the increased recruitment rate when PDGF was present compared to the case when no PDGF was delivered. Hence, the platform proved to be perfectly suited for the study of the recruitment inducing capacity of a healing material on an *in vitro* wound model.

QUANTITATIVE PROTEOMICS TO STUDY ECM SYNTHESIS

The last objective, which is presented in Chapter 6 was motivated by the need to gain knowledge about deciphering the microenvironment created by cells cultivated in 3D synthetic hydrogels. This rationale was supported by decades of research that sought to elucidate the structure of body tissues. More specifically to our case, the components of fetal membranes have been the topic of several published works that highlighted the contribution of each extracellular-membrane protein to the structural stability of the membranes.^{25,26} This interest

Conclusion

became even more relevant when recent discoveries reported that those proteins do not only have a structural function but that they also have a central function in regulating biological signals in the complex cellular environment. Indeed, ECM proteins have been shown to sequester growth factors²⁷⁻³¹ and send biological signals to direct cell fate and behaviour.³²⁻³⁸ Thus, the faithful reproduction of the ECM environment is a determining factor when aiming to mimic native tissues in vitro or when engineering healing materials directing the regeneration of a specific tissue.

Throughout this work, we made use of growth factors as biological signals and potential cues inducing the healing process. Based on previous studies that show growth factor dependency of specific ECM protein synthesis,^{11,22,39-42} we aimed to present a way to identify the proteins produced and deposited in synthetic PEG hydrogels when cultivated in the presence of growth factors. This was successfully done by taking advantage of mass spectrometry analysis and label free quantification to address the variation in ECM components depending on the treatment provided. Our data displayed clear variations after 20 days in culture. Treating cells with PDGF/EGF or with TGF β 1 resulted in a set of ECM proteins present in different quantities. In addition, we could also attribute protein abundance to the order of growth factor delivery, highlighting once more the importance in the choice of the cues as well as the order in which they are presented.

In summary, we managed to present a method that enables the tracking down of the exact ECM components of a newly produced environment by, in opposition to RNA sequencing, detecting signals in a protein level.

6.2 _ FUTURE OUTLOOK

DEVICE OPTIMIZATION

The medical device showed clear potential for the future use, however, several design parameters will need optimization to reach the clinics. First, shape and size of the umbrella-shaped retainer will need to be adapted to optimize its mechanical properties. Despite its workability, it lacks in pulling resistance, which is needed for the reliable placement of it by the physician without visual control. Second, the handling piece used by the surgeon to implant the receptor must be developed following industrial production and regulations requirements. Finally, the choice of gluing material has to be made by preferentially testing various candidates within existing biocompatible adhesives. Their ability to bind the receptor in a stable manner, in wet conditions will be key elements for its adoption. The weak adhesion strength of the two components glues also indicates the need for improvements. The addition of a mixing device at the distal end of the device, adjustment of glue viscosity and speed of application can potentially play a determinant role for optimal membrane defect stabilization. All those elements can be tested on the models set out in Chapter 2.

In addition, cyclic pressure variations could be applied by adapting the models set out in Chapter 2 to simulate contractions and assess the stability of the implanted materials in dynamic conditions.^{2,43} The adhesive strength of those glues will be tested in combination with multiple materials covering the nitinol receptor backbone. For example, ePTFE or silicone mesh will be tested in combination with fibrin glues or cyanoacrylate-based adhesives. Those materials are biocompatible and have the advantage of already being used in clinical applications.⁴⁴⁻⁴⁸

INJECTING HEALING-INDUCING MATERIALS

The device was made to enable the application of any type of injectable materials. In a long-term approach, sealing materials might be replaced by bioactive materials stimulating tissue healing at the site of application. Thus, the establishment of platforms presented in Chapters 3-5 to address the effect of bioactive cues on cellular behaviour is highly relevant in the context of tissue healing. In the next steps, those platforms will be used to investigate the healing processes of a myriad of bioactive signals on the precise cell types of interest. In this precise case of fetal membrane healing, cells harvested from fetal membranes will be cultivated first on the 96-well hydrogel gradients plate to quantify the activation potential of growth factors. Thanks to the automation of production until data analysis, an important number of samples will be analysed. Besides the analysis of cell invasion, the production of ECM will be assessed on the same assay. Since the proteomics approach only requires digestion of the sample, it could be done on the same hydrogel gradients. This way, one could make a direct parallel between invasion index and ECM production.

Conclusion

Moreover, development of new approaches to control the immobilization of biological cues in synthetic hydrogels allows us to illustrate a vast range of possibilities for controlling the exposure of growth factors to cells. For example, it has been shown that ligands can have different binding affinities.⁴⁹ This characteristic can be used to bind multiple growth factors each to one ligand and thus, varying the availability of those cues thanks to their different affinity. Alternatively, one can think of covalently binding growth factors to the hydrogel backbone and linking it to a degradation motif, which, in turn, can also be tuned to vary its degradation kinetics.⁵⁰ This way, one can engineer materials having successive release and presentation of growth factors. The platforms resulting from objectives 2 and 3 are perfectly adapted to this type of study. It would allow the study of the effect of growth factor binding and successive release on the activation potential and on the specific ECM protein production. This could be used as a real platform for screening purposes by tailoring the 4th dimension of complex biomaterials.^{51,52} More specifically for our project, the type, the concentration and the successive presentation of growth factors could be studied to optimize cell recruitment and production of specific ECM proteins like Collagens II, III, V, Laminin and Fibronectin, which form the core structural composition of amnion. Put together, these elements are the necessary tools for the development of the ideal material inducing the healing of fetal membrane defects by producing the native tissue components. This will ultimately need to be tested and verified in combination with the application device on big animal models (Figure 6.1 red).

To conclude, each chapter resulted in a significant contribution to their respective field by bringing novelty on both the medical technology side and on the synthetic tissue engineering domain. Together, all these elements could be combined in the future to engineer injectable smart healing materials that specifically trigger healing processes, going one step towards the complete regeneration of tissue defects.

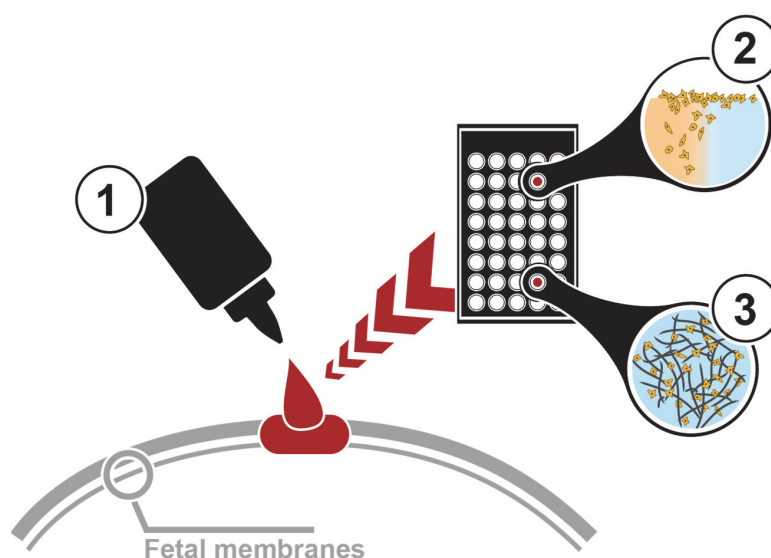


Figure 6.1. Schematic representation of future possibilities enabled by the achievement of objectives 1, 2 and 3. The application device, combined with the assessment of healing process like cell activation and ECM production can result in the delivery of smart materials to efficiently regenerate tissue defects.

6.3 _ REFERENCES

1. Bilic, G., *et al.* Injectable candidate sealants for fetal membrane repair: bonding and toxicity in vitro. *American journal of obstetrics and gynecology* 202, 85 e81-89 (2010).
2. Haller, C.M., *et al.* Mussel-mimetic tissue adhesive for fetal membrane repair: a standardized ex vivo evaluation using elastomeric membranes. *Prenatal diagnosis* 31, 654-660 (2011).
3. Haller, C.M., *et al.* Mussel-mimetic tissue adhesive for fetal membrane repair: an ex vivo evaluation. *Acta biomaterialia* 8, 4365-4370 (2012).
4. Kivelio, A., *et al.* Mussel mimetic tissue adhesive for fetal membrane repair: initial in vivo investigation in rabbits. *Eur J Obstet Gynecol Reprod Biol* 171, 240-245 (2013).
5. Ochsenbein-Kolble, N., *et al.* Enhancing sealing of fetal membrane defects using tissue engineered native amniotic scaffolds in the rabbit model. *American journal of obstetrics and gynecology* 196, 263 e261-267 (2007).
6. Harmanli, O.H., Wapner, R.J. & Lontz, J.F. Efficacy of fibrin glue for in vitro sealing of human chorioamniotic membranes. *The Journal of reproductive medicine* 43, 986-990 (1998).
7. Louis-Sylvestre, C., Rand, J.H., Gordon, R.E., Salafia, C.M. & Berkowitz, R.L. In vitro studies of the interactions between platelets and amniotic membranes: a potential treatment for preterm premature rupture of the membranes. *American journal of obstetrics and gynecology* 178, 287-293 (1998).
8. Papadopoulos, N.A., *et al.* Fetal membrane closure techniques after hysterotomy in the midgestational rabbit model. *American journal of obstetrics and gynecology* 178, 938-942 (1998).
9. Devlieger, R., Gratacos, E., Ardon, H., Vanstraelen, S. & Deprest, J. Factors influencing the flow rate through a surgical defect in human fetal membranes. *Prenatal diagnosis* 22, 201-205 (2002).
10. Gratacos, E., *et al.* Successful sealing of fetoscopic access sites with collagen plugs in the rabbit model. *American journal of obstetrics and gynecology* 182, 142-146 (2000).
11. Lienemann, P.S., *et al.* Locally controlling mesenchymal stem cell morphogenesis by 3D PDGF-BB gradients towards the establishment of an in vitro perivascular niche. *Integr Biol-Uk* 7, 101-111 (2015).
12. Milleret, V., Simona, B.R., Lienemann, P.S., Vörös, J. & Ehrbar, M. Electrochemical Control of the Enzymatic Polymerization of PEG Hydrogels: Formation of Spatially Controlled Biological Microenvironments. *Advanced healthcare materials*, n/a-n/a (2013).
13. Aizawa, Y. & Shoichet, M.S. The role of endothelial cells in the retinal stem and progenitor cell niche within a 3D engineered hydrogel matrix. *Biomaterials* 33, 5198-5205 (2012).
14. Dodla, M.C. & Bellamkonda, R.V. Anisotropic scaffolds facilitate enhanced neurite extension in vitro. *J Biomed Mater Res A* 78, 213-221 (2006).
15. Musoke-Zawedde, P. & Shoichet, M.S. Anisotropic three-dimensional peptide channels guide neurite outgrowth within a biodegradable hydrogel matrix. *Biomedical materials* 1, 162-169 (2006).
16. Wylie, R.G., *et al.* Spatially controlled simultaneous patterning of multiple growth factors in three-dimensional hydrogels. *Nat Mater* 10, 799-806 (2011).
17. Keenan, T.M. & Folch, A. Biomolecular gradients in cell culture systems. *Lab on a chip* 8, 34-57 (2008).
18. Sant, S., Hancock, M.J., Donnelly, J.P., Iyer, D. & Khademhosseini, A. Biomimetic Gradient Hydrogels for Tissue Engineering. *Can J Chem Eng* 88, 899-911 (2010).
19. Peret, B.J. & Murphy, W.L. Controllable Soluble Protein Concentration Gradients in Hydrogel Networks. *Adv Funct Mater* 18, 3410-3417 (2008).
20. Ruhrberg, C., *et al.* Spatially restricted patterning cues provided by heparin-binding VEGF-A control blood vessel branching morphogenesis. *Genes & development* 16, 2684-2698 (2002).
21. Senger, D.R. & Davis, G.E. Angiogenesis. *Cold Spring Harb Perspect Biol* 3, a005090 (2011).
22. Robson, M.C., Steed, D.L. & Franz, M.G. Wound healing: biologic features and approaches to maximize healing trajectories. *Curr Probl Surg* 38, 72-140 (2001).
23. Davis, G.E., Black, S.M. & Bayless, K.J. Capillary morphogenesis during human endothelial cell invasion of three-dimensional collagen matrices. *In Vitro Cell Dev Biol Anim* 36, 513-519 (2000).
24. Fisher, S.A., Anandakumaran, P.N., Owen, S.C. & Shoichet, M.S. Tuning the Microenvironment: Click-Crosslinked Hyaluronic Acid-Based Hydrogels Provide a Platform for Studying Breast Cancer Cell Invasion. *Adv Funct Mater* 25, 7163-7172 (2015).
25. Bryant, S.J. & Anseth, K.S. Hydrogel properties influence ECM production by chondrocytes photoencapsulated in poly(ethylene glycol) hydrogels. *J Biomed Mater Res* 59, 63-72 (2002).

Conclusion

26. Parry, S. & Strauss, J.F., 3rd. Premature rupture of the fetal membranes. *N Engl J Med* 338, 663-670 (1998).
27. Macri, L., Silverstein, D. & Clark, R.A.F. Growth factor binding to the pericellular matrix and its importance in tissue engineering. *Adv Drug Deliver Rev* 59, 1366-1381 (2007).
28. Martino, M.M. & Hubbell, J.A. The 12th-14th type III repeats of fibronectin function as a highly promiscuous growth factor-binding domain. *FASEB J* 24, 4711-4721 (2010).
29. Ramirez, F. & Rifkin, D.B. Extracellular microfibrils: contextual platforms for TGFbeta and BMP signaling. *Curr Opin Cell Biol* 21, 616-622 (2009).
30. Sarrazin, S., Lamanna, W.C. & Esko, J.D. Heparan sulfate proteoglycans. *Cold Spring Harb Perspect Biol* 3(2011).
31. Schultz, G.S. & Wysocki, A. Interactions between extracellular matrix and growth factors in wound healing. *Wound Repair Regen* 17, 153-162 (2009).
32. Guilak, F., *et al.* Control of Stem Cell Fate by Physical Interactions with the Extracellular Matrix. *Cell Stem Cell* 5, 17-26 (2009).
33. Kubow, K.E., *et al.* Crosslinking of cell-derived 3D scaffolds up-regulates the stretching and unfolding of new extracellular matrix assembled by reseeded cells. *Integr Biol (Camb)* 1, 635-648 (2009).
34. Lin, F., *et al.* Fibronectin growth factor-binding domains are required for fibroblast survival. *J Invest Dermatol* 131, 84-98 (2011).
35. Singh, P. & Schwarzbauer, J.E. Fibronectin and stem cell differentiation - lessons from chondrogenesis. *J Cell Sci* 125, 3703-3712 (2012).
36. Wijelath, E.S., *et al.* Heparin-II domain of fibronectin is a vascular endothelial growth factor-binding domain: enhancement of VEGF biological activity by a singular growth factor/matrix protein synergism. *Circ Res* 99, 853-860 (2006).
37. Yamada, Y., Hozumi, K. & Nomizu, M. Construction and Activity of a Synthetic Basement Membrane with Active Laminin Peptides and Polysaccharides. *Chem-Eur J* 17, 10500-10508 (2011).
38. Zhu, J. Bioactive modification of poly(ethylene glycol) hydrogels for tissue engineering. *Biomaterials* 31, 4639-4656 (2010).
39. Ng, F., *et al.* PDGF, TGF-beta, and FGF signaling is important for differentiation and growth of mesenchymal stem cells (MSCs): transcriptional profiling can identify markers and signaling pathways important in differentiation of MSCs into adipogenic, chondrogenic, and osteogenic lineages. *Blood* 112, 295-307 (2008).
40. Kivellio, A., Ochsenbein-Koelble, N., Zimmermann, R. & Ehrbar, M. Engineered cell instructive matrices for fetal membrane healing. *Acta biomaterialia* 15, 1-10 (2015).
41. Murphy, M.B., *et al.* Adult and umbilical cord blood-derived platelet-rich plasma for mesenchymal stem cell proliferation, chemotaxis, and cryo-preservation. *Biomaterials* 33, 5308-5316 (2012).
42. Ponte, A.L., *et al.* The in vitro migration capacity of human bone marrow mesenchymal stem cells: Comparison of chemokine and growth factor chemotactic activities. *Stem Cells* 25, 1737-1745 (2007).
43. Perini, M., *et al.* Mechanical and Microstructural Investigation of the Cyclic Behavior of Human Amnion. *J Biomech Eng-T Asme* 137(2015).
44. Bilsel, Y. & Abci, I. The search for ideal hernia repair; mesh materials and types. *Int J Surg* 10, 317-321 (2012).
45. Hellmund, A., *et al.* Prenatal Diagnosis and Evaluation of Sonographic Predictors for Intervention and Adverse Outcome in Congenital Pulmonary Airway Malformation. *PLoS One* 11, e0150474 (2016).
46. Saygun, O., *et al.* Reinforcement of the suture line with an ePTFE graft attached with histoacryl glue in duodenal trauma. *Can J Surg* 49, 107-112 (2006).
47. Shorr, N., Cohen, M.S. & Lessner, A. Histoacryl closure of eyelid skin grafts. *Ophthal Plast Reconstr Surg* 7, 190-193 (1991).
48. Van Steenberghe, W. The first prospective endoscopic experience with the ePTFE-covered Viabil stent in patients with a distal malignant biliary stenosis. *Acta Gastroenterol Belg* 73, 18-24 (2010).
49. Lienemann, P.S., Lutolf, M.P. & Ehrbar, M. Biomimetic hydrogels for controlled biomolecule delivery to augment bone regeneration. *Adv Drug Deliv Rev* 64, 1078-1089 (2012).
50. Metzger, S., *et al.* Cell-Mediated Proteolytic Release of Growth Factors from Poly(Ethylene Glycol) Matrices. *Macromol Biosci* 16, 1703-1713 (2016).
51. Tibbitt, M.W. & Anseth, K.S. Dynamic microenvironments: the fourth dimension. *Sci Transl Med* 4, 160ps124 (2012).
52. Decaestecker, C., Debeir, O., Van Ham, P. & Kiss, R. Can anti-migratory drugs be screened in vitro? A review of 2D and 3D assays for the quantitative analysis of cell migration. *Med Res Rev* 27, 149-176 (2007).

ACKNOWLEDGEMENTS

The realisation of this work was made possible by the scientific and/or personal participation of many people. There might not be enough space to mention all of them, but I want to thank every person who made those 4 years a memorable chapter in my life. First, big thank to you, reader, who went, without any doubt, thoroughly through this thesis and gave it a reason to exist.

Most importantly, I thank **Dr. Martin Ehrbar** for the support and guidance throughout all the steps of this scientific and personal development. Thanks for trusting in my capacities, for always listening to any idea independently of its relevance and for bringing me back on track when needed.

Huge thank to **Prof. Matthias Lütolf** for recommending me to the Ehrbar Lab, for accepting to be my doctoral father and for always contributing with useful feedbacks.

I am also thankful to the member of my thesis jury, **Prof. Philippe Renaud**, **Prof. Nicole Ochsenbein-Kölble**, **Dr. Mark Tibbitt** and **Prof. Nikolaos Stergiopoulos** for accepting to evaluate my work.

To all the individuals who were part of the Ehrbar Lab. More particularly, I want to thank **Dr. Vincent Milleret** for our numerous conversations, for his precious advice and for his endless source of bad jokes. Also, huge thank to **Dr. Philippe Lienemann** for his amazing tutoring, for his patience, dedication and for his questionable skills at Wii ping-pong. I am also very grateful to have shared my workspace with **Queralt Vallmajó (Martín)**, a continuous source of good energy and contagious positivity. Keep kicking b***! Big thank also to **Ulrich Blache** for being available and always wanting to help, in particular with his great German sayings. I will also always be thankful to **Dr. Anna-Sofia Kiveliö**, for transferring me her project and for always sharing her food. Big hug! Thank you to **Dr. Stef/Stéf/Steph/Stéph (?) Metzger** for her love of details and for transmitting her passion for British actors.

I also want to thank ancient and more recent members of the PATH G community: **Dr. Benjamin Simona**, **Dr. Michela Perrini**, **Eva Avilla Royo**, **Dr. Ali Mirsaidi**, **Sibylle Abt**, **Alexandra Dolder**, **Tabea Vogel**, **Cornelia Bornhauser**, **Lisa Krattiger**, **Tabea Stephan**, **Silvia Züger**, **Dr. Ricardo Urbanet**, **Stefanie Lopes** and **Dr. Paula Simoes-Wüst**, for making our workspace a pleasant and joyful environment.

Special thanks to the pillars of the lab, **Esther Kleiner**, **Aida Kurmanaviciene**, **Yvonne Eisenegger** and **Corina Von Arx** for making the lab the best possible workspace, for their extremely useful technical help, for dealing with my administrative tasks and for taking good care of all the lab members. I am extremely grateful to all of you.

Next, I want to thank external people who contributed to the development of my scientific and personal skills through the years and with whom most of the work could not have been realized. Many thanks to:

Prof. Roland Zimmermann and the **clinics of obstetrics** of the University Hospital Zürich for always being open for discussion and providing enriching inputs.

Stephen Wheeler of the laboratory of biosensors and bioelectronics at ETHZ for his amazing work on concretizing my ideas by manufacturing extremely important elements in the diverse fields of my research.

Dr. Christian Trachsel and **Dr. Jonas Grossmann** from the functional genomics center in Zürich for teaching me the basics of mass spectrometry and contributing actively, with a lot of patience, to the realization of this work.

Olivera Evrova and **Prof. Viola Vogel** for allowing and helping me with the use of their equipment.

Prof. Eberli for providing with Degrapol.

Dr. Glen Kirkham and **Prof. Kevin Shakesheff** from the University of Nottingham for the collaborative work.

Kevin Bircher and **Prof. Edoardo Mazza** for providing with testing devices.

Luca Zimmermann from the ETHZ for the numerous meetings and his valuable inputs on mechanical design optimization.

Dr. Markus Ehrat for the rich conversations that brought me essential knowledge about the entrepreneurial world.

Dr. Christopher Millan for sharing his entrepreneurial knowledge and supporting in the writing of a grant proposal.

Jennifer Duncan for sharing her English skills during the redaction of this work.

Balboa and its team for helping me keeping a balance between body and mind.

Very importantly, I thank **My friends** who were always present to remind me that there is something besides science and always making sure to set up the best leisure environment.

Special thanks to my niece **Margot** for having set a deadline to the end of my thesis by deciding to join the family. I also want to thank my sister **Gabriela** for her tasteful graphical contribution to this thesis and for her unconditional love, support and for always being my example.

Finally, I want to thank my beautiful parents **Lidia** and **Jean-Marc** for their love, patience and dedication in making me a better person every day. I love you.

CURRICULUM VITAE

Yannick Robert Devaud
Fabrikstrasse 21, 8005 Zürich, Switzerland

December 14th 1987
Yannick.devaud@gmail.com

LANGUAGES

French	Mother tongue
Portuguese	Mother tongue
English	Fluid talk and good writing
German	Fluid talk and good writing
Swiss German	Fluid talk

EDUCATION

Master degree in Bioengineering with minor in biomedical technologies at EPFL	2012
Bachelor degree in Life Sciences and Technologies at EPFL	2010
High-school graduation at St.Michel, Fribourg, Switzerland, with Honours	2007

PROFESSIONAL EXPERIENCE

Research assistant as PhD candidate at the laboratory of Tissue Engineering and Stem Cell research, University Hospital Zürich, Switzerland	2013 - present
President of the Ski Club Fribourg, and J+S snowboard instructor	2005 - present
Ceremonialist at my sister's wedding	2015
Speaker at international hockey competitions	2012 - 2014
Live-ticker sports commentator for a national sports channel on the web	2011 - 2014
Intern at the Biomedical Nanotechnologies Laboratory, McGill University, Montréal under the supervision of Dr. David Juncker	2010
Research assistant for the master project at the Laboratory of Cartilage Tissue Engineering, UC San Diego under the supervision of prof. Robert L. Sah	2011-2012

SCIENTIFIC CONTRIBUTION

PUBLISHED ARTICLES

Y.R. Devaud, P. S. Lienemann, R. Reuten, B. R. Simona, M. Karlsson, W. Weber, M. Koch, M. P. Lutolf, V. Milleret and M. Ehrbar. Locally controlling mesenchymal stem cell morphogenesis by 3D PDGF-BB gradients towards the establishment of an in vitro perivascular niche, INTEGRATIVE BIOLOGY, 2015, 7.1, 101:111

G.R. Kirkham, E. Britchford, T. Upton, J. Ware, G.M. Gibson, Y.R. Devaud, M. Ehrbar, M. Padgett, S. Allen, L.D. Buttery, K. Shakesheff. Precision Assembly of Complex Cellular Microenvironments using Holographic Optical Tweezers, SCIENTIFIC REPORTS 5, 2015, Nr. 8577

SUBMITTED MANUSCRIPT

Minimally invasive Surgical device for precise application of bioadhesives to prevent Ipprom, FETAL DIAGNOSIS AND THERAPY, October 2017

MANUSCRIPT TO BE SUBMITTED IN DECEMBER 2017

Label free quantification proteomics for the identification of mesenchymal stem cell matrisome inside 3D poly-ethylene glycol hydrogels, BIOMATERIALS

PATENTS

Minimally invasive surgical device for membrane closure. Nr: EP17154743 February 2017

Electrochemically-controlled polymerization by enzymatic inhibition. Nr EP16206283 December 2016

GRANTS

University of Zürich Proof of Concept grant May 2017

Commission for Technology and Innovation. Nr 27063.1 PFLS-LS August 2017

Academia-Industry Training program, Venturelab. October 2016

AWARDS

1st and 3rd at the Academia-Industry Training pitching competition October 2016

Best Biology and Chemistry high school graduation 2007

Overall number 1 ranking at the secondary school Belluard, Fribourg, Switzerland 2003

INTERESTS

Beach-volleyball junior swiss tour competitor 2006 – 2007

Captain of the floorball/unihockey club Sense-Tafers in the 2nd swiss league 2003 – 2007

Swimming competitor 1998 – 2004

Surf, sailing, hockey, travelling, gardening and DIY activities

